MENTATION PAGE

Form Approved OMB No. 0704-0188

AD-A226 438

1b. RESTRICTIVE MARKINGS

3. DISTRIBUTION/AVAILABILITY OF REPORT
Approved for public release; distribution unlimited

ORMING ORGANIZATION REPORT NUMBER(S)

5. MONITORING ORGANIZATION REPORT NUMBER(S)
ARO 26213.69-EL

E OF PERFORMING ORGANIZATION
irch Laboratory of Electronics
chusetts Institute of Technology

6b. OFFICE SYMBOL (If applicable)

7a. NAME OF MONITORING ORGANIZATION
U.S. Army Research Office

RESS (City, State, and ZIP Code)
issachusetts Avenue
ridge, MA 02139

7b. ADDRESS (City, State, and ZIP Code)
P.O. Box 12211
Research Triangle Park, NC 27709-2211

E OF FUNDING/SPONSORING ANIZATION
. Army Research Office

8b. OFFICE SYMBOL (If applicable)

9. PROCUREMENT INSTRUMENT IDENTIFICATION NUMBER
DAAL03-89-C-0001

RESS (City, State, and ZIP Code)
. Box 12211
earch Triangle Park, NC 27709-2211

10. SOURCE OF FUNDING NUMBERS

PROGRAM ELEMENT NO.	PROJECT NO.	TASK NO.	WORK UNIT ACCESSION NO.
	P-26213-EL		

(Include Security Classification)
Reprinted (Chapters) from RLE Progress Report No. 132, June 1990

ONAL AUTHOR(S)

E OF REPORT	13b. TIME COVERED	14. DATE OF REPORT (Year, Month, Day)	15. PAGE COUNT
RINT	FROM _____ TO _____		

LEMENTARY NOTATION The view, opinions and/or findings contained in this report are se of the author(s) and should not be construed as an official Dept. of the Army position, icy or decision, unless so designated by other documentation.

COSATI CODES		
D	GROUP	SUB-GROUP

18. SUBJECT TERMS (Continue on reverse if necessary and identify by block number)

RACT (Continue on reverse if necessary and identify by block number)

lork by Prof. J. Allen and his collaborators is summarized here.

Document complete per ARO. — RHH

RIBUTION/AVAILABILITY OF ABSTRACT
NCLASSIFIED/UNLIMITED ☐ SAME AS RPT. ☐ DTIC USERS

21. ABSTRACT SECURITY CLASSIFICATION
UNCLASSIFIED

ME OF RESPONSIBLE INDIVIDUAL
S. Greene - RLE Contract Reports

22b. TELEPHONE (Include Area Code)
(617)258-5871

22c. OFFICE SYMBOL

n 1473, JUN 86 Previous editions are obsolete. SECURITY CLASSIFICATION OF THIS PAGE

UNCLASSIFIED

ERRATA

AD-A 226-438

This document contains the following pages per Massachusetts Institute of Technology, Research Laboratory of Electronics: p. 21-23, 35, 41-45, 47-50, 53-57, 59-60, 61-62, 64-66, 73-83, 109-126, 139-142, 148-153, 197-202, 275-279.

DTIC-FDAC
21 Dec 90

RLE Progress Report

No. 132

January 1 - December 31, 1989

Submitted by

Professor Jonathan Allen
Professor Daniel Kleppner

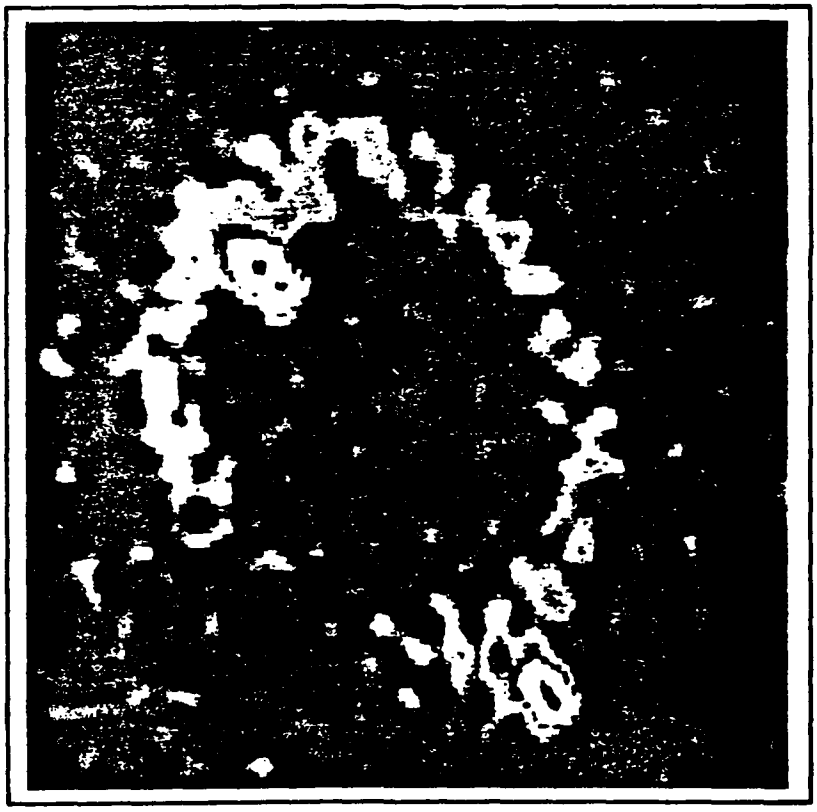

Research Laboratory of Electronics
Massachusetts Institute of Technology
Cambridge, MA 02139 USA

Chapter 1. Submicron Structures Technology and Research

Academic and Research Staff

Professor Henry I. Smith, Professor Dimitri A. Antoniadis, James M. Carter, Professor Jesus A. del Alamo, Professor Marc A. Kastner, Professor Terry P. Orlando, Dr. Mark L. Schattenburg, Professor Carl V. Thompson

Visiting Scientists and Research Affiliates

C.T. Liu,[1] Irving Plotnik,[2] T.P. Smith,[3] Dr. Dan Tsui[1]

Graduate Students

Sergio A. Ajuria, Phillip F. Bagwell, Martin Burkhardt, William Chu, Lawrence A. Clevenger, Kathleen R. Early, Cris Eugster, Jerrold A. Floro, Reza A. Ghanbari, Khalid Ismail, Eva Jiran, Harold Kahn, Yao-Ching Ku, Yachin Liu, Hai Longworth, Udi Meirav, Paul G. Meyer, Alberto Moel, Joyce E. Palmer, Samuel L. Park, Hui Meng Quek, John H.F. Scott-Thomas, Ghavam Shahidi, Siang-Chun The, Anthony Yen

Undergraduate Students

JoAnne Gutierrez, Kenneth Lu, Pablo Munguia, Lisa Su, Flora S. Tsai, Vincent Wong, Howard Zolla

Technical and Support Staff

Donna Martinez, Timothy McClure

1.1 Submicron Structures Laboratory

The Submicron Structures Laboratory at MIT develops techniques for fabricating surface structures with linewidths in the range from nanometers to micrometers, and uses these structures in a variety of research projects. These projects of the laboratory, which are described briefly below, fall into four major categories: development of submicron and nanometer fabrication technology; nanometer and quantum-effect electronics; crystalline films on non-lattice-matching substrates; and periodic structures for x-ray optics, spectroscopy and atomic interferometry.

1.2 Microfabrication at Linewidths of 100 nm and below

Sponsors

Joint Services Electronics Program
Contract DAAL03-89-C-0001
National Science Foundation
Grant ECS 87-09806

Project Staff

Martin Burkhardt, James M. Carter, William Chu, Kathleen Early, Reza A. Ghanbari, Yao-Ching Ku, Alberto Moel, Hui Meng Quek, Dr. Mark L. Schattenburg, Professor Henry I. Smith, Siang-Chun The, Anthony Yen

[1] Princeton University, Princeton, New Jersey.

[2] Hampshire Instruments, Westboro, Massachusetts.

[3] *IBM T.J. Watson Research Center, Yorktown Heights, New York.*

A variety of techniques for fabricating structures with characteristic dimensions of 0.1 μm (100 nm) and below are investigated. These include: x-ray nanolithography, holographic lithography, achromatic holographic lithography, electron-beam lithography, focused-ion-beam lithography, reactive-ion etching, electroplating, and liftoff. Development of such techniques is essential if we are to explore the rich field of research applications in the deep-submicron and nanometer domains.

X-ray nanolithography is of special interest because it can provide high throughput and broad process latitude at linewidths of 100 nm and below, something that cannot be achieved with scanning-electron-beam or focused-ion-beam lithography alone. We are developing a new generation of x-ray masks made from inorganic membranes (Si, Si_3N_4, and SiC) in order to eliminate pattern distortion. To achieve multiple-mask alignment compatible with 50 nm linewidths, we will fix the mask-sample gap at 4 μm, translate the mask piezoelectrically, and detect alignment to < 10 nm by a dual-grating interferometric scheme. Phase-shifting x-ray masks should permit us to achieve 50 nm linewidths at such gaps. In previous studies we showed that a pi-phase-shifting mask improves process latitude by increasing the irradiance slope at feature edges. For linewidths below 50 nm we bring the mask membrane into soft contact with the substrate by electrostatic means. A variety of techniques are used to pattern the x-ray masks including e-beam lithography, focused-ion-beam lithography (FIBL), holographic lithography and sidewall shadowing.

Since the early research on x-ray lithography, it was believed that photoelectrons, released when x-ray photons are absorbed, severely limit the resolution of x-ray lithography for linewidths below 100 nm. For example, it was estimated that using the Al_K x-ray (λ = 0.834 nm, E = 1.5 keV), it would not be possible to reliably achieve linewidths below 100 nm. We explored this issue experimentally and found previous estimates to be in error. Figure 1 shows that a 30 nm wide line on an x-ray mask is faithfully replicated with no measurable linewidth change using any one of three x-ray wavelengths, Al_K

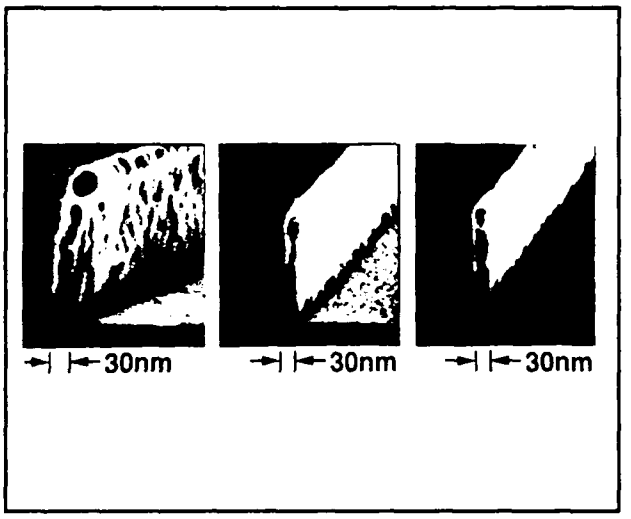

Figure 1. Replication in PMMA of a 30 nm-wide gold absorber line with (a) C_K (λ = 4.5 nm), (b) Cu_L(λ = 1.3 nm), and (c) Al_K(λ = 0.83 nm).

(0.834 nm), Cu_L (1.33 nm), or C_K (45 nm). The implication is that for linewidths down to ~ 10nm, diffraction and not photoelectron range is the factor that will limit resolution.

A new type of achromatic holographic lithography (AHL) was developed that enables us to achieve 100 nm-period gratings (50 nm nominal linewidth). Previously, 200 nm was the minimum period achievable. The AHL scheme is illustrated in figure 2, and the exposure results shown in figure 3. This technology will be used to make gratings for x-ray spectroscopy and atom beam interferometry, and to fabricate new classes of quantum-effect electronic devices.

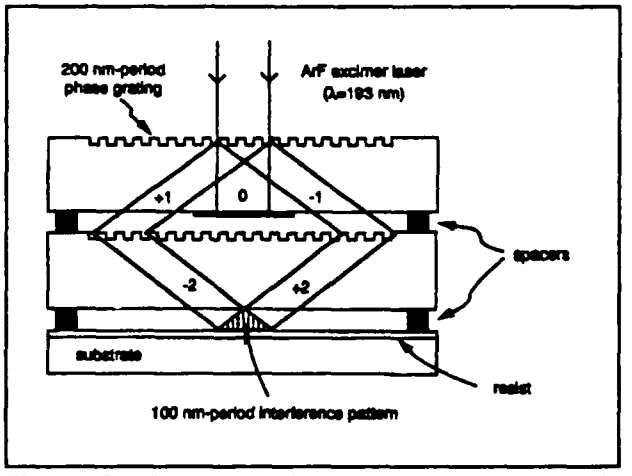

Figure 2. Schematic of the achromatic holographic configuration.

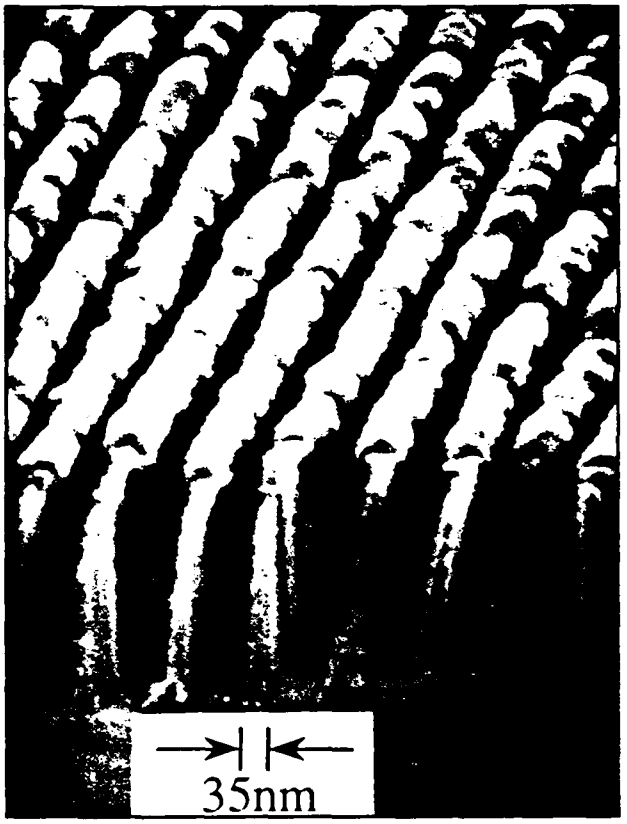

Figure 3. Scanning electron micrograph of 100 nm-period grating lines after exposure, shadow evaporation of nickel and reactive ion etching in an oxygen plasma.

1.3 Improved Mask Technology for X-Ray Lithography

Sponsors

Semiconductor Research Corporation
Contract 87-SP-080
Hampshire Instruments Corporation

Project Staff

Yao-Ching Ku, Kenneth Lu, Professor Henry I. Smith, Lisa Su, JoAnne Gutierrez, Flora S. Tsai

In order to utilize x-ray lithography in the fabrication of submicron integrated electronics, distortion in the x-ray mask must be eliminated. Distortion can arise from stress in the absorber, which is usually gold or tungsten. Tungsten is preferred because it is a closer match in thermal expansion to Si, SiC and other materials used as mask membranes. However, W is usually under high stress when deposited by evaporation or sputtering. Earlier, we demonstrated that for a given type of substrate, zero stress (i.e., less than 5×10^7 dynes/cm^2) can be achieved by controlling the sputtering pressure to within one-tenth of a militorr. We are now developing a computer-controlled system for monitoring in situ, during deposition, the stress in sputtered W on x-ray mask membranes. Stress is determined from the resonant frequency of the membrane.

We have also investigated a number of materials as mask membranes including: Si, Si_3N_4, SiC, and laminates of Si_3N_4/poly Si/Si_3N_4 and $SiO_2/Si_3N_4/SiO_2$. The strongest membranes were Si rich Si_3N_4. A 1.2 μm thick membrane of this material can sustain a full atmosphere pressure differential across a span of 20 mm. There is a concern, however, that Si_3N_4 will undergo stress changes during the heavy x-ray irradiation anticipated in IC production. We are investigating this issue as well as novel approaches to enhance the durability of Si membranes.

1.4 Study of Electron Transport in Si MOSFETs with Deep-Submicron Channel Lengths

Sponsor.

Joint Services Electronics Program
Contract DAAL03-89-C-0001

Project Staff

Professor Dimitri A. Antoniadis, Gregory A. Carlin, Paul G. Meyer, Ghavam Shahidi, Professor Henry I. Smith, Siang-Chun The

Electronic conduction in sub-100 nm channel length Si MOSFETS is being studied in order to observe non-stationary transport effects, i.e., effects arising from rapid spatial variation of the electric field, and the resulting disparity between the actual carrier temperature and the temperature that would correspond with the given field at steady-state conditions. In simple terms, non-stationary effects are observed when transit times across the very short channels become comparable to, or shorter than, energy relaxation times. Previous work has produced NMOS devices with channel lengths down

to 60 nm and gate oxides as thin as 2.5 nm. The devices were fabricated with a combination of x-ray nanolithography and optical projection lithography. Electron velocity overshoot and a reduction of hot-electron effects, as measured from the substrate current, were observed in these devices.

Our focus has now shifted to the fabrication of self-aligned deep-submicron MOSFETs. These devices will use polysilicon gates and cobalt salicidation (self-aligned silicidation). The aim is to reduce parasitic source and drain resistances and gate-source overlaps. This will permit a clearer observation of the non-stationary effects, e.g., in both substrate and gate currents, and will enable us to push device switching speed.

Deep-submicron self-aligned silicided NMOS devices have been successfully fabricated using optical projection lithography followed by partial photoresist ashing to define small features. Devices with effective channel lengths down to 230 nm were fabricated using this technique. As in the non-self-aligned device process, both boron and indium were used as implant species to control punchthrough and threshold voltage. The sheet resistance of the source-drain regions was reduced by silicidation from 110 to 13.6 Ohms per square, and source-drain contact resistances on the devices were reduced from 52 to 10.7 Ohms.

The self-aligned NMOS process is undergoing further development to include x-ray nanolithography for gate polysilicon patterning. This has included the development of inorganic x-ray mask technology to avoid distortion and achieve precise alignment. A simple optical scheme to align x-ray masks to substrates to less than 1 μm has also been developed. The absorber on the x-ray mask will be patterned using a combination of optical lithography and focused-ion-beam (FIB) lithography. In addition, an effort is being made to further improve consistency and control in the salicidation process.

Work is also in progress to develop a corresponding deep-submicron self-aligned PMOS process. This should give us 100 nm-channel-length CMOS circuits fabricated by a technology compatible with commercial mass production.

1.5 Studies of Electronic Conduction in One-Dimensional Semiconductor Devices

Sponsors

Joint Services Electronics Program
Contract DAAL03-89-C-0001
National Science Foundation
Grant ECS-85-03443

Project Staff

Professor Dimitri A. Antonaidis, Stuart B. Field, Professor Marc A. Kastner, Udi Meirav, Samuel L. Park, John H.F. Scott-Thomas, Professor Henry I. Smith

Sophisticated processing techniques and advanced lithography have allowed us to enter what we believe is a fundamentally new regime in the study of electronic conduction in one-dimensional systems. A slotted-gate MOSFET structure (figure 4) was used to produce an electron gas at the Si/SiO_2 interface beneath the gap in the lower-gate. This was done by biasing the upper gate positively, while keeping the slotted gate just below threshold. Fringing fields around the lower gate confined the electron gas to a width substantially narrower ($\sim$ 25 nm) than the distance separating the two halves of the slotted gate ($\sim$ 70 nm). The slotted gate was produced using x-ray nanolithography and liftoff. It was composed of refractory metals to allow a subsequent high temperature anneal. This anneal removed damage created by the e-beam evaporation of the refractory metal, so that the electron gas had a mobility of 15,000 cm^2 / V-sec at 4.2K. The electrical conductance of the 1-D gas was measured as a function of the upper gate voltage for temperatures less than 1K, and a surprising series of periodic oscillations was seen in the conductance (figure 5). Changing the gate voltage can be thought of as changing the number of electrons per unit length of electron gas. Since the conductance is thermally activated, the oscillations reflect a periodic change in the activation energy of the electron gas as the electron density is changed. Computer simulations solving Poission's equation and the single particle Schrodinger

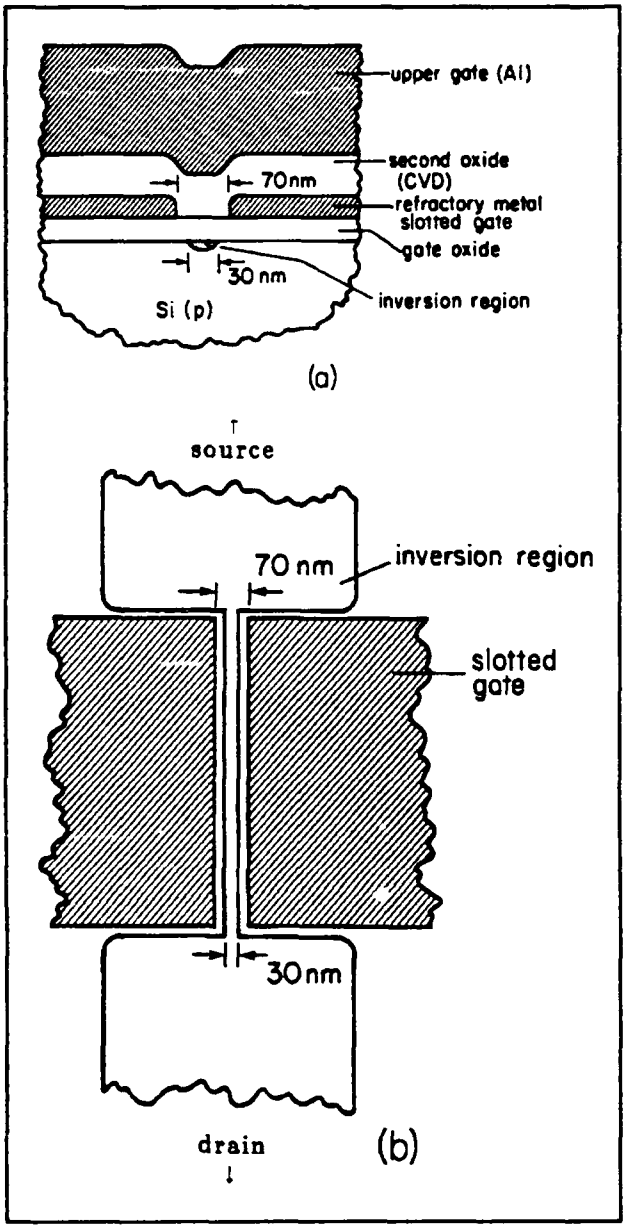

Figure 4. (a) Schematic cross section and (b) top view of the slotted-gate device. The inversion layer, formed by the positively biased upper gate is confined by the lower gate. The thermal oxide and refractory metal lower gate are both 30 nm thick, and the chemical vapor deposition oxide is 45 nm thick. The width of a narrow inversion layer is exaggerated in (b).

wave equation strongly suggest that the electron gas is dynamically one-dimensional when the oscillations are most strongly seen. That is, the electrons are in the lowest quantum energy level of the potential well created by the fringing fields of the slotted gate.

A one-dimensional electron gas will form a charge density wave (CDW) when the electron-electron interaction is the dominant energy. This is the same regime that the device is in when the oscillations are seen. In a CDW, electrons are spaced periodically. This minimizes the total energy of the electron gas. Impurities in the device can pin the CDW. Two impurities in the conducting channel would in turn strongly pin and weakly pin the CDW as the electron density of the gas is changed. This corresponds to commensurability and incommensurability of the CDW with the spacing of the impurities, and results in oscillatory behavior of the conductance with electron density. The period of the oscillations varies randomly from device to device, with no dependence on length. The period changes in the same device when it is heated to room temperature and then cooled. This strongly suggests that mobile impurity atoms are doing the pinning. It should be stressed that these oscillations are seen with no magnetic field, implying

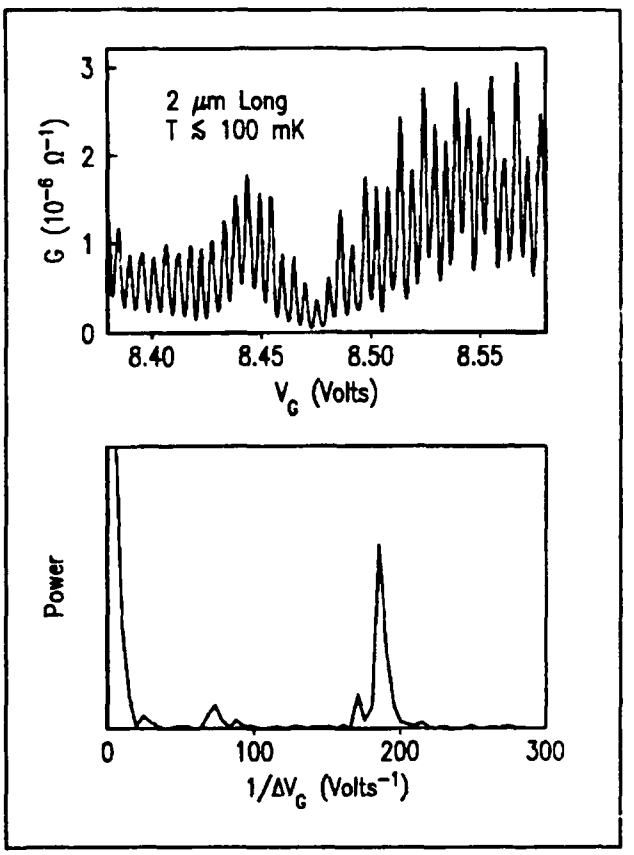

Figure 5. Top panel: Conductance G versus gate voltage V_G for a 2 μm-long inversion layer. Bottom panel: Fourier power spectrum of the top panel data.

that the phenomenon is fundamentally different from phenomena requiring Landau quantization (such as the Quantum Hall Effect). Also, the effect seems to require a many-body theory (i.e., one incorporating electron-electron interactions).

1.6 Surface Superlattice Formation in Silicon Inversion Layers Using 0.2 μm-Period Grating-Gate Field-Effect Transistors

Sponsors

Joint Services Electronics Program
Contract DAAL03-89-C-0001
U.S. Air Force - Office of Scientific Research
Grant AFOSR-88-0304

Project Staff

Professor Dimitri A. Antoniadis, Phillip F. Bagwell, Professor Marc A. Kastner, Professor Terry P. Orlando, Professor Henry I. Smith, Anthony Yen

We have been studying distinctly quantum mechanical effects in electrical conduction using the silicon grating-gate field-effect transistor (GGFET). The Si GGFET is a dual stacked-gate MOS-type structure in which the gate closest to the inversion layer (bottom gate) is a 200 nm period grating made of refractory metal. A SiO_2 insulating layer separates the grating gate and the inversion layer from a second continuous aluminum gate (top gate). Two types of electronic devices are possible in this geometry: (1) a lateral surface superlattice (LSSL) GGFET in which carrier conduction is perpendicular to the grating lines; and (2) a quasi-one-dimensional (QID) GGFET which confines carriers to move in narrow inversion strips beneath the grating lines.

Here we describe our observation of a transition from conduction through ~ 300 multiple parallel quantum wires to conduction in a 2D electron gas (standard MOSFET) using the Q1D GGFET. We can induce such a dimensional transition by varying the two gate voltages of the GGFET. When a strong magnetic field is applied perpendicular to the plane of the inversion layer at temperatures below 4.2K, we observe a large negative transconductance whose onset voltage marks the transition from 1D to 2D conduction.

This is shown in figure 6, where the transition from 1D to 2D behavior occurs at a top-gate voltage around zero volts. The significant observation is that with a magnetic field perpendicular to the plane of the channel, adding more electrons to the MOSFET actually reduces the device conductance at the 1D to 2D transition point. The oscillations below the transition point are due to magnetoelectric subbands, while those above the transition are due to Shubnikov de Haas oscillations as the Landau levels pass through the Fermi level. This striking dimensional transition in a magnetic field has never been observed before.

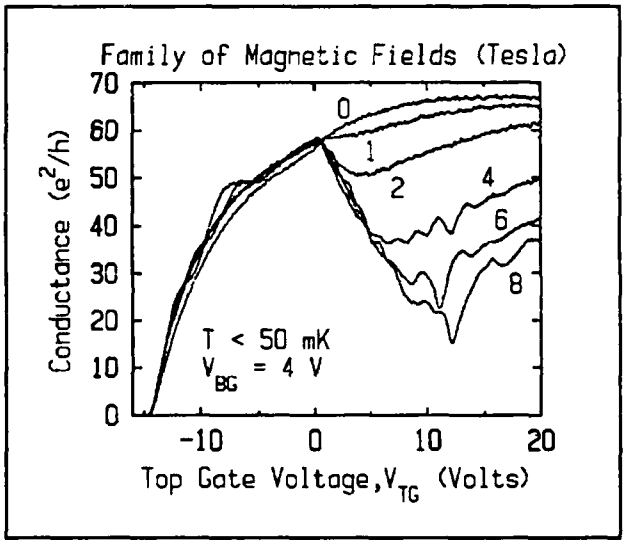

Figure 6. Plot of the conductance of a quasi-1D grating-gate MOSFET as a function the top gate voltage, for several values of the perpendicular magnetic field. At a top gate voltage around zero volts there is a transition from 1D to 2D conduction with an attendant strong negative transconductance.

The origin of the unusual magnetoresistance effects that we have observed is still unclear. At the magnetic fields where the effect becomes prominent, the cyclotron radius is much smaller than the width of the quantum wires, so a semiclassical explanation involving an interplay of the cyclotron radius and wire width is probably inappropriate. Also, the two terminal magnetoresistance measurements significantly complicate interpretation of the data. A noninvasive four-terminal measurement would be ideal, but it is not clear that such a measurement is pos-

sible. Finally, the exact way in which the current feeds into the source contact from the bulk device may also be important. At higher magnetic fields where the magneto-conductance oscillations begin to appear, conduction takes place through edge states. These edge states may also play a role in giving rise to the effect.

1.7 Study of Surface Superlattice Formation in GaAs/GaAlAs Modulation Doped Field-Effect Transistors

Sponsor

U.S. Air Force - Office of Scientific Research
Grant AFOSR-88-0304

Project Staff

Professor Dimitri A. Antoniadis, Martin Burkhardt, William Chu, Professor Jesus A. del Alamo, Reza A. Ghanbari, Khalid Ismail, Professor Marc A. Kastner, Professor Terry P. Orlando, Professor Henry I. Smith, Anthony Yen

We have used the modulation-doped field-effect transistor (MODFET) as a test vehicle for studying quantum effects such as electron back diffraction in a GaAs/AlGaAs material system. In a conventional MODFET the current transport is modulated by a continuous gate between source and drain. In our studies, we have used Schottky metal gratings and grids for the gate, as illustrated in figure 7. Such gates produce a periodic potential modulation in the channel.

The grid was produced by x-ray nanolithography and liftoff. The x-ray mask of the grid was produced by two successive x-ray exposures, at 90 degrees to one another, using a master mask that was fabricated via holographic lithography. The latter yields coherent gratings over areas several centimeters in diameter. A new technique was developed that yields grating and grid patterns only in the channel region between source and drain. This has simplified the overall process and enhanced its reliability.

The MODFET is normally on, that is, a negative gate bias of about -0.2 V must be applied to pinch off conductance from source to drain. As the gate bias is raised above this threshold point, the height of the periodic potential modulation is reduced and, simultaneously, the Fermi energy is raised (or, equivalently, the electron wavelength is reduced) in the 2D electron gas residing at the AlGaAs/GaAs interface. When the electron wavelength phase-matches the periodic potential, electron back-diffraction occurs provided the inelastic length (i.e., the coherence or phase breaking length) is longer than the grating-period. Such back diffraction is manifested by a drop in the conductance. A stronger back diffraction effect is observed in the case of a grid because true minigaps are formed. The measurements of conductance modulation of grating and grid-gate MODFETs agrees with theoretical predictions. In the grid gate devices it was also possible to observe negative differential resistance which might be due to sequential resonant tunneling.

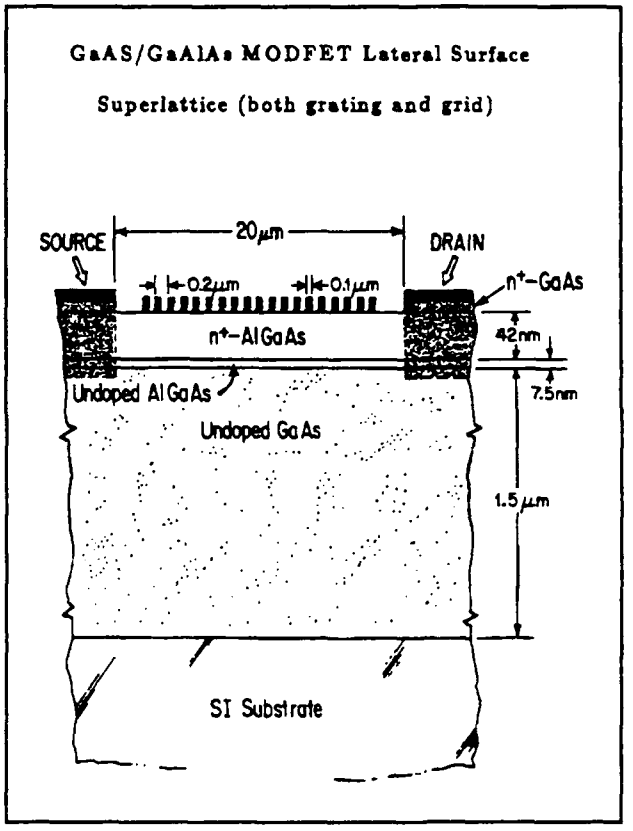

Figure 7. Schematic cross section of a grid-gate MODFET device. Contacts to the grid are made by pads off to the sides of the conduction channel.

We plan to decrease the periodicity of the gratings and grids by a factor of two, to 100 nm period. For devices with such fine grating

periodicity the superlattice effect should become more pronounced and observable at higher temperatures. We will also conduct magnetotransport measurements with devices of 100 and 200 nm periodicity.

1.8 Study of One-Dimensional Subbands and Mobility Modulation in GaAs/AlGaAs Quantum Wires

Sponsors

Joint Services Electronics Program
Contract DAAL03-89-C-0001
U.S. Air Force - Office of Scientific Research
Grant AFOSR-88-0304

Project Staff

Professor Dimitri A. Antoniadis, Phillip F. Bagwell, William Chu, Professor Jesus A. del Alamo, Reza A. Ghanbari, Khalid Ismail, Professor Marc A. Kastner, Professor Terry P. Orlando, Professor Henry I. Smith, Anthony Yen

In order to study one-dimensional conductivity in the AlGaAs/GaAs modulation-doped structure without the conductance fluctuations normally associated with single microscopic systems, we fabricated arrays of 100 parallel quantum wires (MPQW). The measured Hall mobility in the 2-D electron gas at the AlGaAs/GaAs interface was 250,000 cm^2/Vs at 4.2K. The multiple quantum wires were produced by x-ray nanolithography, liftoff of Ti/Au, and ion etching of the AlGaAs. The charge concentration in the quantum wires could be increased by applying a positive bias to a back-side contact or by illumination. (There was no persistent photocurrent in these samples).

Figure 8 shows the measured drain-source current versus backgate bias for the quantum wires (solid line) and for an equivalent 2-D device (dashed line). To explain the structure, we have developed a semi-classical model to calculate the conductivity of these devices. As seen in the dotted line in figure 8, our calculations match the measured data quite well.

Based on our calculations, we conclude that the observed mobility modulation is associated with populating the quasi-one-dimensional subbands. The negative differential transconductance regions arise when higher subbands begin to be populated. Currently, we are working on fabricating new versions of these devices that allow for control of the confining potential, and hence the position of the subbands, by use of a top gate. It is hoped that these devices will verify the validity of our model.

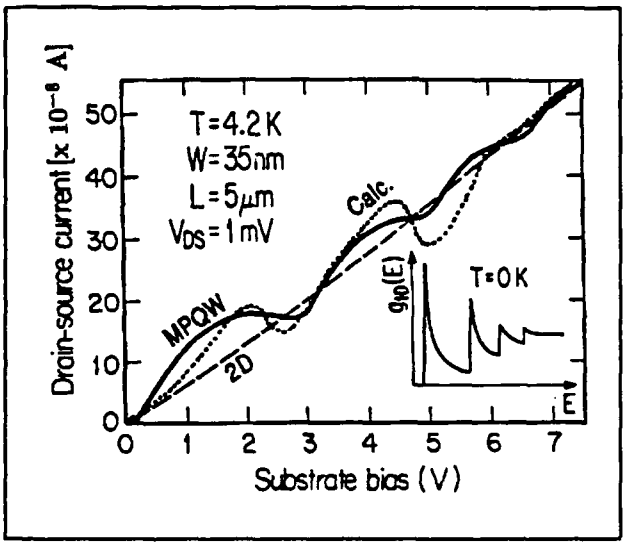

Figure 8. Drain-source current (I_{DS}) as a function of substrate bais (V_{SUB}) for the multiple parallel quantum wires (solid line) and scaled down 2D channel (dashed line). The inset shows the theoretical density of states in a Q1D wire at O K. The dotted line is an analytical calculation.

1.9 Arrays of Field-Effect-Induced Quantum Dots

Sponsors

Joint Services Electronics Program
Contract DAAL03-89-C-0001
U.S. Air Force - Office of Scientific Research
Grant AFOSR-88-0304

Project Staff

Professor Dimitri A. Antoniadis, Martin Burkhardt, William Chu, Professor Jesus A. del Alamo, Reza A. Ghanbari, Khalid Ismail, Professor Marc A. Kastner, C.T. Liu, Professor Terry P. Orlando, Professor Henry I. Smith, T.P. Smith, Professor Dan Tsui

A metal grid on a modulation-doped AlGaAs/GaAs substrate (depicted in figure

9a) produces a two-dimensional periodic potential modulation at the AlGaAs/GaAs interface via the Schottky effect. If a gate electrode is attached to the grid, the potential can be further modified with an external voltage source. By changing the gate voltage from positive to negative values, the potential seen by the electrons located at the AlGaAs/GaAs interface can be varied from uniform (in which case the electrons behave as a 2-D electron gas) to weakly coupled zero-D quantum wells (figure 9b) to isolated zero-D quantum dots (figure 9c). We have made such structures, with spatial periods of 200 nm in both orthogonal directions using technology similar to that described in Section 1.7, but now the grid gate occupies an area of several square millimeters. The isolated quantum dots and the attendant zero-dimensional electronic subbands were examined in collaboration with D. Tsui at Princeton University using far-infrared (FIR) cyclotron resonance. Transitions between the discrete energy levels in the quantum dots were observed as a function of magnetic field. Results were in agreement with a theoretical model.

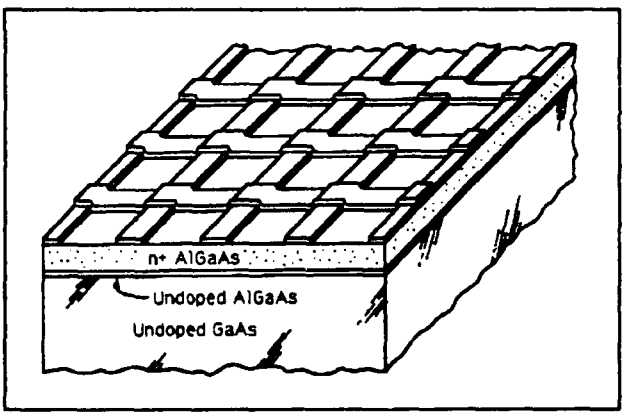

Figure 9a. Metal grid gate on a modulation-doped AlGaAs/GaAs substrate.

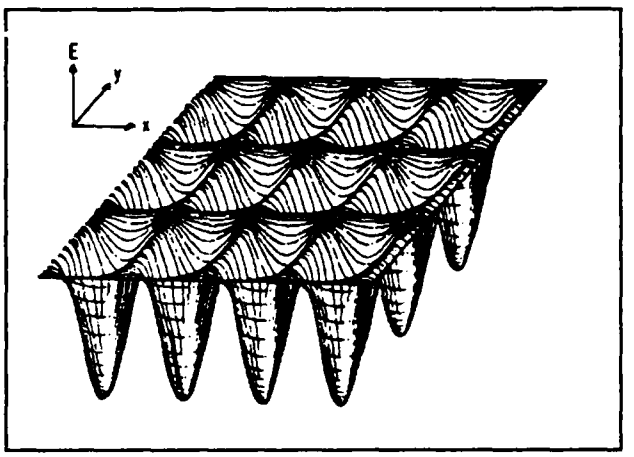

Figure 9b. Depiction of potential seen by electrons at the AlGaAs/GaAs interface for weakly coupled quantum dots.

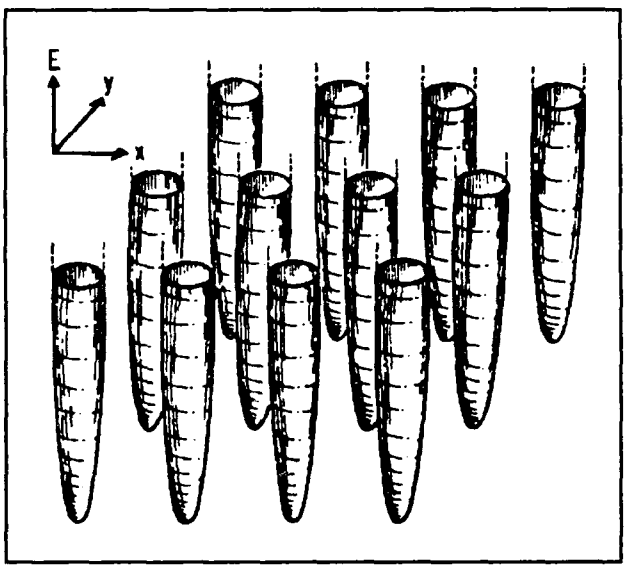

Figure 9c. Potential for the case of isolated quantum dots.

In collaboration with T.P. Smith and K. Ismail at IBM we applied a magnetic field perpendicular to the plane of the grid gate and measured magnetocapacitance as the gate voltage was swept, changing the electronic system from two-dimensional to coupled quantum wells, to insolated quantum dots. The normal oscillations due to Landau level filling are strongly suppressed when the Fermi level lines up with the minibandgaps. Thus, these measurements give important confirmation of the minband structure we observed earlier in transport. In the weakly-coupled-quantum-dot regime the magnetocapacitance oscillations show evidence of fractal behavior when the number of flux

quanta per unit cell of our grid is a rational number (i.e., 1/2, 1/3, 3/5, etc.).

We are currently fabricating a new set of grid-gate MODFETS, using an improved fabrication process and will study their transport, capacitance, and absorption properties as a function of magnetic field.

1.10 Planar-Resonant-Tunneling Field-Effect Transistors (PRESTFETs)

Sponsor

U.S. Air Force - Office of Scientific Research
Grant AFOSR-85-0154

Project Staff

Professor Dimitri A. Antoniadis, William Chu, Khalid Ismail, and Professor Henry I. Smith

Encouraged by the observation of negative differential resistance in the surface-superlattice MODFET (Section 1.7), we have proceeded to fabricate and test a double-barrier MODFET shown schematically in figure 10. Under the gate electrodes, the energy level diagram is as sketched in figure 11. With proper biasing, resonant tunneling should be observable, hence the name of the device PRESTFET (Planar-Resonant Tunneling Field-Effect Transistor).

Three types of measurements were performed (at 4.2 K) on a PRESTFET device in which the gate electrodes were 60 nm long and separated by 60 nm: (1) gate electrodes are connected together, the drain-to-source voltage is held fixed (< 5 mV), and the gate voltage is swept; (2) the electrodes are connected together and the intensity of an illuminating LED is scanned; (3) one gate bias is fixed while the other is swept.

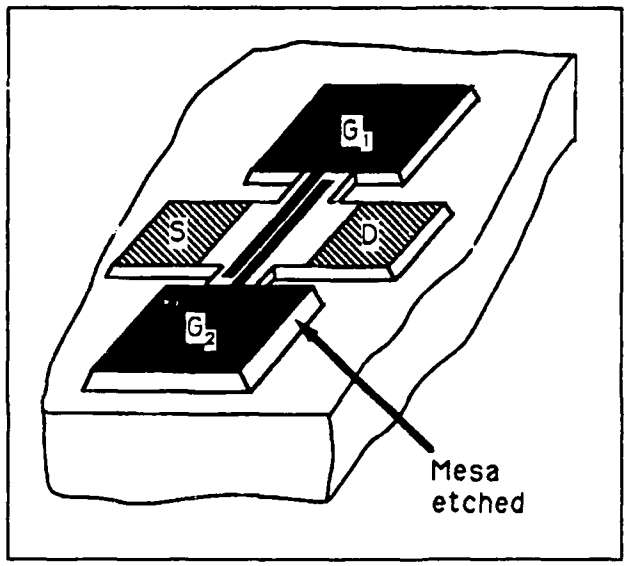

Figure 10. Sketch of the layout of a 4-terminal, double-barrier, planar-resonant-tunneling field-effect transistor (PRESTFET).

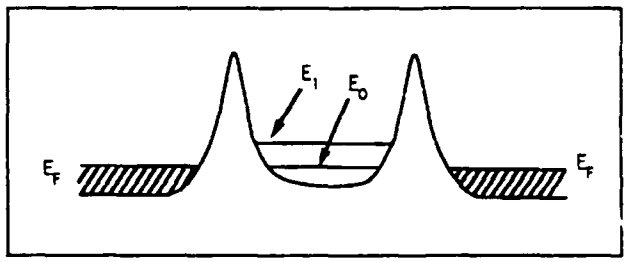

Figure 11. Energy level diagram of a symmetric, double-barrier PRESTFET.

In all three cases, clear resonances were observed in the drain-to-source current. In figure 12, a plot of the results of the third experiment is shown. The results of these three measurements provide clear evidence that resonant tunneling occurs through the quantized well states.

We are currently fabricating PRESTFET devices with even finer electrodes and developing a high-throughput PRESTFET fabrication process using x-ray nanolithography.

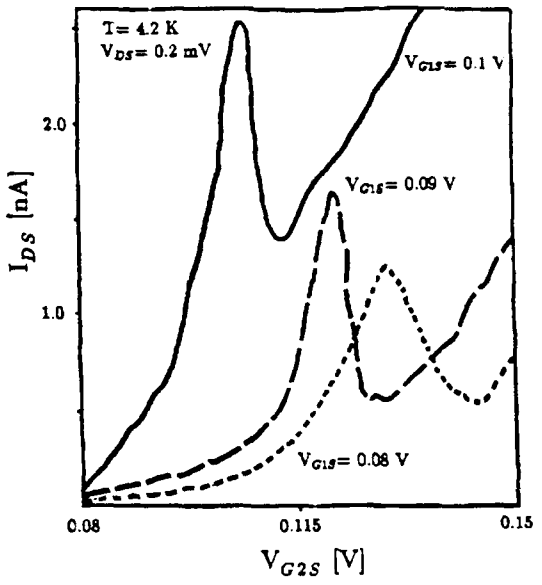

Figure 12. Drain-source current as a function of bias on gate 2 for three different bias conditions, below threshold, on gate 1.

1.11 Submicrometer-Period Gold Transmission Gratings for X-Ray Spectroscopy and Atom-Beam Interferometry

Sponsor

Joint Services Electronics Program
Contract DAAL03-89-C-0001
X-Opt., Incorporated

Project Staff

Dr. Mark L. Schattenburg, Professor Henry I. Smith

Gold transmission gratings with periods of 0.2 to 1.0 μm, and thicknesses ranging from 0.1 to 1 μm are fabricated using x-ray lithography and electroplating. The x-ray masks are made with holographic lithography. Transmission gratings are either supported on thin (1 μm) membranes or are made self-supporting by the addition of crossing struts. They are supplied to external laboratories for spectroscopy of the x-ray emission from a variety of sources. Over 15 laboratories around the world are using MIT-supplied gratings, and this project constitutes the sole source for these diffractors. Self-supporting transmission gratings in both gold and thin-film chromium are being provided to Professor David Pritchard's group for use in experiments to study the diffraction of neutral sodium atoms by gratings. The sodium atoms have a de Broglie wavelength of $\sim$ 17 pm. Clear demonstrations of atomic diffraction have been made with these gratings. The gratings can also be used to divide and recombine an atomic beam coherently, and may provide the easiest route to the realization of an atom wave interferometer.

1.12 High-Dispersion, High-Efficiency Transmission Gratings for Astrophysical X-Ray Spectroscopy

Sponsor

National Aeronautics and Space Administration
Contract NAS8-36748

Project Staff

Professor Claude R. Canizares, Dr. Mark L. Schattenburg, Professor Henry I. Smith

Gold gratings with spatial periods of 0.1 to 1.0 μm make excellent dispersers for high resolution x-ray spectroscopy of astrophysical sources in the 100 eV to 10 keV band. These gratings are planned for use in the Advanced X-Ray Astrophysics Facility (AXAF) that will be launched in the mid-1990s. In the region above 3 keV, the requirements of high dispersion and high efficiency dictate the use of the finest period gratings with aspect ratios approaching 10 to 1. To achieve this, we first expose a grating pattern in 1.0 μm-thick PMMA over a gold plating base using x-ray nanolithography. Gold is then electroplated into the spaces of the PMMA to a thickness up to 1 μm. Flight prototype gratings have been fabricated and undergone space-worthiness tests. In the initial stage of this program we used the carbon K x-ray ($\lambda = 4.5$ nm) which required that the mask and substrate be in contact to avoid diffraction. This, in turn, caused distortion of the grating. To avoid this problem we are developing a new technology of microgap x-ray nanolithography using the copper L x-ray (λ = 1.33 nm) and Si_3N_4 membrane masks.

Chapter 2. Microstructural Evolution in Thin Films of Electronic Materials

Academic and Research Staff

Professor Carl V. Thompson, Dr. Paul Evans, Professor Clifton G. Fonstad, Jr., Dr. En Ma, Dr. John Melngailis, Professor Henry I. Smith

Visiting Scientists and Research Affiliates

Chenson K. Chen,[1] Dr. Roberto R. DeAvillez,[2] David J. Edell,[3] Harold J. Frost,[4] David A. Smith,[5] King-N. Tu[5]

Graduate Students

Sergio A. Ajuria, Geoffrey Burns, Jaeshin Cho, Lawrence A. Clevenger, Andrew D. Dubner, Jerrold A. Floro, James S. Im, Eva Jiran, Harold Kahn, Yachin Liu, Hai Longworth, Joyce E. Palmer, Hui Meng Quek, Jaesang Ro

Undergraduate Student

Howard Zolla

Technical and Support Staff

Celia Slattery

2.1 Modeling of Microstructural Evolution in Thin Films

Sponsors

Joint Services Electronics Program
Contract DAAL03-89-C-0001
National Science Foundation
U.S. Air Force - Office of Scientific Research
Contract AFOSR 85-0154

Project Staff

Professor Carl V. Thompson, Harold J. Frost, Jerrold A. Floro, Yachin Liu

We are developing analytic models for normal, secondary and epitaxial grain growth in continuous thin films as well as particle coarsening in discontinuous films. The effects of surface or interface energy anistropy play especially important roles in these processes. We have developed computer models for film formation by crystal nucleation and growth to impingement under a variety of conditions. The topology and geometry of grain structures have been shown to strongly depend on the conditions of film formation. We have also developed computer simulations for two-dimensional normal grain growth and secondary grain growth.

We are developing analytic models and computer simulations in parallel with experimental studies in model systems. Computer

---

[1] MIT Lincoln Laboratory.

[2] Pontificia Universidade Catolica, Department of Materials Science and Metallurgy, Rio de Janiero, Brazil.

[3] Harvard-MIT Health Sciences Program.

[4] Thayer School of Engineering, Dartmouth College, Hanover, New Hampshire.

[5] IBM, Thomas J. Watson Research Center.

simulations have allowed us to explain microstructrual features which are generally characteristic of thin films, including: (1) stagnation of normal grain growth, (2) development of lognormal distributions of grain sizes and (3) abnormal grain growth which leads texture development or epitaxy. Grain growth models also provide a theoretical context for research on microstructure engineering using impurities, ion bombardment, substrate-surface-topography and precipitates.

Publications

Thompson, C.V. "Coarsening of Particles on a Planar Substrate: Interface Energy Anistropy and Application to Grain Growth in Thin Films." *Acta Metall.* 36:2929 (1988).

Thompson, C.V. "Observations of Grain Growth in Thin Films." In *Microstructural Science for Thin Film Metallizations in Electronic Applications,* 115. Eds. J. Sanchez, D.A. Smith, and N. Delanerolle. Warrendale, Pennsylvania: the Minerals, Metals, and Materials Society, 1988.

2.2 Reliability and Microstructures of Interconnects

Sponsors

Joint Services Electronics Program
Contract DAAL03-89-C-0001
Semiconductor Research Corporation

Project Staff

Jaeshin Cho, Harold Kahn, Hai Longworth, Professor Carl V. Thompson

We are investigating the use of precipitates to produce metallic films and interconnects with engineered microstructures. We deposit initially layered alloy films (e.g., films deposited in a sandwich structure with a pure W layer between pure Al layers). When heated, precipitates form in the center of these films. These precipitates lead to a drag force which impedes grain boundary motion and supresses normal grain growth. Eventually, at elevated temperatures, a minor fraction of the grains begin to break free of the precipitates and grow abnormally. This can ultimately lead to very large grains and also changes in the crystallographic texture of films. With this technique, it is possible to control the grain sizes, the distribution of grain sizes, and the distribution of grain orientations over very broad ranges. We have now observed these effects in a number of aluminum alloy systems including Al-Cu-Cr, Al-Ag-Cr, Al-Mn-Cr, Al-Mn, and Al-W.

We are also developing new techniques which allow statistical characterization of failure of contacts and interconnects for silicon-based integrated cricuit technology. We are using these techniques to correlate failure rates and mechanisms with microstructures of interconnect lines and contact diffusion barriers. We are investigating techniques for controlling microstructures in order to improve contact and interconnect reliability, especially under conditions which can lead to electromigration.

We have recently shown that interconnect lines with bimodally distributed grain sizes have drastically reduced reliabilities. Also, for lines with monomodally distributed (uniform) grain sizes, increasing the grain size (relative to line width) results in an increase of both the median time to electromigration-induced failure and the lognormal standard deviation in the time to failure, see figures 1-3. The net result, in large populations of lines with monomodal grain size distributions, is little or no change in the time to the first failure. We have explained these results in terms of a "failure unit model" in which grain boundaries are taken to be the individual units which are responsible for the reliability of a line. The successful application of this model indicates the importance of the properties of individual grain boundaries in controlling interconnect reliability. We are now investigating the statistical reliability of lines with single, controlled grain boundaries in order to understand in detail the type of microstructural features which limit interconnect reliability.

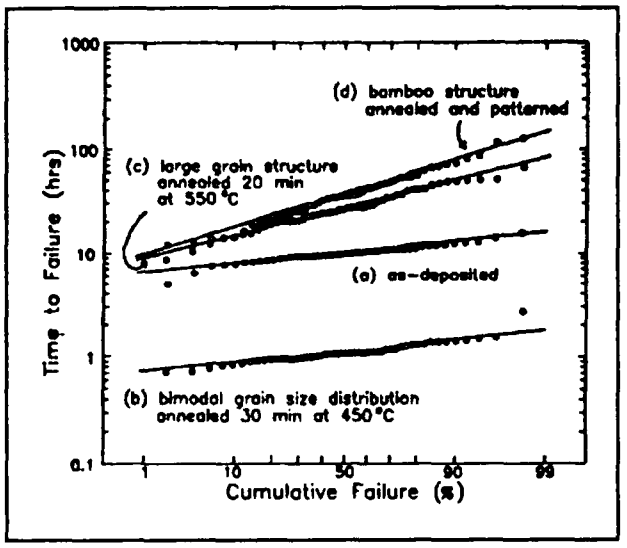

Figure 1. Distribution of failure times for 2.2-μm-wide, Al-2%Cu-0.3%Cr lines: (a) as-deposited (MTTF = 9.8 h, DTTF = 0.197), (b) after annealing for 30 min. at 450°C to develop a bimodal grain size distribution (MTTF = 1.08 h, DTTF = 0.223), (c) after annealing for 20 min. at 550°C to obtain mono-modally distributed large grains (MTTF = 26.3 h, DTTF = 0.465), and (d) after annealing for 20 min at 550°C before patterning, to obtain bamboo microstructures (MTTF = 35.0 h, DTTF = 0.580).

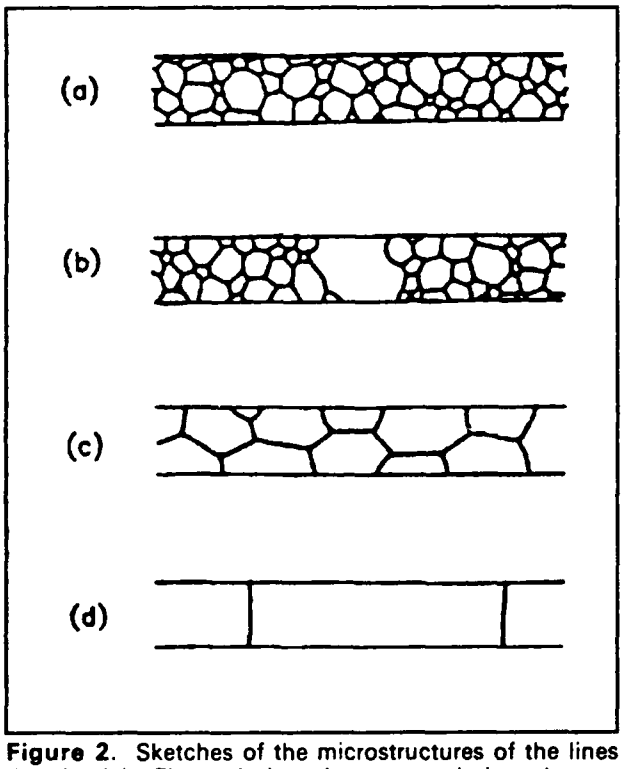

Figure 2. Sketches of the microstructures of the lines described in Figure 1, based on transmission electron microscopy.

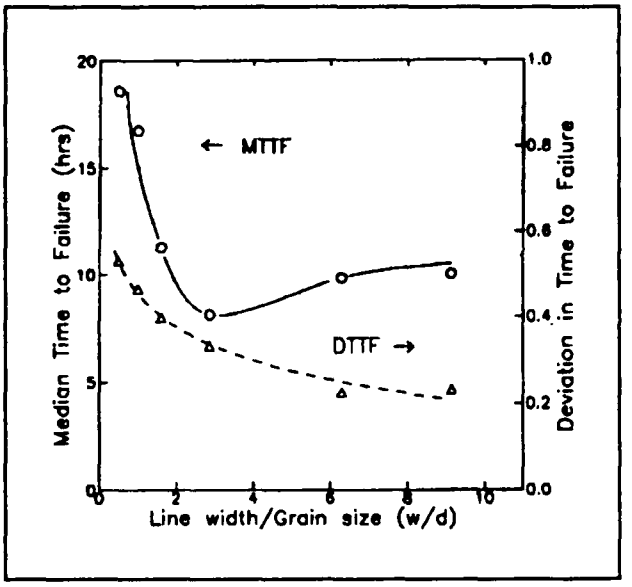

Figure 3. Median time to failure and deviation in the time to failure vs. linewidth/grain size ratio for Al-2%Cu-0.3%Cr lines with monomodally distributed grain sizes.

Publication

Cho, J., and C.V. Thompson. "The Grain Size Dependence of Electromigration Induced Failures in Narrow Interconnects." *Appl. Phys. Lett.* 54:2577 (1989).

2.3 Epitaxial Grain Growth

Sponsors

AT&T

U.S. Air Force - Office of Scientific Research
Contract AFOSR 85-0154

Project Staff

Jerrold A. Floro, Professor Carl V. Thompson, Professor Henry I. Smith

In the past year, we demonstrated that grain growth in polycrystalline films on single crystal substrates can lead to epitaxial films. This new approach to obtaining heteroepitaxial films can lead to ultrathin films with reduced defect densities compared to films deposited using conventional techniques. In epitaxial grain growth, ultrathin polycrystalline films are deposited on single crystal substrates. When these polycrystalline films are heated to elevated temperatures, epitaxial grains with low

Chapter 4. Chemical Reaction Dynamics at Surfaces

Academic and Research Staff

Professor Sylvia T. Ceyer, Dr. Kenneth B. Laughlin, Dr. Kevin J. Maynard

Graduate Students

John D. Beckerle, David J. Gladstone, Andrew D. Johnson, Marianne McGonigal, Michelle Schulberg, Qingyun Yang

Undergraduate Student

Gerald Cain

4.1 Chemical Reaction Dynamics on Semiconductor Surfaces

Sponsor

Joint Services Electronics Program
Contract DAAL03-89-C-0001

Project Staff

Professor Sylvia T. Ceyer, Dr. Kenneth B. Laughlin, David J. Gladstone, Marianne McGonigal, Michelle Schulberg, Gerald Cain

The etching of semiconductor materials in halocarbon plasma environments is a complex chemical process. The plasma is used to produce species that are highly reactive with the semiconductor surface. Because many different reactive species, including radicals, ions, and highly excited neutral molecules are produced in a plasma, the mechanism of the etching reaction is difficult to probe. Our program is aimed at using molecular beam reactive scattering techniques to systematically examine the role of each of these species in the etching process.

The initial goal of this project was to measure the barrier to F_2 dissociative chemisorption on Si(100). Contrary to popular belief, we found essentially no barrier to the dissociation of F_2 on the unfluorinated surface. The dissociative chemisorption of F_2 on Si(100) proceeds with unit probability for translational energies of the incident F_2 molecules as low as 0.5 kcal/mol. However, there is a substantial barrier to dissociation above fluorine coverages of 0.5 monolayer. Higher fluorine coverages sufficient to produce the etch product SiF_4 require a higher translational energy of the F_2 molecule. We have observed efficient etching of Si(100) at 300 K for an incident kinetic energy of F_2 of 15 kcal/mol. The angular and translational energy distributions of the SiF_4 — as measured in our newly constructed scattering apparatus consisting of two beams incident on a surface and a rotatable, triply differentially pumped quadrupole mass spectrometer — indicate that the last step of the reaction is the thermal desorption of the product SiF_4 molecule.

We have established that silicon can be etched without the use of molecules incident with energies of hundreds of electron volts, such as those present in plasma etching environments. Molecular beam techniques utilize molecules with energies only slightly higher than thermal (<1 eV), and therefore do not introduce radiation damage or defects into the Si lattice, which is a typical result of plasma etching. We are continuing our work on this system to understand the lack of F_2 energy dependence on the formation of a second reaction product, SiF_2.

We have also recently observed a new kind of mechanism for dissociative chemisorption. In the limit of zero fluorine coverage, we observed that the Si surface strips one of the fluorine atoms from the incident F_2 molecule, leaving the other fluorine atom to scatter into the gas phase. Although this stripping reaction is analogous to the well-known stripping reactions in gas phase chemical reaction dynamics, this is the first observation of its kind from a surface.

Chapter 5. Measurement of Electron-phonon Interactions Through Large-amplitude Phonon Excitation

Academic and Research Staff

Professor Keith A. Nelson

Visiting Scientists and Research Affiliates

Dan E. Leaird,[1] Dr. Andrew M. Weiner[1]

Graduate Student

Gary P. Wiederrecht

5.1 Introduction

Sponsor

Joint Services Electronics Program
Contract DAALO3-89-C-0001

The main goal of this project is to measure the strengths of electron-phonon interactions in semiconductors to understand the effect of these interactions on electron mobility at different temperatures. A secondary goal -- extremely important for ultrafast electronics -- is to determine the responses of electronic materials to input signals which are both fast (i.e., pulses of short duration) and high in repetition rate (i.e., many short pulses in rapid succession).

5.2 High Repetition-rate Signals and Resonant Responses of Crystalline Solids

We have successfully characterized the electronic and vibrational responses of a wide variety of solids to single femtosecond pulses. With earlier JSEP support, we demonstrated that ultrashort optical pulses passing through nearly any material initiate coherent vibrational oscillations that influence the material's transient optical and electrical responses. This finding is important for fast electronics because it indicates the response of materials to fast electrical and optical signals. The material's response to sufficiently short signal duration (i.e., optical or electrical pulse duration) can include transient vibrational oscillations, negatively affecting its usefulness in possible applications such as information processing.

At the same time, the initiation of coherent lattice vibrational oscillations with ultrashort pulses provides us with a unique spectroscopic tool. We can record femtosecond time-resolved "stop-action" spectroscopic observations of coherently vibrating crystal lattices, permitting characterization of well defined, nonequilibirium crystal structures at various stages of vibrational distortion. Characterization of the effects of lattice vibrations (phonons) on electonic energy levels is of particular importance in semiconductors since temperature-dependent carrier mobilities are influenced by electron-phonon interactions.

Figure 1 shows the typical effects of a single ultrashort pulse on a crystalline solid. A femtosecond pulse exerts an "impulse" force on lattice vibrational modes, initiating vibrational oscillations. These oscillations influence the material's optical and electrical properties. The Terahertz-frequency oscillations in the data (shown in figure 1) correspond to individual lattice vibrational oscillation cycles, observed in real-time.

---

[1] Bell Communications Research (Bellcore).

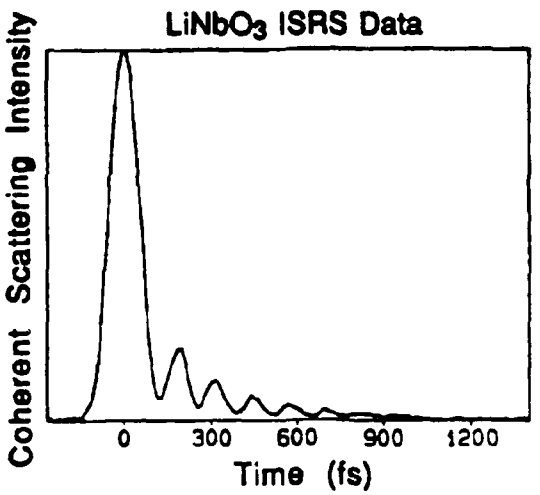

Figure 1. *Impulsive stimulated Raman scattering* (ISRS) data in which optic phonon oscillations and decay in lithium niobate are monitored. In this noncentrosymmetric crystal, the optic phonon mode is both Raman and IR active, and is strongly coupled to the polariton mode associated with infrared light propagation. The phonon oscillations induced through ISRS are therefore accompanied by IR radiation at the same frequency. Femotosecond pulses have therefore been used to excite phonons and also to produce tunable Terahertz-frequency (far-IR) radiation. The phonon frequency and damping rate depend on the ISRS scattering angle.

We are monitoring the material responses to high-density signals instead of a single signal for two main reasons. First, in any real-world high-speed signal-processing application, it is essential to process signals which are not only short in duration but also frequent, i.e., signals with high information density. It is important, therefore, to understand the differences between a material's response to one isolated pulse and its response to many pulses in rapid succession, the latter being far more relevant to applications.

Second, the data in figure 1 illustrate our ability to use short light pulse to control solid-state structure and behavior in a very precise way. We can use pulses to literally move ions or molecules in crystals toward or away from each other. In addition, we can monitor the motions and their effects in real time. Unfortunately, the extent of our optical control is limited because, with a single pulse, we can only move material very small distances — less than 10^{-3} Å. These small distances have dramatic effects in signal processing, as figure 1 illustrates. However, if we could drive lattice vibrations much harder — for example, to amplitudes exceeding 0.1 Å — we could induce permanent structural changes in solids, fabricate new materials, etc. We could also characterize electron-phonon interactions over a wide range of phonon displacements.

To measure material responses to high repetition-rate sequences of femtosecond pulses, we first needed to generate the pulse sequences. We could have approached this problem by splitting a single femtosecond pulse many times with partial reflectors and aiming all the resulting beams into a sample with desired timing. This extremely cumbersome approach would have involved dozens of partial and high reflectors, lenses, and precision delay lines. Instead, we chose to collaborate with scientists at Bellcore who have

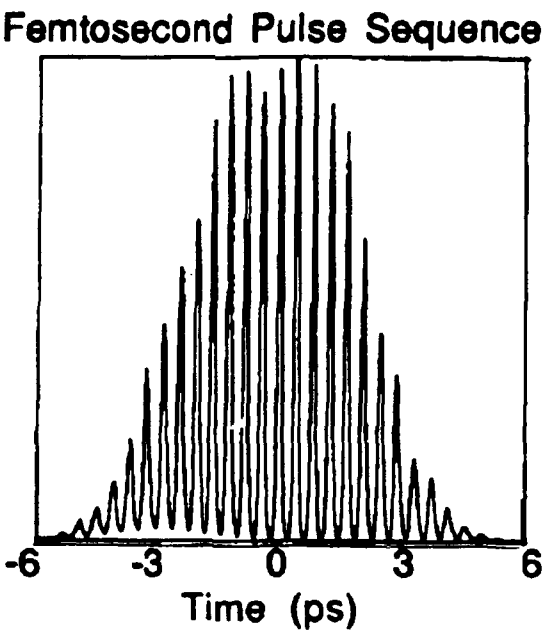

Figure 2. Cross-correlation trace of a sequence of femtosecond pulses at Terahertz repetition rates produced through pulse-shaping techniques. A single femtosecond pulse was passed through two gratings, two lenses, and a spatially varying mask to produce the output shown. The output can be used to exert repetitive "impulsive" driving forces on selected vibrational modes to achieve larger amplitudes than can be driven with a single pulse.

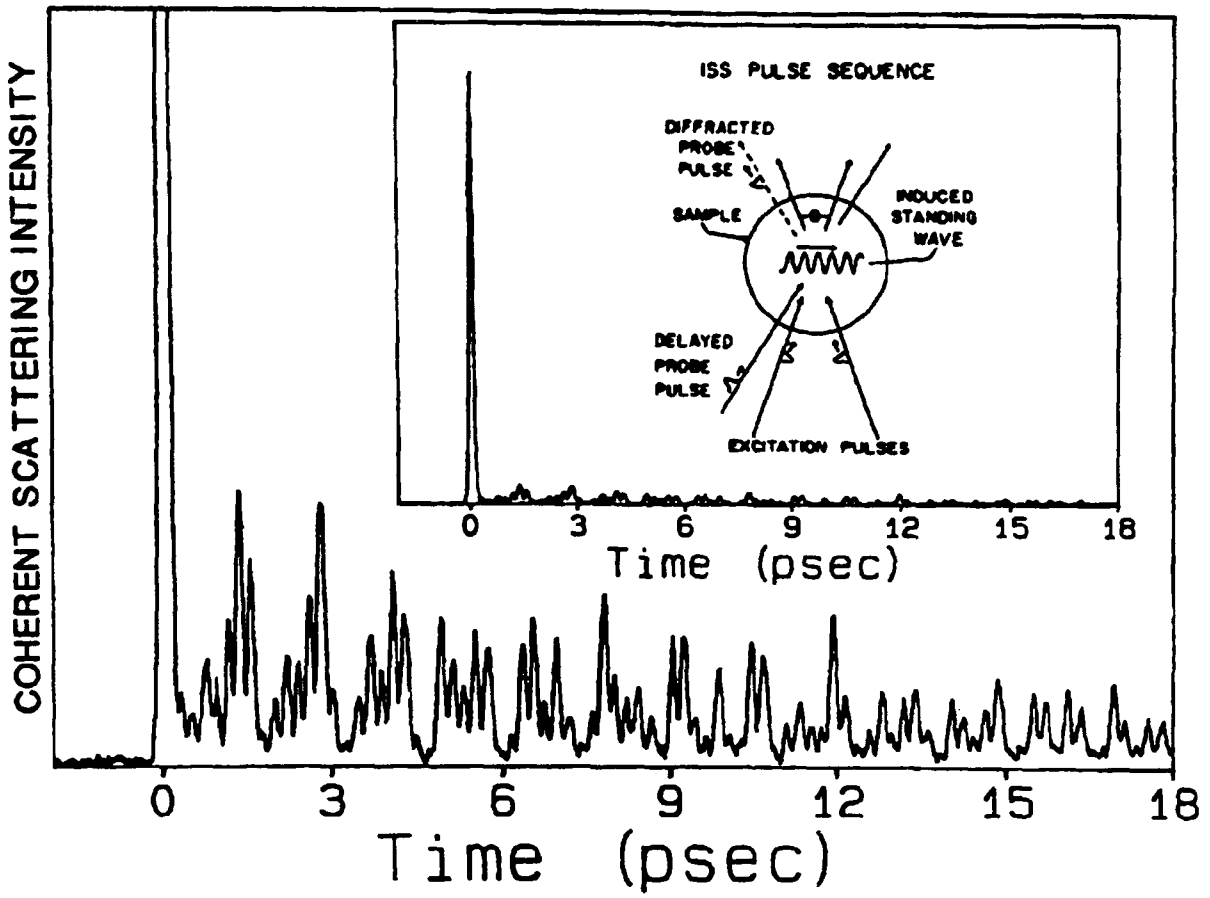

Figure 3. ISRS data from the α-perylene organic molecular crystal. Several phonon modes are excited by the femtosecond excitation pulses. This gives rise to the characteristic "beating" pattern which contains sum and difference frequencies. The "spike" at t = 0 is due to the essentially instantaneous electronic response of the crystal to the excitation pulses. The inset shows that the vibrational signal intensity is only about 4% that of the spike. In some signal processing applications (especially those involving threshhold devices), the comparatively slow response due to vibrations could be disregarded.

recently developed femtosecond optical "pulse-shaping" techniques through which a single femtosecond pulse can be converted into a sequence with the desired timing. In this technique, a single pulse, passed through a simple optical network consisting of only two lenses, two gratings, and a spatially varying mask, yields a pulse sequence similar to the one shown in figure 2. Sequences with different temporal profiles are selected by changing the mask.

Figures 3 and 4, respectively, show crystalline responses to single- and multiple-pulse excitation. For the initial demonstration, we used an organic molecular crystal since its vibrational and electronic properties were well understood. Figure 3 shows the response to a single femtosecond pulse. The "impulse" force exerted by the pulse drives several lattice vibrational modes whose simultaneous oscillations yield the "beating" pattern in the data. The "spike" in the data at t = 0 is caused by the instantanous electronic response of the crystals to the excitation pulses. The signal due to lattice vibrations is only about 4 percent as strong as that due to the electronic response. In some signal processing applications, this "slow" signal could be disregarded, using instead the ultrafast electronic response as the basis for a rapid switch.

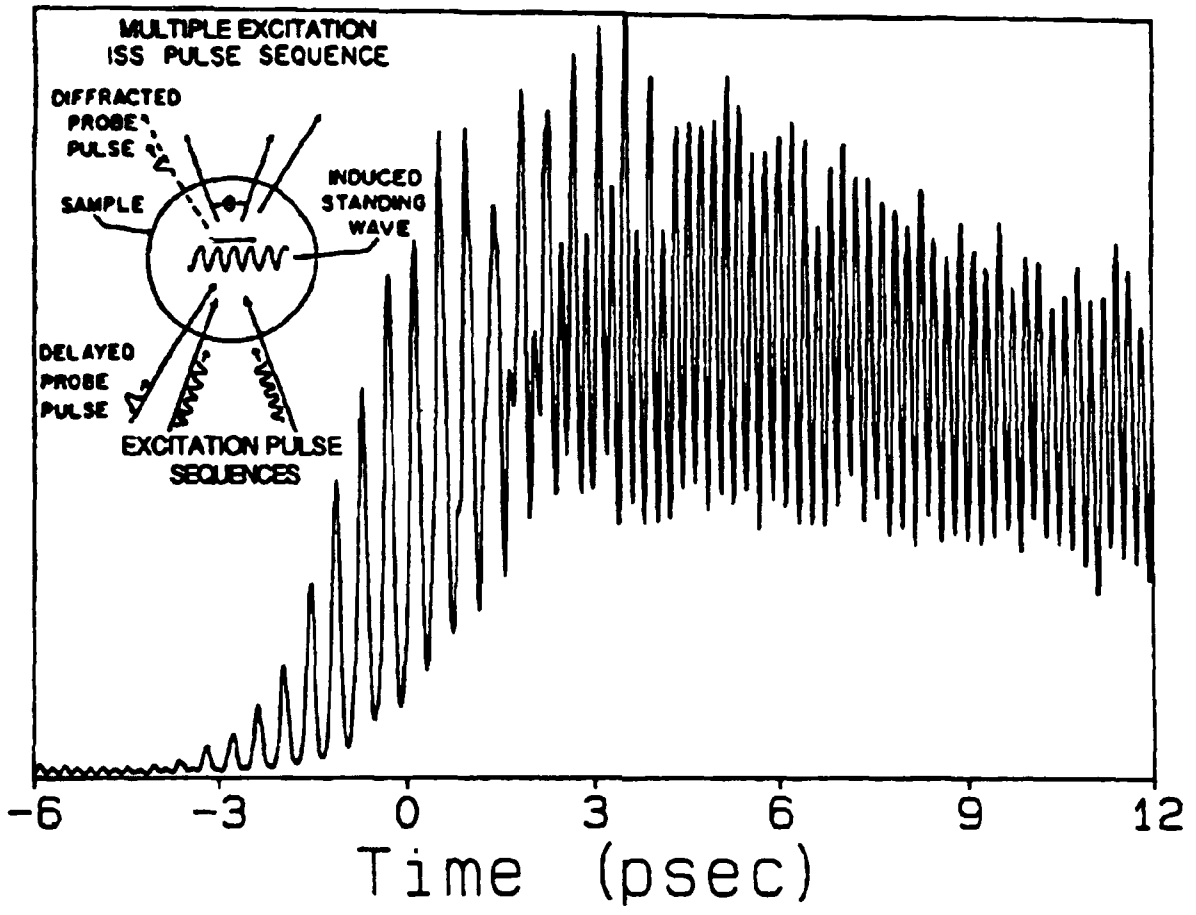

Figure 4. ISRS data from the perylene crystal driven by the pulse sequence shown in figure 2, which is tuned to drive the 80 cm^{-1} lattice vibrational mode. At first the signal is dominated by the instantaneous electronic response of the sample to each of the pulses in the sequence. After about 10 pulses, signal due to repetitively driven lattice vibrations is apparent. Signal from the vibrational mode grows stronger with each successive pulse, eventually reaching intensity levels comparable to the strongest electronic response. Selective amplification of the 80 cm^{-1} mode has been demonstrated. The strong response due to the amplified vibrational mode could not be ignored in any signal processing application.

Figure 4 shows the crystal's response to the sequence of pulses shown in figure 2. We have crafted this sequence so that the time between pulses (419 fs) is precisely equal to the oscillation period of one of the lattice vibrational modes. The impulse forces exerted by the pulses resonantly drive this mode in a manner analogous to repetitively pushing a child on a swing so that larger oscillation amplitudes are reached in time. The data show that for the first several pulses, the intense "spike" due to the electronic response dominates the signal. After about 10 pulses, however, the amplified vibrational response is apparent. By the end of the pulse sequence ($t > 3ps$), the signal due to vibrations is as intense as the strongest electronic "spike." This illustrates one important difference between the response of the material to high-density input signals versus the response to a single pulse. *We could not ignore the long-lived vibrational response in any real-life signal-processing application.*

The results also illustrate the increased optical control over the sample afforded by judicious multiple-pulse excitation. In this case, through repetitive excitation, we increased the vibrational amplitude by almost a factor of 10. Amplification is also highly mode-selective, since the pulse sequence is timed to drive only one of the lattice

vibrations. This is clear from the single-frequency oscillations in the data, as compared to the beating pattern in figure 3 that results from excitation of several vibrational modes.

At present, we are beginning experiments in which these techniques are applied to semiconductors. We expect to drive large-amplitude vibrational responses and to observe their effects on electronic energy levels. This will permit characterization of the electron-phonon interactions. Another very interesting application will be to multiple quantum well structures. Repetitive excitation should lead to large-amplitude responses of acoustic-like phonons which traverse a single well in the time between pulses of the sequence.

It is worth noting that our primary outside collaborator in this project, Dr. Andrew M. Weiner, performed research for his Ph.D. under the supervision of Professor Erich P. Ippen. Under earlier JSEP support, we collaborated with Dr. Weiner and Professor Ippen to conduct some of the first femtosecond time-resolved spectroscopy experiments on molecular crystals.

Our work in this area is widely recognized within the ultrafast optics and electronics community. *Optics News* described our research in a summary of 1989 highlights, and an article in *Science* is forthcoming. At present, we are preparing more detailed reports.

Publications

Nelson, K.A. "Impulsive Stimulated Raman Scattering with Single-pulse and Multiple-pulse Excitation." *Proceedings of the 12th International Conference on Raman Spectroscopy.* Forthcoming.

Nelson K.A., and E.P. Ippen. "Femtosecond coherent spectroscopy." *Adv. Chem. Phys.* 75: 1-35 (1989).

Weiner, A.M., D.E. Leaird, G.P. Wiederrecht, and K.A. Nelson. "Femtosecond Multiple Pulse Impulsive Stimulated Raman Scattering." *Optics News* 15(12): 29-31 (1989).

Weiner, A.M., D.E. Leaird, G.P. Wiederrecht, and K.A. Nelson. "Femtosecond Pulse Sequences Used for Optical Manipulation of Molecular Motion." *Science.* Forthcoming.

Weiner, A.M., D.E. Leaird, G.P. Wiederrecht, M.J. Banet, and K.A. Nelson. "Spectroscopy with Shaped Femtosecond Pulses: Styles for the 1990s." *Proceedings of the SPIE Conference on Optoelectronics and Lasers.* Forthcoming.

Chapter 6. Chemical Beam Epitaxy of Compound Semiconductors

Academic and Research Staff

Professor Leslie A. Kolodziejski, Stephen C. Shepard

Visiting Scientists and Research Affiliates

Dr. Hidehito Nanto[1]

Graduate Student

Dana H. Lee

Technical and Support Staff

Angela R. Odoardi

6.1 Chemical Beam Epitaxy Facility

Sponsors

3M Company Faculty Development Grant
AT&T Research Foundation
Special Purpose Grant
Joint Services Electronics Program
Contract DAAL03-89-C-0001
National Science Foundation
Grants ECS 88-46919 and ECS 89-05909
Purdue University
Subcontract No. 530-0716-07
U.S. Navy - Office of Naval Research
Contract N00014-88-K-0564

We made substantial progress in 1989 toward establishing a chemical beam epitaxy (CBE) facility for the epitaxial growth of compound semiconductors. The major part of our effort was in the development and assembly of the CBE hardware including the growth, transfer, introduction, and bake chambers. By the end of 1989, the CBE system was approximately 85 percent complete. We expect delivery from the manufacturer by the middle of February 1990.

Figure 1 is a photograph of the CBE system showing its growth reactor module and some associated electronics. Within the black metal frame outlining the exhausted enclosure are the gas manifold (upper left side), ultrahigh vacuum growth chamber (right side), and the pumping subsystem (bottom left). Figure 2 shows the transfer, introduction, and bake chamber modules. The black metal frame outlines a fully exhausted, filtered laminar flow enclosure.

The CBE growth reactor is equipped with four individual gas injectors for metalorganics of Zn, Ga and In, Se, and for the hydride arsine. The temperature of each gas injector can be varied between 0 to 1250 degrees Celsius so that the molecules can be "cracked" or thermally decomposed prior to impingement on the heated single crystalline substrate. Three typical effusion cells, such as those used in molecular beam epitaxy, can be used with dopant or alloying elements. In situ analysis facilities include reflection high energy electron diffraction, a residual gas analyzer, and a quartz crystal flux monitor. Four symmetrically placed heated sapphire viewports can be used to direct a laser beam at incident angles to the growing surface front and to collect the reflected laser beam.

The design of the original CBE system was expanded to include an additional ultrahigh vacuum analytical/metalization chamber, which will added in mid-1990. Attached to the transfer chamber, this new chamber will

[1] Professor, Department of Electronics, Kanazawa Institute of Technology, Kanazawa, Japan.

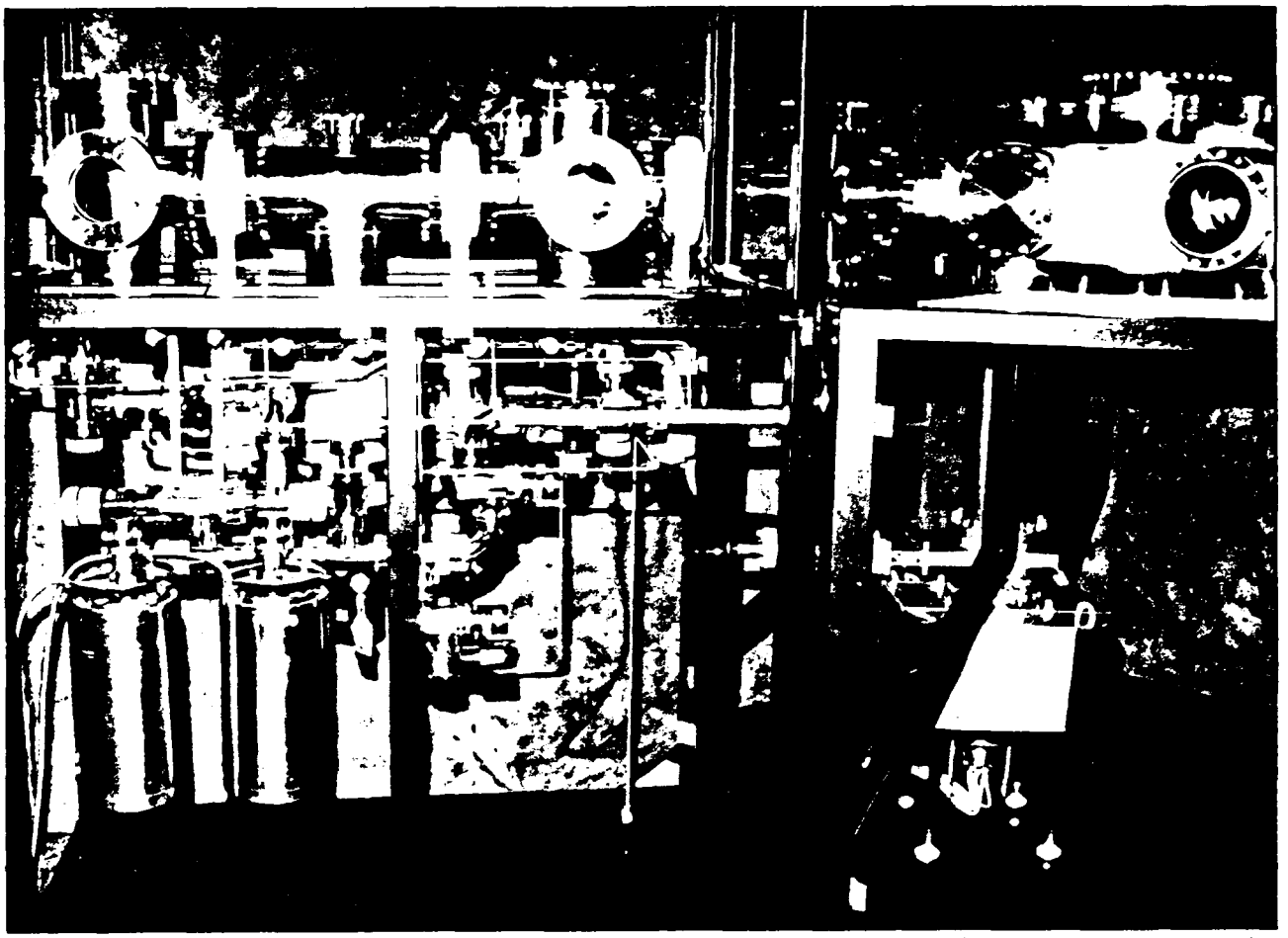

Figure 1. Growth reactor module and partially complete electronics rack of the chemical beam epitaxy system (as of November 1989).

allow samples to remain in the UHV environment before and after analysis or metalization. The additional chamber is subdivided to include both in situ analysis and metalization capabilities. Initially, the chamber will contain Auger electron spectroscopy (AES) and will be configured to have the associated ports, sample heater and manipulator, shutters, etc., necessary to add the electron beam evaporators to perform metalizations. Additional viewports will be provided to illuminate samples during Auger electron spectroscopic analysis and metalization with a coherent source of light. The source of photons will be provided by various lasers or lamps having a multitude of powers and wavelengths.

We envision that the laser-aided investigations carried out in the analytical/-metalization chamber will complement laser-assisted experiments planned during the epitaxial growth of semiconductor layers. We anticipate that both types of experiments will provide clues to understanding the effect of photons on the physisorption, chemisorption and incorporation processes which occur during the chemical beam epitaxial growth process.

Funds for obtaining the analytical/-metalization chamber were provided by the National Science Foundation, Defense Advanced Research Projects Agency, and by a donation from Emcore Corporation.

The space which will house the new CBE system was completely remodeled. Renovation included: (1) major demolition of walls to create one large (1200 square foot) lab from three smaller labs; (2) an increase in the services available such as power, water, nitrogen, etc.; and (3) installation of a very sophisticated exhaust system, a design

Figure 2. Front view of the bake chamber (left), introduction chamber (center), and transfer chamber (right).

requirement for the custom CBE system. (Both the growth reactor module and the introduction chamber module are fully enclosed and exhausted.) The laboratory also includes a small entry room, typical for a clean room environment, and a substrate preparation area. The substrates can be chemically cleaned in dedicated solvent hoods followed by etching in dedicated acid hoods in adjacent laboratory space. The laboratory will also house a surface profilometer for studying film thickness and a Normarski interference microscope for studying surface morphology.

6.2 Controlled Substitutional Doping of ZnSe Grown by Chemical Beam Epitaxy

Sponsors

Joint Services Electronics Program
Contract DAAL03-89-C-0001
U.S. Navy - Office of Naval Research
Contract N00014-88-K-0564

The potential of the II-VI compound semiconductor family for optical device applications has been relatively underutilized. There are substantial difficulties in preparing them by any growth technique to be amphoterically doped in a controlled manner. In the past, because bulk, liquid phase, or vapor phase growth techniques required very high temperatures for fabrication of ZnSe, control of the carrier type could not be achieved. The resultant ZnSe exhibited n-type transport properties or the as-grown

material was so heavily compensated that the material was highly resistive. Newer growth technologies such as molecular beam epitaxy (MBE) and chemical beam epitaxy (CBE) provide promise for circumventing the doping problems of the II-VIs and ZnSe as one example, due to the non-equilibrium nature of the growth, and by their ability to affect the growth, with photon illumination. Once ZnSe is controllably doped as p-type and n-type material, many device applications could take advantage of the wide, direct bandgap (2.67 eV at room temperature) which provides for the emission of blue light. Blue light emitting diodes, blue semiconductor injection lasers, and flat panel electroluminescent display devices are representative of the many possible optical devices. The blue wavelength range will be useful in (1) underwater communication, (2) visible holography, (3) laser disc recording, where a shorter wavelength would allow for a ten-fold increase in the density of stored information, and (4) for short range communications where new polymer fibers can be utilized.

Studies of dopant incorporation reported in the literature for ZnSe were complicated by the presence of unintentional impurities found in both elemental and compound source material which is used in the MBE growth process. In most cases, undoped ZnSe grown by MBE, using commercially available source material, has been reported to be n-type with low resistivity ($\sim 1\Omega$-cm). The low resistivity of the "undoped" ZnSe material implied that the ZnSe was of correct stoichiometry because a relatively small deviation from a Zn-to-Se flux ratio of one-to-one toward either Zn-rich or Se-rich conditions was found to result in high resistivity material. (The defects generated during growth under non-stoichiometric conditions appeared to compensate for the non-intentionally incorporated impurities giving rise to the high resistivity.)

Although major progress was recently made in the molecular beam epitaxy of ZnSe, controlled substitutional n- and p-type doping is still significantly limited. The technique of chemical beam epitaxy (CBE), however, combines the many advantages of molecular beam epitaxy and metalorganic chemical vapor deposition (MOCVD) growth techniques while eliminating their many disadvantages.

An ultrahigh vacuum environment, similar to that used in MBE, is utilized in CBE. Because in CBE the solid source material of MBE is replaced by gaseous source material, CBE is similar to MOCVD in that respect. The gas sources are controlled by precision mass flow controllers, permitting constant flux ratios at reasonable growth rates. By employing metalorganic gaseous sources for the Zn and Se species, we will obtain a greater degree of control of the flux intensities. The MBE technique of employing low temperature, high vapor pressure sources of Zn and Se cannot achieve this control. Because the elements originate from a gas bottle, long-term operation is possible since very little gaseous material is consumed. We will eliminate many hardware problems encountered during the growth of II-VI compounds by using CBE. We also anticipate that the use of the CBE technique will allow us to solve crystal growth problems. Scientists and device engineers will be able to capitalize on the many attractive material properties of the II-VI compound semiconductors.

With research support from the Office of Naval Research, we will explore the CBE of ZnSe. We will determine its optimum growth parameters following microstructural, optical, and electrical evaluation of the epitaxial layers. After we achieve high quality, ultrapure, undoped ZnSe, our objective under the program supported by the Joint Services Electronics Program will be to incorporate the impurity species in ZnSe.

6.3 Laser-Assisted Chemical Beam Epitaxy of Wide Bandgap Blue/Green II-VI Semiconductors

Sponsor

Purdue University
Subcontract No. 580-0716-07

In addition to the more typical growth experiments described above, chemical beam epitaxy (CBE) is naturally suited for experiments designed to modify or affect the

Chapter 7. High-Frequency InAlAs/InGaAs Metal-Insulator-Doped Semiconductor Field-Effect Transistors (MIDFETs) for Telecommunications

Academic and Research Staff

Professor Jesus A. del Alamo

Graduate Student

Sandeep Bahl

Undergraduate Student

Walid Azzam

Technical and Support Staff

Angela R. Odoardi

7.1 Introduction

Sponsors

Joint Services Electronics Program
Contract DAAL03-89-C-0001
Charles S. Draper Laboratory
Contract DL-H-404180

The goal of this project is to design, fabricate, test, and model submicron InAlAs/InGaAs Heterostructure Field-Effect Transistors (HFETs) on InP. These devices are of great interest for applications in long-wavelength optical communications and ultra-high frequency microwave telecommunications. We expect that extraordinary device performance will result from the unique combination of: (1) the large conduction bandgap discontinuity between InAlAs and InGaAs, (2) the large $\Gamma - L$ separation in InGaAs, and (3) the high velocity of electrons in InGaAs.

We have recently pioneered HFETs in which the InGaAs channel is heavily doped but the InAlAs insulator is undoped (MIDFETs for Metal-Insulator-Doped semiconductor FET).[1] We have found that these devices display a performance comparable to InAlAs/InGaAs Modulation-Doped FETs (MODFETs) of similar gate length. In addition, these devices offer a number of unique benefits not found in other device structures: reduced transconductance[1] and f_T collapse,[2] higher breakdown voltage,[1] and freedom to optimize gate insulator parameters.[3] A new *modulation-doped channel* MIDFET also displays unprecedented microwave characteristics.[4]

During 1989, we obtained the first working InAlAs/InGaAs MIDFETs on InP fabricated

---

1 J.A. del Alamo and T. Mizutani, "An $In_{0.52}Al_{0.48}As/n^+In_{0.53}Ga_{0.47}As$ MISFET with a Heavily-Doped Channel," *IEEE Electron Device Lett.* EDL-8 (11): 534-536 (1987).

2 J.A. del Alamo and T. Mizutani, "Bias Dependence of f_T and f_{max} in an $In_{0.52}Al_{0.48}As/n^+$-$In_{0.53}Ga_{0.47}As$ MISFET," *IEEE Electron Device Lett.* EDL-9 (12): 654-656 (1988).

3 J.A. del Alamo and T. Mizutani, "A Recessed-Gate $In_{0.52}Al_{0.48}As/n^+$-$In_{0.53}Ga_{0.47}As$ MIS-type FET," *IEEE Trans. Electron Devices* ED-36 (4): 646-650 (1989).

4 J.A. del Alamo and T. Mizutani, "An $In_{0.52}Al_{0.48}As/n^+$-$In_{0.53}Ga_{0.47}As$ MISFET with a Modulation-Doped Channel," *IEEE Electron Device Lett.* EDL-10 (8):394-396 (1989).

at MIT.[5] The performance and properties of these MIDFETs are similar to those fabricated elsewhere.[3] More relevant to the problem, we fabricated, for the first time, strained-insulator InAlAs/InGaAs MIDFETs. This report gives a detailed description of our research on these devices.

We have exploited the inherent flexibility of gate insulator design of a MIDFET by increasing the AlAs content in the InAlAs insulator from the lattice-matching composition to InP ($In_{0.52}Al_{0.48}As$), straining it towards larger bandgaps. This rapidly effects an enhancement in the conduction band discontinuity (ΔE_c) between the InAlAs and the InGaAs channel (figure 1). We expect, in this manner, to obtain the following benefits:

- reduced gate leakage
- improved gate breakdown voltage
- reduced real-space transfer of hot electrons from the channel to the gate.

We have demonstrated all of these benefits experimentally while largely unaffecting the rest of the device parameters (threshold voltage, transconductance, etc.).

7.2 Experiments

We grew four wafers by molecular-beam epitaxy in MIT's Riber 2300 system. Following standard procedures, we prepared the surface of the InP wafer. Figure 2 shows the cross section of the grown heterostructures. The layer structure is similar to those utilized previously,[1] except for:

1. The channel design is more aggressive: doping is higher, $4 \times 10^{18}\ cm^{-3}$, and thickness is lower, 100 Å. This channel is expected to result in superior performance.

2. The Al composition in three of the wafers is increased over lattice matching conditions, i.e., wafers were grown in which x in the $In_{(1-x)}Al_xAs$ layer is 0.48, 0.52, 0.60, and 0.70 (all insulator layers are 300 Å thick). This is the main purpose of the present experiment.

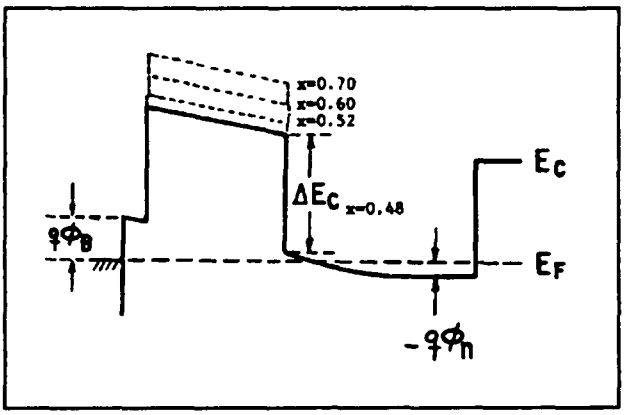

Figure 1. Cross-sectional equilibrium band diagram of device structure indicating the increase in ΔE_g with increase in Al composition.

We continued fabrication after growth with mesa isolation utilizing a selective chemical etchant, AuGeNi ohmic contact formation, TiAu interconnect, and TiAu gate layer formation. Figure 2 shows the resulting device cross section.

We have integrated a number of devices of varying dimensions and a large set of test structures into a $2.9 \times 2.7\ mm^2$ chip. We present here DC I-V measurements on MIDFETs with a nominal gate length of 1.5 μm and a gate width of 30 μm.

7.3 Device Results

Figure 3 shows a plot of the transconductance versus gate to source voltage for four representative devices with varying $In_{(1-x)}Al_xAs$ insulator compositions. As expected from simple theory, the threshold voltage is, to the first order, unaffected by the introduction of strain in the insulator. The lattice-matched device has a maximum transconductance of 220 mS/mm. This value is higher than for any of the InAlAs/InGaAs MIDFETs previously reported in the literature with a similar gate length and overall epitaxial structure (the best was 160

[5] S. Bahl, W.J. Azzam, and J.A. del Alamo, "Fabrication of an InAlAs/n^+-InGaAs MIDFET," unpublished paper presented at the Fourth New England MBE Workshop, Cambridge, Massachusetts, May 4, 1989.

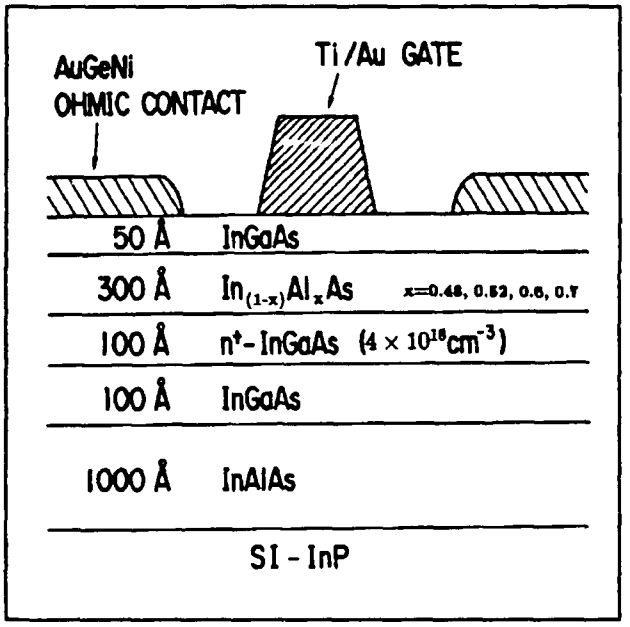

Figure 2. Cross section of device structure.

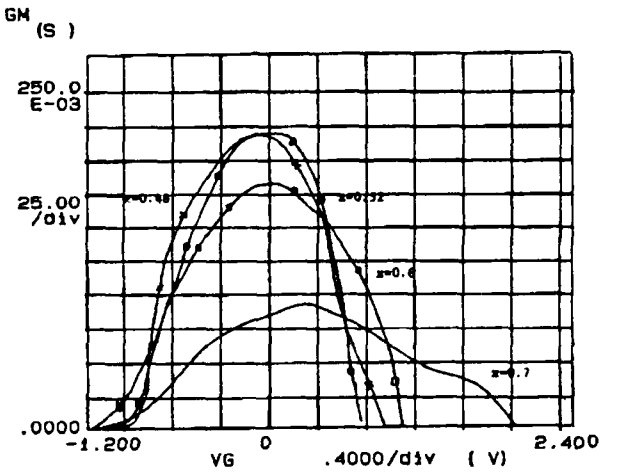

Figure 3. *Transconductance versus gate to source voltage for* V_{ds} = 4 V.

mS/mm).[3] We believe that is due to the enhanced channel doping in this new device structure.

An increase of AlAs composition in the $In_{(1-x)}Al_xAs$ gate insulator from the lattice-matched condition x = 0.48 to x = 0.6 brings about a slight reduction of peak g_m due to an enhanced contact resistance. First order theory predicts this result. A further increase of x to 0.7 results in a catastrophic reduction in g_m that cannot be explained by a larger source resistance. It appears that, from an electrical point of view, the critical layer thickness for the 300 Å $In_{(1-x)}Al_xAs$ insulator has been exceeded in going from x = 0.6 to x = 0.7.

While there is a small reduction of g_m with AlAs composition, the g_m curve broadens in V_{gs}, as figure 3 indicates, because gate current is being suppressed due to the enhanced conduction band discontinuity (discussed below). Thus, the maximum current driving capability of the devices is not degraded. In fact, this capability improves with AlAs composition up to 0.6. The maximum drain current obtained is 300 mA/mm for the x = 0.6 device. This is better than that which had been reported previously in similar devices and is a very competitive value for any 1.5 μm gate length HFET.

Increasing the AlAs composition results in a drastic reduction of forward gate current. Figure 4 illustrates gate current as a function of drain-source voltage for $V_{gs} = 1.2$ V. As the AlAs composition increases, gate current at all values of V_{ds} is drastically suppressed. This results in broader g_m versus V_{gs} characteristics (shown in figure 3) and higher $I_{D\,max}$, as mentioned above.

A more significant result, shown in figure 5, is the impact of AlAs composition on the real-space transfer of hot electrons from the channel to the gate. Such a phenomenon is very clearly observed in the devices with AlAs composition of 0.48 and 0.52. Its unique signature is an increase in the gate current as V_{ds} increases for a given V_{gs}. This increase is due to electrons that are heated by the high electric field prevalent inside the channel and then acquire sufficient energy to overcome the conduction band discontinuity between the channel and the gate insulator. The drain current saturates when the device itself enters saturation. An AlAs composition of 0.6 results in a sufficient conduction band discontinuity to completely suppress this phenomenon. This may be a major advantage of submicron strained-insulator MIDFETs in which the electric field in the channel can reach a very high value.

Figure 5 shows that real-space transfer of hot electrons to the gate causes a small negative differential output resistance. Because elec-

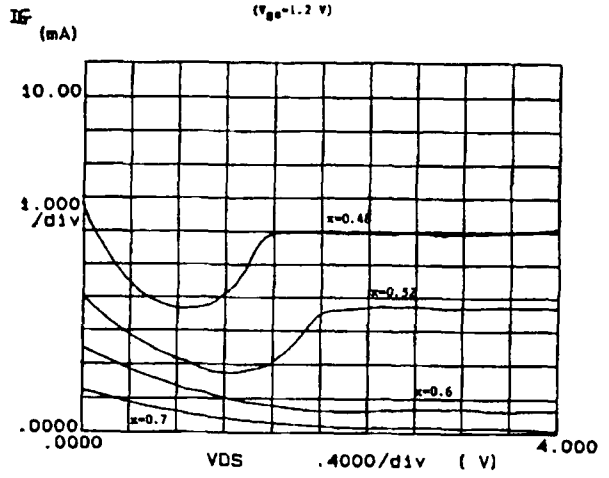

Figure 4. Gate current versus V_{ds} at $V_{gs} = 1.2$ V, as a function of AlAs composition.

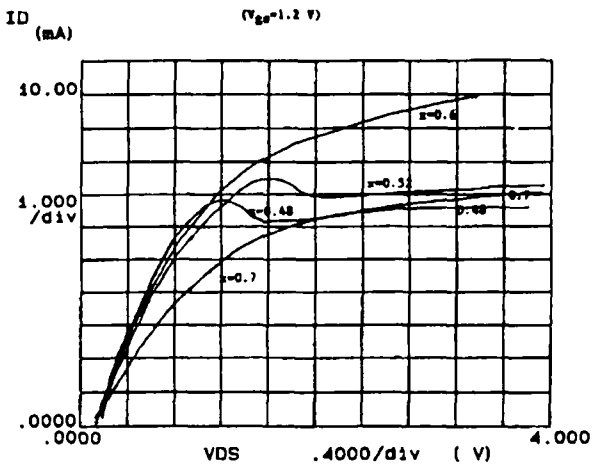

Figure 5. Drain current versus V_{ds} at $V_{gs} = 1.2$ V, as a function of AlAs composition.

trons are lost to the gate, this phenomenon results in drain current reduction. In addition, it may produce device instabilities and oscillations. For the x = 0.6 device, real-space transfer is completely suppressed and the drain current reaches higher values, as figure 5 indicates. Overall, the x = 0.6 device has ten times less gate current than the x = 0.48 device at practical operating points.

A final advantage of the strained-insulator MIDFETs is the enhanced reverse-bias gate breakdown voltage. Figure 6 shows the gate I-V characteristics measured with drain and source shorted. We obtain a rather hard breakdown for all devices. If we define breakdown at a reverse current of 1 mA, the breakdown voltage for the lattice matched device is 17 V. As the AlAs composition is increased in the insulator, the breakdown voltage increases very quickly, up to 28 V for x = 0.7.

The combination of the unique features investigated above makes strained-insulator InAlAs/n^+-InGaAs MIDFETs very suitable candidates for high-power microwave applications. Figure 7, for example, shows that $In_{0.40}Al_{0.60}As/n^+$-$In_{0.53}Ga_{0.47}As$ MIDFETs displayed excellent I-V characteristics up to $V_{ds} = 10$ V.

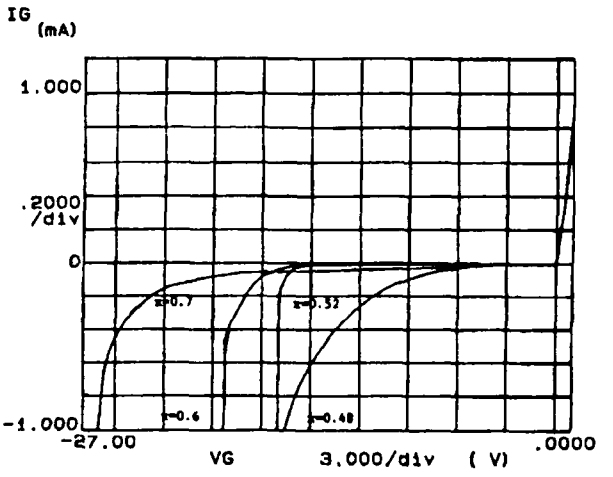

Figure 6. Reverse gate current characteristics of FETs as a function of AlAs composition $V_{ds} = 0$ V.

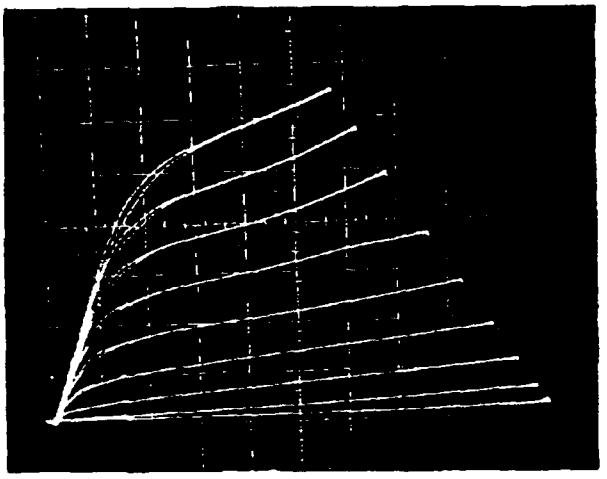

Figure 7. I-V characteristics of fabricated $In_{0.40}Al_{0.60}As/n^+$-$In_{0.53}Ga_{0.47}As$ MIDFET. Scales: I_D: 1mA/div,V_{ds}:1V-div,V_{gs}:0.2V/step, V_{gs}(max) = 0 V.

7.4 Publications

Bennett, B.R., and del Alamo, J.A. "Index of Refraction Anysotropy in Mismatched InGaAs/InP Heterostructures Measured by Ellipsometry." Paper presented at the Symposium on Layered Heterostructures - Heteroepitaxy, Superlattices, Strain and Metastability of the 1989 Fall Meeting Materials Research Society, Boston, Massachusetts, November 27-December 2, 1989. Symposium *Proceedings*. Forthcoming.

del Alamo, J.A., and Azzam, W.J. "A Floating-Gate Transmission-Line Model (FGTLM) Technique for Accurate Measurement of Source Resistance in HFETs." Paper presented at 1989 Workshop on Compound Semiconductor Materials and Devices, Hilton Head, South Carolina, February 20-22, 1989.

del Alamo, J. A. and Mizutani, T. "A Recessed-Gate $In_{0.52}Al_{0.48}As/n^+$-$In_{0.53}Ga_{0.47}As$ MIS-type FET." *IEEE Trans. Electron Devices* ED-36 (4): 646-650 (1989).

del Alamo, J. A. and Mizutani T. "An $In_{0.52}Al_{0.48}As/n^+$-$In_{0.53}Ga_{0.47}As$ MISFET with a Modulation-Doped Channel." *IEEE Electron Device Lett.* EDL-10 (8): 394-396 (1989).

del Alamo, J.A., and Azzam, W.J. "A Floating-Gate Transmission-Line Model (FGTLM) Technique for Measuring Source Resistance in Heterostructure Field-Effect Transistors." *IEEE Trans. Electron Devices* 36 (11): 2386-2393 (1989).

Chapter 8. Novel Superconducting Tunneling Structures

Academic and Research Staff

Professor John M. Graybeal

Graduate Student

George E. Rittenhouse

8.1 Project Description

Sponsor

Joint Services Electronics Program
Contract DAAL03-89-C-0001

In this program, we examine the behavior of the superconducting Josephson channel in electronically gated resonant tunneling structures. These hybrid superconducting/semiconducting structures represent the first attempt at Josephson coupling via resonant tunneling. A significant consequence of this approach is that the quantum confinement levels, not the semiconducting gap voltage, set the energy scale for modulating the Josephson coupling. Having made significant progress in the fabrication of such a device, we expect to have test devices available for initial measurements in coming months.

The envisioned device will use a thin silicon layer (<1000 Å) as a superconducting weak link between the superconducting source and drain electrodes. The superconducting counterelectrodes are separated from the silicon layer by a thin oxide layer. The weak link also defines a quantum well in which the superconducting Cooper pairs can interfere with each other (either constructively or destructively). This creates a resonant tunneling channel for Cooper pairs (i.e., the Josephson channel) between the source and drain in parallel with the normal quasiparticle (or single electron) channel. The applied gate voltage biases the levels within the semiconducting well, modulating the Josephson current by varying the wavelength of the tunneling electrodes. In many ways, this structure is analogous to a Fabry-Perot interferometer. Previous efforts on similar hybrid Josephson devices have not utilized either resonant tunneling or quantum confinement. Thus, there is a mismatch between the semiconducting and superconducting gap energy scales.[1] The key motivation for our devices is that the energy scale is set by quantum confinement and can be tuned separately from either gap energy. For silicon well widths in the range of 500–1000 Å, the energy levels separation in the well can be set more than ten times smaller than the semiconducting gap.

Current progress focuses on two areas. The first is the development of ultrathin uniform oxide tunneling barriers for the resonant quantum well. This tunnel barrier must be thin enough to enable a substantial number of Cooper pairs to tunnel through it, yet be thick enough to provide adequate isolation between the gate and the output. We have successfully fabricated ultrathin oxide layers of very high quality, grown at 800°C in a dilute (0.8 percent) oxygen atmosphere. Oxide layers have been fabricated with thicknesses of 15, 20, 25, 30 and 35 Å, and all appear to have healthy barrier heights with no observable trap states (from C-V analysis).

The second area of progress is the examination of two different device structures. The first device structure has a vertical geometry

[1] A.W. Kleinsasser, T.N. Jackson, G.D. Pettit, H. Schmid, J.M. Woodall, and D.P. Kern, "Prospects for Proximity Affect Superconducting FETs," *IEEE Trans. Mag.* MAG-25 (2): 1274-1277 (1989) and references within.

and uses a silicon membrane as the weak link, a geometry that has been fabricated before albeit for much thicker silicon membrane thicknesses. The second structure is a novel new structure, done in collaboration with Professor Henry I. Smith. This structure has a lateral geometry with a silicon wall as the weak link. Both are shown in figure 1. The operational physics of the two structures is identical.

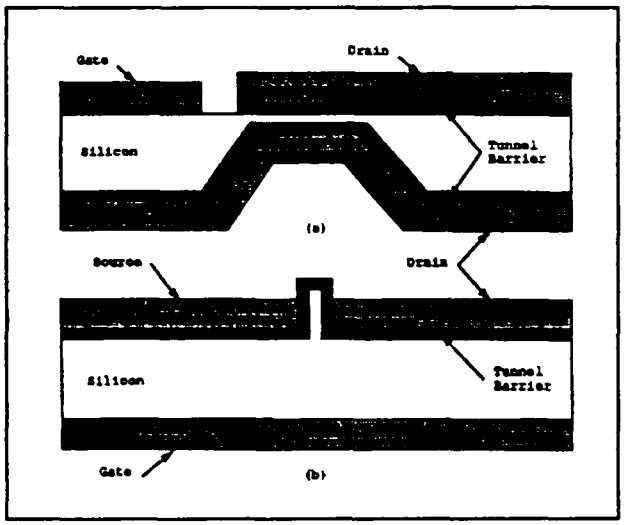

Figure 1. (a) Vertical device geometry, and (b) lateral device geometry. Note: drawings are not to scale.

In the vertical structure, the membrane is formed by an isotropic etch in ethylenediamine-pyrocatechol. This etch stops on a heavily boron-doped 1.75 μm thick layer deposited at the surface of the wafer. After this etch, the membrane is thinned to the desired thickness. Two disadvantages of this structure are its extreme fragility and its process limitation, being only heavily boron-doped. The advantage of the structure is that its fabrication requires only one level of conventional VLSI optical lithography. However, we have found the fabrication of membranes much thinner than 1 μm to be exceedingly difficult, primarily due to fabrication-induced mechanical stresses. We have therefore stopped work on this particular structure.

The second device structure has a lateral topology, as shown in figure 1(b). The starting material for this device is (100) Si. The wall is formed by a strongly anisotropic potassium-hydroxide wet etch. As this weak link is defined by a mask layer, no etch stop is necessary. Therefore, this fabrication route places no constraints on the dopant type or level in the wafer, which is very desirable. Also, the mechanical integrity of this device is substantially more robust. In addition, the lateral structure allows it to be more easily integrated into circuits.

The primary difficulty in fabricating this lateral device is the production of the mask and the alignment of the mask pattern to the crystalline axes of the underlying wafer. We believe that both of these problems are surmountable, and our work is progressing on both fronts. Indeed, although we need to make some refinements, we have successfully produced thin silicon walls on test chips (figure 2). After finalizing the fabrication route, we will then begin careful measurement and analysis of the device behavior.

Figure 2. Nanow (500Å) wall structure (on right) etched into Si<110> wafer. Note scale at bottom of figure.

Chapter 9. Heterostructures for High Performance Devices

Academic and Research Staff

Professor Clifton G. Fonstad, Jr., Dr. Elias D. Towe, Richard R. Perilli

Visiting Scientists and Research Affiliates

Dr. Herve Blanck,[1] Dr. Sheila Prasad[2]

Graduate Students

Thomas P.E. Broekaert, Geoffrey Burns, Woo-Young Choi, Isako Hoshiro, Lung-Han Peng, Yakov Royter, Richard Singer, James Vlcek

Undergraduate Students

Eric Monson, Melissa Frank, Debra Miller

Technical and Support Staff

Angela R. Odoardi

9.1 Introduction

The broad objective of our research effort is to develop III-V quantum heterostructures for high performance electronic, optoelectronic, and photonic devices for high speed optical communications and signal processing. To this end, we are developing (1) new, higher performance materials systems including InP-based InGaAlAs heterostructures and <111> oriented strained layer superlattices; (2) a new family of quantum-well-base, tunnel-barrier n-n-n transistors and near- and far-infrared optoelectrical devices; and (3) new damage-free in situ processing techniques for fabricating advanced quantum structures and embedded heterostructures.

The following sections describe our progress during the past year in the research areas listed above. Our group works closely with Professors Hermann Haus, Erich Ippen and James Fujimoto to develop the optical device application, characterization and modeling aspects of this program and with Professor Sylvia Ceyer to develop new in situ processing techniques.

9.2 Computer Controlled Growth of Lattice-Matched InGaAlAs Heterostructures on InP

Sponsors

Charles S. Draper Laboratory
Contract DL-H-315251
Joint Services Electronics Program
Contract DAAL03-89-C-0001
National Science Foundation Grant
Grant EET 87-03404

Project Staff

James Vlcek, Professor Clifton G. Fonstad

The InGaAlAs material system, lattice-matched to InP substrates, includes alloy compositions with bandgaps that match the low-loss windows of silica-based optical

[1] Thomson CSF.

[2] Northeastern University, Boston.

fibers at 1.3 and 1.55 microns. Since the constituent "elements" of the pseudo-ternary alloy InGaAlAs (InAs, GaAs, and AlAs) each have the same anion, this compound is better suited to traditional molecular beam epitaxial (MBE) growth techniques than the more commonly used InGaAsP alloy system.

In electronic and optical semiconductor devices, the need for both graded-composition and hyper-abrupt metallurgical junctions frequently arises, but it is difficult to build these structures with solid-source Molecular Beam Epitaxy. In the case of graded junctions, the fluxes of the constituent elements must be precisely controlled during the growth process to maintain lattice matching of the epitaxial layer to the substrate, while varying the ratios of two or more beam fluxes to each other. This control is accomplished by ramping the setpoint temperature of the effusion cells for the constituent elements of the growing crystal. Achieving hyper-abrupt junctions, on the other hand, is complicated by use of mechanical shutters to block the beam fluxes during the growth process. Opening and closing of these shutters changes the thermal characteristics of the effusion cell, leading to transients in the emitted flux which must be removed to achieve truly abrupt metallurgical junctions.

Complications encountered in the growth of both graded layers and hyper-abrupt junctions can be addressed by a common solution: construction of a model for the effusion cell which takes into account not only the nonlinear relationship between flux and temperature, but also the temporal response of the cell to setpoint changes. This model is then used to construct the proper setpoint temperature profiles to achieve either a time-varying flux profile for a graded layer, or a flat flux profile to remove a shutter transient. These temperature profiles are executed by a digital computer which communicates with the feedback-loop (or PID, for Proportional Integral Derivative controllers which stabilize the effusion cells).

With this scheme, we have grown compositionally graded layers with maximum deviation from the desired flux profile maintained below one percent, reducing flux transients from values in the range of 10 to 25 percent to less than 1.5 percent. Current research on this topic includes extending models of the effusion cell and eliminating overlapping shutter transients similar to those that would occur in superlattice structures (multiple, closely-spaced abrupt heterojunctions).

9.3 InGaAlAs Multiple Quantum Well Heterostructures for Guided Wave Optics

Sponsors

National Science Foundation Grant
Grant EET 87-03404

Project Staff

James Vlcek, Professor Clifton G. Fonstad, Jr., in collaboration with Mary R. Phillips and Professor Hermann A. Haus

Through the use of quantum confinement at InGaAs/InAlAs heterojunctions, emission and absorption edges of epitaxial grown structures can be continuously varied over the wavelength range of 1.3 to 1.6 microns, making them compatible with silica fiber communications. In addition to use in semiconductor lasers for optical emission and photodetectors for signal detection, these heterostructures can be employed for all-optical devices such as waveguides and modulators. The dynamics of optical nonlinearities in the transparent region of these structures will be an important factor in the speed of refractive, all-optical switches.

To measure subpicosecond optical nonlinearites just below the superlattice bandgap, we have fabricated InGaAs/InAlAs multiple quantum well heterostructures. In a pump-probe experiment, we collaborated with Mary R. Phillips and Professor Hermann A. Haus of RLE to measure the refractive and absorptive nonlinearities of these samples.

A typical heterostructure consisted of 72 periods of an InGaAs/InAlAs superlattice, each with periods of 70 Å. This structure was grown using the computer-automated MBE system described in Section 9.2. Room temperature infrared absorption measurements of our best sample showed clear, strong excitonic absorption lines for both n=1 and n=2 transitions. Both the n=1 light and

in the literature. Now, we are in the process of optimizing our layer structure, growth conditions, and device fabrication technology which should greatly enhance device performance.

In addition to multiple quantum well laser diodes, we are investigating the use of graded-index optical confinement structures for (1) an optimal gain profile with minimal angular dispersion of the emitted beam and (2) structures utilizing controlled amounts of lattice mismatch strain in the active layer to further enhance the quantum size effects of the confined carriers. To achieve our long range goal of producing ultra-narrow linewidth devices, we are extensively analyzing various theoretical techniques for reducing laser linewidth. Our ultimate goal is to produce room temperature laser diodes with emission linewidths below 100 kHz.

9.5 InGaAlAs Strained-Layer Heterostructures on 111 GaAs and InP for Optical for Modulator Applications

Sponsors

Joint Services Electronics Program
Contract DAAL03-89-C-0001
National Science Foundation Grant
Grant EET 87-03404

Project Staff

Richard Singer, Professor Clifton G. Fonstad, Jr., in collaboration with Stuart D. Brorson, Daryl Smith,[3] B. Laurich,[3] Christian Mailhoit,[4] Bruce D. McCombe,[5] and Bernie A. Weinstein[5]

When epitaxial layers with a slight lattice mismatch are deposited upon (111)-oriented GaAs or InP substrates, piezoelectric fields are generated. Whether a field points <111>A or <111>B is a function of whether a given epilayer is under tensile or compressive strain. Our group was the first to produce these structures and to demonstrate experimentally the existence of piezoelectric fields. We are now applying this effect to optoelectronic devices.

If a quantum well structure is grown through appropriate choice of ternary composition and layering, the strain-induced field will red-shift the excitonic resonance of the well. This is the familiar Quantum Confined Stark Effect (QCSE). In the present structures, the internal strain-induced field provides a bias on the order of 105 V/cm. An applied voltage will either enhance or counteract the strain-induced field around a bias point in a highly sloped, nearly linear region of the field verses index and/or absorption characteristics of these structures. Thus, the external bias is expected to dramatically affect the transmittance or reflectance of the multiple quantum well structure at a given wavelength. Practical, low voltage modulation of optical signals should be possible.

Presently, we are seeking to grow, fabricate, and characterize window and waveguide p-i-n modulators in both the GaAs and InP material systems. Material of good surface morphology has been successfully grown by molecular beam epitaxy on (111) GaAs, and samples of (111)-oriented strained layer heterostructures have been distributed to a number of researchers interested in studying them. Recently, reflection modulators consisting of a mirror region of quarter wave plates and an active region of strained multiple quantum wells have been grown and tested with no applied bias. Work is currently underway to process these devices so that we can study their response to applied voltages.

MBE growth on InP is more difficult because of the conflicting requirements of a low substrate temperature and high As overpressure to stabilize the volatile (111) surface, on the one hand, and the opposite growth conditions needed to enhance surface mobility of Al on the other. To overcome this diffi-

---

[3] Los Alamos National Laboratory.

[4] Lawrence Livermore National Laboratory.

[5] State University of New York at Buffalo.

culty, we will attempt a variation of migration enhanced epitaxy in which we will keep both the substrate temperature and As overpressure low.

9.6 Molecular Beam Epitaxial Growth on (h11) Vicinal Surfaces

Sponsor

MIT Funds

Project Staff

Dr. Elias D. Towe, Professor Clifton G. Fonstad, Jr., in collaboration with H.Q. Le,[6] and J.V. Hryniewicz[6]

Traditionally, III-V compound semiconductors have been synthesized on (100) substrate surfaces. Because it is desirable to fabricate devices on chemically etch-structured (100) surfaces, an understanding of molecular beam epitaxial growth on high-index planes vicinal to the (100) surface is important. Understanding the properties of material grown on such surfaces is also necessary. The particular planes of interest are those denoted by (h11).

We have continued our work on the growth of epi-layers on (h11) vicinal surfaces of GaAs. In particular, the growth conditions and characteristics on the (111)B, (211)B and (511)B surfaces for acceptable quality layers are fairly well understood. GaAs and (Al, Ga)As layers with luminescence superior to that of layers on the (100) surface have been grown on these surfaces.

Our interest in the epi-layers on the (h11) surfaces is due to the potential for improved-performance and for their use in novel optical devices. We are currently studying some laser devices with strained-layer active regions on (111)-GaAs substrates. The devices have been fabricated, and we will test them soon. Some waveguide structures on (211) substrates have also been fabricated so that an undergraduate thesis student can evaluate them with a tunable Ti:sapphire laser.

We expect that the threshold current densities of the lasers on the (111)-GaAs substrates will be lower than those on the conventional (100) substrates. This expectation is based on the fact that the relative photoluminescence emission of the layers on these substrates is higher than that on the (100) substrates.

9.7 Pseudomorphic AlAs/InAs/InGaAs Resonant Tunneling Structures

Sponsor

Joint Services Electronics Program
Contract DAAL03-89-C-0001

Project Staff

Thomas P.E. Broekaert, Professor Clifton G. Fonstad, Jr.

A fundamental objective in the design of resonant tunneling diodes (RTDs) for microwave oscillators and digital switching is achievement of the highest possible peak current density at the lowest possible peak voltage, while maintaining a high peak-to-valley current ratio and wide valley region. The InGaAlAs material system, lattice matched to InP, has the design flexibility to optimize the RTD for microwave performance and switching applications in terms of peak current density and peak voltage of the RTD.

Thus far, by using very thin, three monolayer AlAs barriers and InGaAs wells, within bounding regions of InGaAs lattice-matched to InP, we have achieved room temperature peak current densities in excess of 1 MA/cm^2, the highest reported value for RTDs to date, at peak voltages as low as 0.55 V. The peak-to-valley current ratio of these devices is approximately 2 to 4.

For the diode structure, a turn-on threshold voltage is apparent in the I-V characteristics. This threshold characteristic can be removed

---

[6] MIT Lincoln Laboratory.

by widening the well or by including a low bandgap material, i.e., InAs, in the well. Diode structures of this type have been fabricated and display linear initial I-V characteristics with no turn-on threshold and a low peak voltage.

The combination of thin AlAs barriers and InAs containing wells should allow us to further optimize the RTDs.

9.8 Three-Terminal Quantum Well Base/Tunnel Barrier Devices

Sponsors

Joint Services Electronics Program
Contract DAAL03-89-C-0001

Project Staff

Thomas P.E. Broekaert, Lung-Han Peng, Professor Clifton G. Fonstad, Jr.

We have gained our objective of making direct electrical contact to a populated conduction band quantum well in a resonant tunneling configuration. Recently, in a significant breakthrough, we succeeded in etching away the layers above the InAs quantum well layer in an AlAs/InAs/InGaAs resonant tunneling diode and making electrical contact directly to this 2 to 5 nm thick layer. This major advance in this technique opens the door to development of a new class of ultra-high performance electronic, optoelectronic, and photonic devices. We are currently beginning an aggressive program of research utilizing this advance to investigate quantum-well base, tunnel-barrier n-n-n transistors; tunnel injection, quantum-well-level laser diodes for the 2 to 5 micron region; sub-picosecond quantum-well-level, tunnel-barrier infrared photodiodes; and ultrafast quantum-well-level, tunnel-barrier optoelectronic modulators and non-linear optical components.

The basis for all these devices is the AlAs/InAs/InGaAs double barrier resonant tunneling structure discussed in the previous section. There are at least three unique features of this structure which make it ideally suited for these structures. First, the AlAs tunnel barriers are unusually high relative to the InGaAs injectors and the InAs well, which yields multiple confined well states and sharp quantum structure at room temperature. Second, the InAs well lies below the band edges of the InGaAs injectors so that when it is suitably wide and doped, the first well level will be populated. This provides all-important lateral conduction in the plane of the well and the necessary ground-state population for detector and optical modulator applications. Third, the very wide range of materials in these structures has allowed us to develop a selective etch which, in turn, makes it possible to make electrical contact to the very thin quantum well layer.

9.9 Design and Fabrication of GaAlAs Heterostructure Laser Diodes for Monolithic Integration with Si Circuits

Sponsors

International Business Machines Corporation
National Science Foundation
Grant ECS 8[illegible]13178

Project Staff

Geoffrey Burns, Dr. Herve Blanck, Professor Clifton G. Fonstad, Jr., in collaboration with Professor Carl V. Thompson

Prospects for monolithic integration of III-V electrical and optical devices with Si circuits have focused vigorous research efforts in direct heteroepitaxial growth of these compounds on Si substrates. Developing III-V optical sources useful for VLSI optical interconnects is one goal which has been pursued by several groups. Along these lines, we have focused upon the laser diode due to its capacity for high speed modulation and large power output. During previous years, we have developed processes for direct epitaxial growth of GaAs on Si using molecular beam epitaxy. With particular attention to details of Si surface preparation, GaAs growth initiation, and in situ annealing, we have been able to repeatably produce GaAs layers with smooth growth fronts and reduced defect density. This growth sequence has been extended to produce AlGaAs\GaAs heterostructures for laser fabri-

Chapter 1. Optics and Quantum Electronics

Academic and Research Staff

Professor Hermann A. Haus, Professor Erich P. Ippen, Professor James G. Fujimoto, Professor Peter L. Hagelstein, Dr. Santanu Basu, Dr. Jyhpyng Wang, Dr. Beat Zysset

Visiting Scientists and Research Affliates

Dr. Hiroyuki Yokoyama[1]

Graduate Students

Kristen K. Anderson, Keren Bergman, John Paul Braud, Stuart D. Brorson, Tak K. Cheng, James G. Goodberlet, Cris Eugster, Katherine L. Hall, Wei-Ping Huang, Charles T. Hultgren, Janice M. Huxley, Joseph M. Jacobson, Sumanth Kaushik, Michael J. LaGasse, Yinchieh Lai, Ling-Yi Liu, Martin H. Muendel, John D. Moores, Ann W. Morganthaler, Robert W. Schoenlein, Morrison Ulman

Undergraduate Students

Daniel Tauber

Technical and Support Staff

Mary C. Aldridge, Mary Ellen Butts, Donna L. Gale, Cynthia Y. Kopf

1.1 The Nonlinear Waveguide Interferometer

Sponsors

Charles S. Draper Laboratory
Contract DL-H-404179
Joint Services Electronics Program
Contract DAALO3-89-C-0001
National Sciences Foundation
Grant EET 87-00474

Project Staff

Professor James G. Fujimoto, Professor Hermann A. Haus, Professor Erich P. Ippen, Michael J. LaGasse, John D. Moores, Keren Bergman

Section 1.2 describes a single-arm interferometer invented in our laboratory that has been used for low power all-optical switching. We are currently investigating a switch very similar to the single arm interferometer, which is based on a fiber (waveguide) ring reflector, similar to, yet different from, the ring reflector demonstrated by the group at British Telecom.[2] In our research, we have shown that the fiber ring reflector is an excellent candidate for soliton switching and for producing squeezed light.[3] Consequently, since any experiments limited by quantum noise (i.e., detector shot noise) must take into account the quantum properties of light, we have become interested in developing a self-consistent quantum theory

---

[1] NEC, Japan.

[2] N.J. Doran, K.J. Blow, and D. Wood, *Proc. SPIE* 836:238-243 (1987).

[3] J.D. Moores, K. Bergman, H.A. Haus, and E.P. Ippen, "Optical Switching Using Fiber Ring Reflectors," submitted for publication; H.A. Haus, K. Watanabe, and Y. Yamamoto, "Quantum-Nondemolition Measurement of Optical Solitons," *J. Opt. Soc. Am. B* 6:1138-1148 (1989); Y. Lai and H.A. Haus, "Characteristic Functions and Quantum Measurements of Optical Observables," *J. Quant. Opt.*, forthcoming; M. Shirasaki and H.A. Haus, "Squeezing of Pulses in a Nonlinear Interferometer," *J. Opt. Soc. Am. B*7(1): 30-34 (1990).

for optical solitons.[4] The promise of a simple squeezing mechanism using optical pulses in fibers has also kindled our interest in developing a fiber gyro that would operate at a noise level below the standard quantum limit shot noise.

The fiber ring is one realization of a fiber ring gyro utilizing the Sagnac effect. Unfortunately, the ring cannot be used directly as a gyro with squeezed noise, because the noise that is in phase with the Sagnac signal is not reduced below the vacuum level. However, our theory predicts that a cascade of two rings, one as a squeezer and one as a gyro, can be made to perform at a level below the standard quantum limit. Ongoing experiments should determine whether squeezing is achieved in the ring. The squeezing process is broadband so that pulses can be used in the experiments. Nonlinearity is enhanced because the duty cycle enhances peak power. Through our experiments, we need to identify the several classical sources of noise that could prevent squeezing.

1.2 Picosecond Optical Signal Sampling

Sponsor

National Science Foundation
Grant EET 87-00474

Project Staff

Professor James G. Fujimoto, Professor Hermann A. Haus, Wei-Ping Huang, Michael J. LaGasse

The goal of our work is to develop optical waveguide devices for high rate all-optical switching. This objective involves development of (1) analytical and computer tools for the characterization of optical waveguide properties and (2) computer programs for describing optical pulse interactions and for experimentally verifying their predicted performance.

Through our pioneering work, we have achieved a better understanding of coupling modes theory and prediction of crosstalk in waveguide couplers.[5] Our paper on this subject was selected for publication in an IEEE volume of reprints on optical couplers.

Along with our work on coupled mode theory, we have clarified the theory of transfer of power in grating assisted couplers[6] and have developed a self-consistent theory for tapered couplers.[7] In addition, we have developed simple computer programs for the IBM PC that characterize optical waveguide modes.[8] In cooperation with Dr. Donnelly of MIT Lincoln Laboratory, we continued the work by Dr. L. Molter Orr, who was supported by the preceding National Science Foundation grant while working on her Ph.D. at MIT. This research has led to an improved understanding of the crosstalk problem in waveguide couplers.[9]

---

[4] Y. Lai and H.A. Haus, "Quantum Theory of Solitons in Optical Fibers. I. Time-Dependent Hartree Approximations," *Phys. Rev. A* 40:844-853 (1989); Y. Lai and H.A. Haus, "Quantum Theory of Solitons in Optical Fibers. II. Exact Solution," *Phys. Rev. A* 40:854-866 (1989); H.A. Haus and Y. Lai, "Quantum Theory of Soliton Squeezing - A Linearized Approach," *J. Opt. Soc. Am. B* 7(3): 386-392 (1990).

[5] H.A. Haus, W.P. Huang, S. Kawakami, and N.A. Whitaker, "Coupled-Mode Theory of Optical Waveguides," *J. Lightwave Tech.* LT-5:16-23 (1987).

[6] W.P. Huang and H.A. Haus, "Power Exchange in Grating-assisted Couplers," *J. Lightwave Tech.* 7:920-924 (1989).

[7] H.A. Haus and W.P. Huang, "Mode Coupling in Tapered Structures," *J. Lightwave Tech.* 7:729-730 (1989); W.P. Huang and H.A. Haus, "Selfconsistent Vector Coupled-Mode Theory for Tapered Optical Waveguides," *J. Lightwave Tech.*, forthcoming.

[8] H.A. Haus, W.P. Huang, and N.M. Whitaker, "Optical Waveguide Dispersion Characteristics from the Scalar Wave Equation," *J. Lightwave Tech.* LT-5:1748-1754 (1987).

[9] J.P. Donnelly, L.A. Molter, and H.A. Haus, "The Extinction Ratio in Optical Two-Guide Coupler $\Delta\beta$ switches," *J.*

All-optical switching and all-optical logic gates require that the output of gates and switches are reasonably undistorted versions of input pulses. We have demonstrated an all-optical switch with a record low switching intensity of 0.5 W and with a very low distortion of the switched out pulse.[10] We achieved the low switchout power by using a long propagation distance through an optical fiber. The switch, invented in our laboratory by a visiting Japanese researcher, is interferometric, using a single fiber and two orthogonally polarized versions of the pulse that interfere with each other. One of the two pulses is acted upon by a control pulse. Because only a single fiber is used, the interferometer is stable even when considerably long (i.e., 100 m). Modifications of the switch into integrable form will be feasible, when sufficient nonlinearities have been realized in semiconductor waveguides.

1.3 Nonlinear Dynamics in Active Semiconductor Waveguides

Sponsors

Joint Services Electronics Program
Contract DAAL03-89-C-0001
National Science Foundation
Grant EET 88-15834
U.S. Air Force - Office of Scientific Research
Contract F49620-88-C-0089

Project Staff

Katherine L. Hall, Charles T. Hultgren, Professor Erich P. Ippen

We have continued our study of carrier dynamics and nonlinear optical interactions in active semiconductor waveguide devices. Using 100-fs-duration pulses in the 800–900 nm regime obtained by fiber compression of synch-pumped dye laser pulses and similar pulses in the 1.45–1.65-μm band from APM F-center lasers, we are investigating nonlinear dynamic behavior in both GaAlAs and InGaAsP devices under various excitation conditions. Varying the wavelength of the pump and probe beams, as well as injection current in our diode waveguide structures, we are studying interactions in the presence of gain, loss, or nonlinear transparency. In all of these cases, an injected carrier density on the order of $10^{18}/cm^3$ makes the nonlinear optical behavior considerably different from that observed in passive devices.

In both GaAlAs and InGaAsP devices, we have discovered a strong nonlinearity due to nonequilibrium carrier heating. Heating of the carrier gas with respect to the lattice has a recovery time on the order of 1 ps in GaAlAs and 650 fs in InGaAsP. Since heating occurs via free electron absorption without a change in carrier number, recovery is complete. During the past year, we have documented gain and loss dynamics, which include two-photon absorption and hole-burning effects in addition to heating in a variety of different devices. In our present experiments, we are observing the index of refraction changes associated with these nonlinearities and evaluating their potential for use in all-optical switching.

During 1989, we have also demonstrated a novel means for detecting nonlinear optical interactions in the active regions of diodes by monitoring changes in diode voltage. The forward bias voltage is measured as a function of time delay between two pulses passing through the active region. The result is a nonlinear autocorrelation measurement that, when compared with optical pump-probe data, allows us to distinguish between those interactions involving carriers in the active region and other interactions.

Quant. Electron. 25:924-932 (1989); J.P. Donnelly, H.A. Haus, and L.A. Molter, "Cross Power and Crosstalk in Waveguide Couplers," *J. Lightwave Tech.* 6:257-268 (1988).

[10] M.J. LaGasse, D. Liu-Wong, J.G. Fujimoto, and H.A. Haus, "Ultrafast Switching with a Single-Fiber Interferometer," *Opt. Lett.* 14:311-313 (1989).

1.4 Saturation Characteristics of Semiconductor Optical Amplifiers

Sponsors

Joint Services Electronics Program
Contract DAAL03-89-C-0001
National Science Foundation
Grant EET 88-15834
U.S. Air Force - Office of Scientific Research
Contract F49620-88-C-0089

Project Staff

Katherine L. Hall, Yinchieh Lai, Professor Erich P. Ippen

Although in the future optical amplifiers will be essential components of optical communication networks and integrated photonic circuits, very little is known about their nonlinear behavior. We need to improve our understanding of this behavior to properly evaluate the gain saturation and intermodulation distortion effects limiting device performance. In our laboratory, we have studied amplifier characteristics as a function of pulse duration and energy in the nonlinear regime. We have also developed an analytical model to describe the observed behavior.

In our experiments, we have been the first to observe pulsewidth-dependent gain in diode laser amplifiers. We have obtained data by measuring amplifier gain (output pulse energy/input pulse energy) as a function of input pulse energy. At low input energies, the amplification of ultrashort (100 fs) pulses is the same as that for longer (20 ps) pulses. As energy increases, however, the gain for the 100-fs pulses decreases more rapidly than that for the 20-ps pulses. This effect, observed at 1.5 μm in both conventional and quantum-well quaternary devices, results in a 3-db roll-off for the 100-fs pulses at an output energy that is about a factor of ten lower than that for the longer pulses.

We have modeled this behavior with a system of coupled differential equations that includes changes in gain due to nonequilibrium carrier distributions. The standard set of two equations describing the coupling between photon density and excited state carrier density is supplemented by a third, and in some cases a fourth, equation that represents the faster nonequilibrium dynamic. The time constant of this dynamic determines the pulsewidth at which gain roll-off occurs. The parameters of the model are consistent with results from time-resolved pump-probe experiments performed on the same devices. We have obtained excellent agreement with the observed saturation data. This model predicts that a more rapid sequence of femtosecond pulses should be able to extract full energy. Although individual ultrashort pulses are restricted to lower gains, gain recovery between them is faster.

1.5 Femtosecond Studies of Metallic and High T_c Superconductors

Sponsors

Joint Services Electronics Program
Contract DAAL03-89-C-0001
U.S. Air Force - Office of Scientific Research
Contract F49620-88-C-0089

Project Staff

Stuart D. Brorson, Tak K. Cheng, Professor Erich P. Ippen

Femtosecond pump-probe observations of reflectivity dynamics on metal surfaces provide a unique measure of nonequilibrium electron dynamics. Because of the high electron density, incident optical energy is absorbed directly by the electron gas. The resulting rise in electron temperature produces a dynamic change in reflectivity. Relaxation of this change occurs as the electrons lose energy to the lattice via phonon emission. The rate is governed by the electron-phonon coupling strength.

We have begun to systematically study the strength of electron-phonon coupling, an important component in BCS theory of superconductivity, in collaboration with Professor M. Dresselhaus' group. In a series of experiments, we measured $\lambda\{\omega^2\}$ for ten different metals (four of them superconducting). The agreement between the values obtained with those described in the literature was excellent. In addition, our method for measuring $\lambda\{\omega^2\}$, the temperature relaxation rate, has several advantages over other techniques such as tunneling or heat

capacity measurements because it: (1) is a direct measurement, (2) works at room temperature, and (3) can be applied to non-superconducting as well as superconducting samples. We have also demonstrated that thin overlayers of Cu, which has d-band transitions in the visible, can enhance the experimental reflectivity changes on metals which are otherwise too small to detect. This enhancement extends the method for use with any metal film.

We have also performed a series of pump-probe and transmission experiments on three high-T_c thin films: $YBa_2Cu_3O_{7-\delta}$, $Bi_2Sr_2CaCu_2O_{8+x}$, and $Bi_2Sr_2Ca_2Cu_3O_{10+y}$. In these materials, too, we have observed a strong correlation between observed relaxation rates and T_c. At present, there is no clear theoretical explanation for these results. We are performing additional experiments to improve our understanding of the observed correlation.

1.6 Suppressed and Enhanced Spontaneous Emission from Microcavities

Sponsor

Joint Services Electronics Program
Contract DAAL03-89-C-0001

Project Staff

Hiroyuki Yokoyama, Stuart D. Brorson, Professor Erich P. Ippen

Optical microcavities could prove useful in the construction of efficient, high speed semiconductor lasers. One particularly interesting possibility is using a cavity to alter the spontaneous emission rate of the device. This alteration has been observed with atoms and molecules. However, altering the emission rate in a semiconductor device is more difficult because the broad spontaneous emission bandwidth requires cavity dimensions on the order of a wavelength. To determine its potential application in semiconductor devices, we have analyzed the radiation modes of oscillating dipoles in planar (one-dimensional confinement) and optical-wire (two-dimensional confinement) structures. When we used a mode counting method equivalent to, but less complex than, traditional classical and quantum electrodynamical approaches, we found that an idealized planar metallic mirror cavity could suppress the spontaneous emission with respect to free space by no more than a factor of two. Emission was suppressed to a lesser degree with use of a real dielectric stack. Theory shows, however, that we could achieve greater suppression by restricting the dimensionality to that of the optical wire. Then, enhanced spontaneous emission should be easier to observe. With GaAs quantum-well cavities fabricated at NEC, Dr. Yokoyama observed reductions in the luminescence times by factors of two due to cavity effect. We have recently achieved femtosecond up-conversion detection of spontaneous emission from these structures and we are now attempting to observe more dramatic reductions with multiple-quantum-well structures grown at MIT by Professor Clifton G. Fonstad's group.

1.6.1 JSEP Publications

Ippen, E.P., H.A. Haus, and L.Y. Liu. "Additive Pulse Mode Locking." *J. Opt. Soc. Amer. B* 6(9): 1736-1745.

Ippen, E.P., L.Y. Liu, and H.A. Haus. "Self-starting Condition for Additive-pulse Mode-locked Lasers." *Opt. Lett.* 15(3): 183-185 (1990).

Kesler, M.P. and E.P. Ippen. "Femtosecond Time-Domain Measurements of Group Velocity Dispersion in AlGaAs Diode Lasers." *Electron. Lett.* 25(10): 640-641 (1989).

Nelson, K.A. and E.P. Ippen, "Femtosecond Coherent Spectroscopy." *Advances in Chemical Physics*. Vol. 75 (1989).

Mark, J., L.Y. Liu, K.L. Hall, H.A. Haus, E.P. Ippen. "Femtosecond Pulse Generation in a Laser with a Nonlinear External Resonator." *Opt. Lett.* 14(1): 48-50 (1989).

1.7 New Ultrashort Pulse Laser Technology

Sponsors

Joint Services Electronics Program
Contract DAAL03-89-C-0001
National Science Foundation
Grant ECS 85-52701
U.S. Air Force - Office of Scientific Research
Contract F49620-88-C-0089

Project Staff

Professor James G. Fujimoto, Dr. Jyhpyng Wang, James G. Goodberlet, Joseph M. Jacobson, Robert W. Schoenlein, Morrison Ulman

1.7.1 Introduction

Development of new ultrashort pulse laser technology is the cornerstone for studies of ultrafast phenomena and high speed optical measurement and communication techniques. In the area of ultrashort pulse generation and measurement technology, we are developing new techniques to extend the range of applications and resolution of ultrafast studies. In particular, development of tunable wavelength femtosecond sources is important for a wide range of spectroscopic as well as optoelectronic device studies. High repetition rate femtosecond amplifier technology permits the generation of high peak intensities for the study of nonlinear optical effects. Finally, our research places special emphasis on developing new solid state laser materials and diode pumping techniques. These developments could represent next generation technology, ultimately replacing existing dye laser systems to yield more compact and viable short pulse sources suitable for a wider variety of engineering applications.

1.7.2 Tunable Femtosecond Ti:Al_2O_3 Laser

Solid state lasers provide an attractive alternative to existing ultrashort pulse dye laser technology. Working in collaboration with researchers at MIT Lincoln Laboratory, we have developed a novel ultrashort pulse generation modelocking technique in the Ti:Al_2O_3 laser.[11] Ti:Al_2O_3 is a promising new solid state laser material which features room temperature operation, high energy storage, and a broad tuning range of 670 nm to 1000 nm. The broad gain bandwidth of this material make it ideal for femtosecond pulse generation and amplification. In addition, the tuning range is especially useful for the study of GaAs-based electronic and optoelectronic materials and devices.

Our ultrashort pulse generation technique is an extension of a pulse shortening technique developed in color center lasers known as additive pulse modelocking (APM).[12] However, in the Ti:Al_2O_3 laser, modelocking is achieved without the need for active gain or loss modulation. This self-starting additive pulse modelocking results in a significant reduction in the system cost and complexity since high frequency active modulation is not required for the laser system. Extending this technique to other laser materials holds the promise of developing a compact and low cost ultrashort pulse laser technology suitable for commercial application.

The self-starting additive pulse modelocking technique uses an external cavity which contains an optically nonlinear medium (a length of optical fiber). The nonlinear external cavity functions resemble a nonlinear Fabry Perot. The reflectivity of the Fabry Perot is a function of the relative cavity lengths or phase of the optical field. Since the optical fiber has a nonlinear index of refraction, the reflectivity of the Fabry Perot is intensity

---

[11] J. Goodberlet, J. Wang, J.G. Fujimoto. and P.A. Schulz, "Femtosecond Passively Mode-locked Ti:Al_2O_3 Laser with a Nonlinear External Cavity," *Opt. Lett.* 14:1125-1127 (1989).

[12] P.N. Kean, X. Zhu, D.W. Crust, R.S. Grant, N. Langford, and W. Sibbett, "Enhanced Mode Locking of Color-Center Lasers," *Opt. Lett.* 14:39-41 (1989); K.J. Blow and D. Wood, "Mode-Locked Lasers with Nonlinear External Cavities," J. Opt. Soc. Am. B 5:629-632 (1988); J. Mark, L.Y. Liu, K.L. Hall, H.A. Haus, and E.P. Ippen, "Femtosecond Pulse Generation in a Laser with a Nonlinear External Resonator," *Opt. Lett.* 14:48-50 (1989); E.P. Ippen, H.A. Haus, and L.Y. Liu, "Additive Pulse Mode Locking," *J. Opt. Soc. Am. B* 6:1736-1745 (1989).

dependent. If the relative cavity lengths are controlled appropriately, the nonlinear cavity will function like a fast saturable absorber to enhance intensity fluctuations in the laser. This produces the pulse formation process.

The additive pulse modelocked laser incorporates an all-optical switch in the form of a nonlinear Fabry Perot which produces pulse shortening. Alternatively, this system can be viewed as the analog of an RF or microwave feedback system, except that the feedback is nonlinear, operating at optical frequencies. Figure 1 shows a schematic diagram of the Ti:Al_2O_3 laser. In Ti:Al_2O_3, pulses as short as 1.4 ps have been generated directly from the laser with pulse durations of 200 fs obtained by externally compensating for chirp.

During the past year, we have studied the starting dynamics of the ultrashort pulse formation process and the scaling behavior of the laser system and performance. This research is relevant to extending the short pulse generation technique to other solid state laser materials at other wavelengths as well as to higher and lower power solid state lasers.

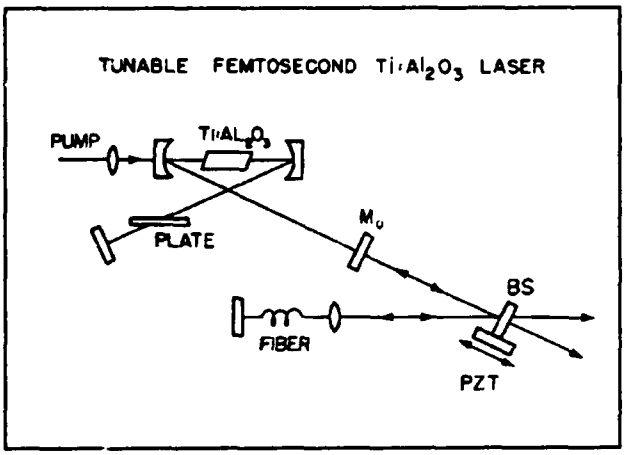

Figure 1.

1.7.3 Diode Pumped Modelocked Nd:YAG Lasers

During preliminary studies in collaboration with investigators at MIT Lincoln Laboratory, we demonstrated the extension of this short pulse generation technique to a diode pumped Nd:YAG laser.[13] Other studies at RLE by Professors Ippen and Haus have achieved short pulse generation in a lamp pumped Nd:YLF laser. Results suggest that self-starting additive pulse modelocking can be applied to a range of solid state laser materials.

The diode pumped Nd:YAG laser combines the advantages of diode pumping which offers high inherent stability, compactness, and low cost with the technique of additive pulse modelocking which has a simple design and especially short pulse generation. We have achieved a pulse width of 1.7 ps, which is the shortest pulse generated to date in a modelocked Nd laser. Preliminary measurements show that this system has excellent interpulse arrival time or phase stability, making it a suitable source for optoelectronic diagnostic studies that require synchronization of optical and electronic signals.

One of the key features of this technology is that the laser power and repetition rate can be scaled up or down. The extension of diode pumped self-starting additive pulse modelocking to lower output powers would permit development of extremely compact short pulse sources. Since the cavity length can be varied, this approach provides a method for obtaining variable pulse repetition rates. The development of compact short pulse sources could prove useful for a number of commercial applications including high speed optoelectronic sampling measurements and device diagnostics as well as possible applications for high speed signal processing using optical techniques.

---

[13] J. Goodberlet, J. Jacobson, J.G. Fujimoto, P.A. Schulz, and T.Y. Fan, "Self Starting Additive Pulse Modelocked Diode Pumped Nd:YAG Laser," *Opt. Lett.*, forthcoming.

1.7.4 Multistage Femtosecond Dye Amplifier

While solid state laser systems are an important area of investigation for the next generation of ultrashort pulse laser technology, current measurement technology is based on dye laser systems and amplifiers. We are investigating new laser generation and high repetition rate amplification techniques for studying ultrafast phenomena, placing special emphasis on development of a multistage, high repetition rate, dye amplifier. The amplifier has a modular construction and may be easily configured for a variety of tasks.

The ultrashort pulse source for our system is a colliding pulse modelocked ring dye laser (CPM).[14] This laser produces 50 fs pulses at 620 nm wavelength. The wavelength is not tunable because the laser is passively modelocked. The output of the CPM is amplified using a copper vapor laser pumped dye amplifier.[15] The copper vapor laser operates at a repetition rate of 8 kHz which facilitates the use of signal averaging and lock-in detection techniques for high sensitivity measurements.

We have developed a new multistage copper vapor laser pumped dye cell amplifier system.[16] The compact, multistage design allows the amplifier to be easily configured for advanced short pulse generation techniques. In comparison with earlier designs, we have improved its efficiency and experimental convenience while keeping the overall system complexity within manageable limits.

The high pulse intensity available from just one stage of amplification (2—3 microjoules) permits use of nonlinear optical techniques to generate wavelength tunable pulses in the near infrared. After the first amplification stage, the femtosecond beam is focused in a cell of flowing water to generate a broadband continuum. A single wavelength may be selected from this continuum and amplified using an infrared dye in the second stage.

We are also currently investigating a third configuration which will produce compressed amplified pulses with pulse durations shorter than 20 fs. In this arrangement, a short single mode optical fiber is placed after the first stage of amplification. This increases bandwidth of the pulses because of self-phase modulation. After a second stage of amplification, the pulses can be compressed with a dispersive delay line or phase filter.

Thus, the high repetition rate amplifier forms the basis for a wide range of studies of ultrafast phenomena. Using nonlinear continuum generation techniques, the system provides a wavelength tunable source. For very high time resolutions, we can apply pulse compression techniques, achieving 20 fs measurement resolutions.

1.8 Ultrafast Processes in Waveguide Devices

Sponsors

International Business Machines Corporation
Joint Services Electronics Program
Contract DAAL03-89-C-0001
National Science Foundation
Grant ECS 85-52701
U.S. Air Force - Office of Scientific Research
Contract F49620-88-C-0089

Project Staff

Professor Hermann A. Haus, Professor James G. Fujimoto, Kristen K. Anderson, Claudio Chamon, Michael J. LaGasse

---

[14] J.A. Valdmanis, R.L. Fork, and J.P. Gordon, "Generation of Optical Pulses as Short as 27 Femotseconds Directly from a Laser Balancing Self-Phase Modulation, Group-Velocity Dispersion, Saturable Absorption, and Saturable Gain," *Opt. Lett.* 10: 131-133 (1985).

[15] W.H. Knox, M.C. Downer, R.L. Fork, and C.V. Shank, "Amplified Femtosecond Optical Pulses and Continuum Generation at 5 kHz Repetition Rate," *Opt. Lett.* 9: 552-554 (1984).

[16] M. Ulman, R.W. Schoenlein, and J. G. Fujimoto, "Cascade High Repetition Rate Femtosecond Amplifier," Paper FR3, presented at the Annual Meeting of the Optical Society of America, Orlando, Florida, October 15-20, 1989.

1.8.1 Optical Switching and Nonlinear Index in GaAs and MQW Waveguides

Femtosecond investigations of bandedge nonlinear dynamics in guided wave devices are directly relevant to the development of high-speed all-optical switches. Our group has recently developed a novel technique for nonlinear index measurements. This technique uses time division multiplexing to perform high resolution transient interferometric measurements on a nonlinear index. This approach reduces contributions from thermal and acoustic artifacts which traditionally limit interferometric measurements. The system can detect phase shifts as small as $\lambda/1000$.[17]

For studies in semiconductor devices, we took measurements using a synchronously-pumped, tunable femtosecond dye laser system. Using the dye Styryl 9, we obtained 430 fs pulses in the wavelength range 780 nm to 880 nm. We performed systematic studies to characterize the nonlinear response in AlGaAs ridge waveguide devices.[18] We took the first direct measurement of the wavelength dependence of the instantaneous nonlinear index in this semiconductor. The results show values of n_2 in the range of 10^{-12}cm/W. Femtosecond time-resolved studies permit us to separate the real from the virtual contributions to the nonlinear index.

In one area of our investigation, we study new materials for all-optical switching. Other materials we are currently investigating include multiple quantum well (MGW) GaAs waveguides. After performing preliminary measurements of femtosecond nonlinear effects, we are now in the process of systematically characterizating the wavelength dependence of the nonlinear index as well as its linear optical properties.

A second material system of interest to us is nonlinear optical polymers. We have recently begun studies in collaboration with investigators at Bell Communications Research to characterize the nonlinear index and absorption behavior in polydiacetelene waveguides. Nonlinear optical polymers are a rapidly emerging research area, and the combination of Bellcore's unique materials growth and fabrication capabilities with our capabilities in femtosecond optics will permit state-of-the-art studies to be performed.

1.8.2 Time Domain Optoelectronic Diagnostics

Femtosecond dye laser systems as well as future generation Ti:Al_2O_3 solid state laser systems can provide a tunable source of femtosecond pulses in the near IR wavelength range. This technology can form the basis for a wide range of diagnostics in optoelectronic devices. Diagnostics of optical waveguide devices can be divided roughly into two catagories, measurement of nonlinear and linear properties.

As discussed in the previous section, high peak intensities associated with short pulses can be applied to study nonlinear index or n_2 effects in waveguide devices. In addition, other nonlinear effects such as two photon absorption can also be important in waveguide devices. We have measured the two-photon absorption coefficient β in GaAs waveguide devices. Since two-photon absorption produces excited carrier populations, this is an important limiting process for almost any application requiring high intensities in a waveguide.

In addition to nonlinear properties, we can also develop time domain techniques to measure linear absorption, group velocity, and dispersion. Since femtosecond pulse durations have a spatial extent which is less than the cavity round-trip of most waveguide devices, the transient linear response can be measured. For example, if a short pulse is

---

[17] M.J. LaGasse, K.K. Anderson, H.A. Haus, and J.G. Fujimoto, "Femtosecond All-Optical Switching in AlGaAs Waveguides Using a Single Arm Interferometer," *Opt. Lett.* 14:314 (1989).

[18] M.J. LaGasse, K.K. Anderson, C.A. Wang, H.A. Haus, and J.G. Fujimoto, "Femtosecond Measurements of the Nonresonant Nonlinear Index in AlGaAs," *Appl. Phys. Lett.* 56:417 (1990).

injected into the waveguide, the pulse will be reflected internally within the device and several echoes will be emitted corresponding to multiple round-trip paths through the device. Using a cross-correlation technique, the time resolved behavior of the echoes can be measured. The decay of the echoes contains information about the facet reflectivity and absorption of the device. The delay time or time of flight between the echoes gives the group velocity dispersion. Finally, measurements performed as a function of wavelength permit us to characterize absorption versus wavelength and group velocity dispersion. We have used GaAs passive waveguide devices to demonstrate these techniques.

By extending techniques further, we should be able to measure a wide range of optoelectronic device properties. With development of more compact and cost effective solid state tunable wavelength femtosecond lasers, a time domain optoelectronic diagnostic technology can become a viable alternative to continuous wave and other diagnostic approaches currently used for device characterization.

1.9 Image Potential and Electron Dynamics in Metals

Sponsors

Joint Services Electronics Program
Contract DAAL03-89-C-0001
National Science Foundation
Grant ECS-85-52701
U.S. Air Force - Office of Scientific Research
Contract F49620-88-C-0089

Project Staff

Professor James G. Fujimoto, Robert W. Schoenlein, Morrison Ulman

An improved understanding of electron dynamics in metals and at metal-semiconductor interfaces is necessary for the development of high speed electronic devices. Semiconductors and metals are the major constituents of devices. As device speeds increase with the advent of new high electron mobility and quantum transport effects in semiconductors, dynamic processes in metals will also become an important factor in affecting device performances. Since the density of electrons in metals is high, nonequilibrium processes and excited state dynamics occur extremely rapidly. Femtosecond optical measurement, with its high sensitivity and ultrafast temporal resolution, provide one of the few techniques for directly measuring dynamical processes in metals.

We have continued our investigation of the transient dynamics of image potential states in metals. The image potential state has been a topic of recent active investigation in surface science. Image potential occurs when an electron, excited from the surface of a metal, is bound to its image charge in the bulk.[19] The electronic states form a Rydberg-like series somewhat analogous to a two-dimensional electron gas in semiconductor quantum wells. Because the electronic wavefunction is maximized outside the metal surface, scattering processes are reduced, and the electron relaxes by tunneling from the image potential state to bulk states. Thus, the image potential state provides an important model system for investigating electron dynamics in metals.

Working in collaboration with researchers from General Motors Research Laboratories, our previous investigations combined femtosecond pump-probe spectroscopy with photoemission techniques to directly measure, for the first time, the lifetime of an image potential state in a metal.[20] In our studies, ultraviolet femtosecond pulses are used to populate the image potential states. The image potential dynamics are probed by photoemitting electrons out of these levels with a visible femtosecond pulse delayed in

---

[19] D. Straub and F.J. Himpsel, "Identification of Image-Potential Surface States on Metals," *Phys. Rev. Lett.* 52:1922-1924 (1984).

[20] R.W. Schoenlein, J.G. Fujimoto, G.L. Eesley, and T.W. Capehart, "Femtosecond Studies of Image-Potential Dynamics in Metals," *Phys. Rev. Lett.* 61:2596 (1988).

time. The energy spectrum of the photoemitted electrons is measured with a cylindrical mirror analyzer. This approach has allowed us to map the population of image potential states as a function of both time and electron energy. Studies performed on the the surface of Ag(100) revealed an $n = 1$ image potential lifetime of 15–35 fs, representing one of the highest time resolution transient photoemission measurements ever made.

To test theoretical models for image potential electron dynamics, it is important to systematically study different states in the Rydberg series using different metal surfaces. For the image potential state to be long-lived, the image potential energy must occur in a range where there is a gap of bulk states. The image potential electron must be confined in the potential barrier outside the metal from the crystal lattice by Bragg reflection. In this case, the image potential state relaxes by inelastic scattering. Conversely, if a different metal surface is examined where the image potential is resonant with allowed bulk states, then the dominant relaxation channel is elastic scattering with electronic states in the bulk.

We have continued our earlier measuring efforts to examine the $n = 1$ and $n = 2$ image potential dyanmics in Ag(100) and Ag(111).[21] These experimental results can help explain differences in theoretical models based on simple single partical wavefunction analysis versus many-body effects. The image potential state has well defined quantum properties, providing an attractive model system for studying electronic quantum effects in metals.

1.10 Laser Medicine

Sponsors

Massachusetts General Hospital
Contract N00014-86K-0117
National Institutes of Health
Grant 2-RO1-GM35459

Project Staff

Dr. Jyhpyng Wang, David Huang, Professor James G. Fujimoto, Professor Erich P. Ippen

1.10.1 Heterodyne Ranging for Opthalmic Diagnostics

The ability of excimer lasers to remove corneal tissue in submicron increments has led to interest in lasers in keratorefractive surgery. In this technique, the curvature or refractive power of the cornea is altered surgically to achieve refractive correction of a person's vision without glasses. To exploit the potential for micron-precision ablation control available with laser surgery requires a precise method for monitoring the incision depth. Previously, we had developed a femtosecond optical ranging technique for measurement of corneal incision depth.[22] This technique is analogous to those used in radar or ultrasound except that short pulses of light are used to perform precise measurements of distance. Using this technique in corneal and intra-ocular surgery, distances in the eye can be measured noninvasively, i.e., without contact with the eye. Although this technique has achieved high sensitivity measurement performance, it required use of ultrashort pulse femtosecond lasers, and thus has limited potential for clinical applications.

Our recent research has focused on development of an alternate technique employing a short coherent length light source (AR-coated laser diode) and optical heterodyne detection to perform optical ranging. This method achieves measurement with longitudinal and transverse resolutions (10 μm

[21] R.W. Schoenlein, J.G. Fujimoto, G.L. Eesley, and T.W. Capehart, "Femtosecond Image-Potential Dynamics in Metals: n = 2," *Phys. Rev. B* 41:5436-5439 (1990).

[22] D. Stern, W.Z. Lin, C.A. Puliafito, and J.G. Fujimoto, "Femtosecond Optical Ranging of Corneal Incision Depth," *Inv. Ophthal. Vis. Sci.* 30:99-104 (1989).

Chapter 1. Statistical Mechanics of Surface Systems and Quantum-Correlated Systems

Academic and Research Staff

Professor A. Nihat Berker, Dr. Joseph O. Indekeu

Graduate Students

William Hoston, Kenneth Hui, John F. Marko, Roland Netz

Undergraduate Students

Joseph E. Hilliard, Galen T. Pickett

Technical and Support Staff

Imadiel Ariel

1.1 Introduction

Sponsor

Joint Services Electronics Program
Contract DAAL03-89-C-0001

Correlated fluctuations play an important role in systems with electronic and structural degrees of freedom. This role is most ubiquitous at phase transitions, but is also considerable away from phase transitions, extending down to the lowest temperatures due to quantum mechanics. The renormalization-group method is a new calculational method that can systematically deal with correlated fluctuations at each successive scale length. Since we can include even the consequences of defects, for the first time we can obtain predictive microscopic theories for realistic systems.

1.2 Finite-Temperature Phase Diagram of Vicinal Si(100) Surfaces

Project Staff

Professor A. Nihat Berker

With the collaboration of Professor John D. Joannopoulos and Dr. Oscar L. Alerhand, we have combined electronic energy calculations and such statistical mechanics to obtain ab initio descriptions of finite-temperature semiconductor surfaces and interfaces. The entropy, free energy, and other properties have been evaluated for the silicon (100) surface. The single-step/double-step phase diagram in the variables of crystal cut angle and temperature, as well as other observable properties such as step profiles, are predicted in very good agreement with ongoing experiments. Contrary to previous suggestions that only double-layer steps should appear on the equilibrium surface, it is predicted that the single-layer stepped surface is at equilibrium for small misorientation angles. This structure is stabilized by strain relaxation and by the thermal roughening of the steps. For annealed surfaces, the critical angle at which the transition between the single- and double-layered stepped surface occurs is calculated to be $\theta_c \approx 2°$.

1.3 Absence of First-Order Phase Transitions in Physical Surface Systems

Project Staff

Professor A. Nihat Berker, Kenneth Hui

Most recently, we made a theoretical prediction using the renormalization-group method that appears to have general and far-reaching consequences: we discovered that even an infinitesimal amount of randomness in interactions (e.g., distribution of defects) in

surface systems, converts first-order phase transitions, characterized by discontinuities, to second-order phase transitions, characterized by infinite reponse functions. In bulk systems, as (calculable) threshold randomness is needed for this conversion to occur. This general prediction appears to be supported by experiments on doped $KMnF_3$.

1.4 New Orderings in Systems with Competing Interactions

Project Staff

Professor A. Nihat Berker, William Hoston, Roland Netz

Our studies of realistic, complex systems with competing interactions have led to several new results. We have recently developed a new method that blends Monte Carlo simulation and mean-field theory. We are able to distinguish, for the first time, the effect of dimensionality on frustrated magnetic systems. We have obtained two ordered phases that nevertheless have considerable entropy. Also, we have recently obtained novel phases and multicritical points in systems with competing dipolar and quadrupolar interactions.

Publications

Alerhand, O.L., A.N. Berker J.D. Joannopoulos, D. Vanderbilt, R.J. Hamers, and J.E. Demuth. "Finite-Temperature Phase Diagram of Vicinal Si(100) Surfaces." Submitted to *Phys. Rev. Lett.* (1989).

Berker, A.N. "Harris Criterion for Direct and Orthogonal Quenched Randomness." Submitted to *Phys. Rev. B* (1990).

Hilliard, J.E. *Monte Carlo Simulation of a One-Dimensional Ising System with Competing Interactions Using Domain Walls.* S.B. thesis, Dept. of Physics, MIT, 1989.

Hui, K., and A.N. Berker. "Random Field Mechanism in Random-Bond Multicritical Systems." *Phys. Rev. Lett.* 62:2507 (1989).

Hui, K. "Domain Wall Study of the Stacked Frustrated Triangular Lattice." Submitted to *Phys Rev. Lett.* (1989).

Hui, K. *Quenched Disorder and Competing Interactions in Spin Systems.* Ph.D. diss. Dept. of Physics, MIT, 1989.

Marko, J.F. *On Structure and Scaling at First- and Second-Order Phase Transitions.* Ph.D. diss. Dept. of Physics, MIT, 1989.

Marko, J.F. "Exact Pair Correlations in a One-Dimensional Fluid of Hard Cores with Orientational and Translational Degrees of Freedom." *Phys. Rev. Lett.* 62:543 (1989).

Marko, J.F. "First-Order Phase Transitions in the Hard-Ellipsoid Fluid from Variationally Optimized Direct Pair Correlations." *Phys. Rev. A* 39:2050 (1989).

McKay, S.R., and A.N. Berker. "Magnetization of the d-Dimensional Random-Field Ising Model: An Intermediate Critical Dimension." In *New Trends in Magnetism.* Ed. S.M. Rezende. Teaneck, New Jersey: World Scientific, 1989.

Pickett, G.T. *Asymptotic Behavior of the Spectrum of Generalized Dimensions in Multifractal Tree Growth.* S.B. thesis. Dept. of Physics, MIT, 1989.

Chapter 2. X-Ray Diffuse Scattering

Academic and Research Staff

Professor Robert J. Birgeneau, Dr. Kenneth Blum, Dr. Joel Brock

Graduate Students

Kenneth Evans-Lutterodt, Hawoong Hong, Alan Mak, Do-Young Noh, William Nuttall

Technical and Support Staff

Elizabeth M. Salvucci

2.1 Introduction

Sponsor

Joint Services Electronics Program
DAAL03-89-C-0001

In this research program, we use modern x-ray scattering techniques to study structures and phase transitions in thin films and on surfaces. We have two principal experimental facilities, one at MIT and the other at the National Synchrotron Light Source at Brookhaven National Laboratory. At MIT, we have four high-resolution computer-controlled x-ray spectrometers using high intensity rotating anode x-ray generators. The angular resolution can be made as fine as 1.8 seconds of arc, which enables us to probe the development of order from distances of the order of the x-ray wavelength, ~ 1Å, up to 30,000 Å. The sample temperature can be varied between 2 K and 500 K with a relative accuracy of 2×10^{-3} K. At the National Synchrotron Light Source at Brookhaven National Laboratory, we have, in collaboration with IBM, three fully instrumented beam lines. Two of these beam lines allow studies with photons varying in energy between 3 and 12 keV; the third has a fixed energy of 18 keV. These facilities make possible high resolution scattering experiments with a flux more than three orders of magnitude larger than that from a rotating anode x-ray generator, opening up a new generation of experiments.

As part of this JSEP program, we have built an x-ray compatible high vacuum single crystal apparatus. This enables us to use synchrotron radiation to study the structures and transitions occuring at a single surface, and, indeed, such experiments are now becoming routine. Our current experiments in this program are concentrated on the phases and phase transitions of metal and semiconductor surfaces and surface overlayers.

2.2 Metal Surface Studies

We have carried out detailed studies of the reconstruction of the (110) surface of gold: Au(110). Many noble metal facets are known to favor reconstructed structures at low temperatures. Further, at some temperature T_c a reconstructed surface will typically undergo a reversible "deconstruction" to a high temperature structure which is no longer reconstructed. One such transition which has been studied theoretically as well as with electron diffraction is the Au(110) 1×2 to 1×1 deconstruction. While the "missing row" model of the reconstructed 1×2 surface is well established, the nature of the deconstruction transition itself remains controversial.

Previous work by our group has demonstrated that x-ray scattering is an effective means of studying surface phase transitions. Specifically, the lineshapes of bulk-forbidden surface peaks provide information about the surface height-height (or step-step) correlation functions and are thus a sensitive probe of the surface roughening transition. This transition is characterized by a proliferation of atomic steps which results in logarithmically divergent height fluctuations of the crystalline surface. We have carried out

glancing angle synchrotron x-ray scattering experiments as a means of studying the Au(110) structures and deconstruction transition. The results have been quite remarkable. The so-called 2 × 1 "missing row" model discussed above is a special case of a more general model in which one has (111) microfacets on the Au(110) surface. More extended microfacets can lead to reconstructions with longer periods: 1 × 3, 1 × 4, 1 × 5, etc., and these are very close in energy to the 1 × 2.

In our first set of experiments, the stable phase of the specific Au(110) surface turned out to be 1 × 3 rather than 1 × 2. The basic structure and the possible step excitations are shown in figure 1. For this structure superlattice peaks occur at (0 0 ℓ/3) positions. We find that at 485°C the surface undergoes a continuous, reversible transition. At this transition the 1 × 3 long range order is lost and the local period becomes incommensurate. This behavior results from the proliferation of atomic steps (such as those shown in figure 1b and 1c), which act as domain walls between coherent regions of the reconstructed surface. In fact, by further studies we can determine that both types of steps are present. This means that the 1 × 3 surface both deconstructs and roughens simultaneously.

After further treatment of this same Au crystal, we were able to obtain a stable 1 × 2 phase on the (110) surface. This latter structure is the one most commonly observed in previous experiments. The deconstructive transition of this surface appears to be fundamentally different from that of the 1 × 3 phase. First, the structure remains commensurate even in the disordered phase. Second, there is no evidence of roughening. Third, we have some indication of 2D Ising critical behavior. Further analysis and measurements are required to elucidate the 1 × 2 deconstruction fully.

2.3 Semiconductor Surface Studies

We have investigated the surface disordering transition of Ge (111) near the bulk melting point. The experiment was performed at the National Synchrotron Light Source beamline X20A during the summer of 1989. Our observation was made on Ge wafers resistively heated inside a surface chamber which has a base pressure of 1.3×10^{-10} torr. The sample surface was prepared by sputtering for 30 minutes and subsequent annealing at the same temperature for one hour. Auger-electron spectroscopy was done in situ to check the surface cleanliness. The sample and surface chamber were oriented such that the in-plane (i.e., grazing incidence) (10) and (20) surface peaks, as well as the (11) bulk peak, were observable.

We have studied the evolution of the (10) and (20) surface peaks between 700 K and 1170 K, finding radical changes in intensity. The surface peaks remain resolution limited

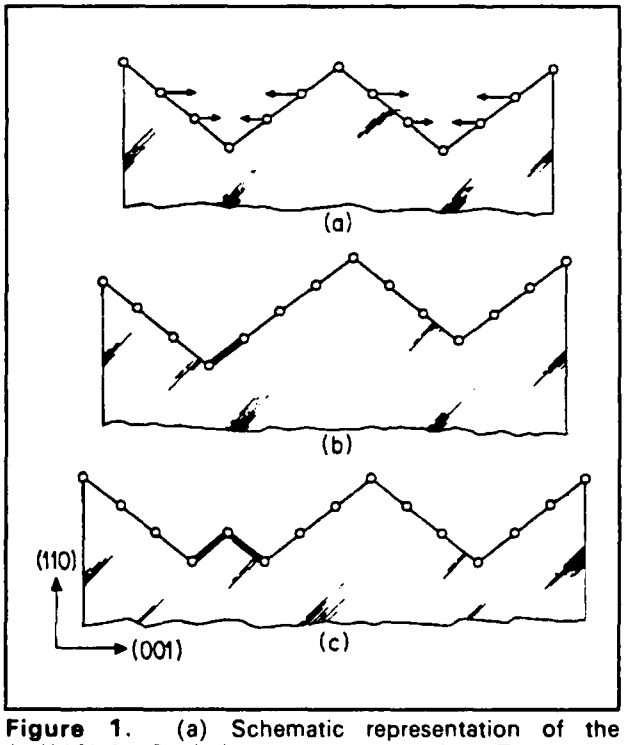

Figure 1. (a) Schematic representation of the Au(110) 1 x 3 missing-row reconstruction. The arrows indicate the southward atomic distrotions observed in the second and third rows from the surface. (b) A single atomic step thermal excitation of the 1 x 3 surface. (c) A paried-step thermal excitation of the 1 x 3 surface.

in the radial direction and the transverse widths stay the same throughout the entire temperature range. As the temperature goes up from 700 K, the intensity of the (10) surface peak decreases exponentially with a Debye-Waller factor of 0.001 K^{-1}. At about 1000 K the rate of decrease of the (10) peak intensity per degree K intensifies. The peak intensity goes through a minimum at about 1100 K and then recovers partially. The transition shown here is reversible with temperature, indicating that it is indeed an equilibrium phase transition. Similar behavior is observed for the (20) surface peak. We have also looked for signs of a surface fluid layer which should manifest itself as a broad ring in reciprocal space, but found no indication of such a layer. Subsequent to the x-ray scattering experiment, we have performed mass spectroscopy measurement on some Ge(111) samples. Each sample was placed one inch away from and with the normal pointing towards the probe. Our data show that there is an exodus of Ge atoms from the surface starting at about 1050 K.

None of the existing models of surface disordering — surface roughening and surface melting — can explain the data. The partial recovery of the surface peak intensity at about 100 K below bulk melting is particularly intriguing. We propose a model which would give a surface peak intensity that is consistent with our observation. A Ge crystal with an ideally terminated (111) surface consists of bilayers of atoms, stacked in an ..ABCABC.. sequence. The structure factor is identically zero at the surface peak position in reciprocal space because the scattering from every three bilayers of atoms exactly cancel. However, the penetration depth of x-rays in the direction normal to the surface is drastically reduced at grazing incidence, due to absorption and total internal reflection. The magnitude of the wave amplitude caused by a layer is maximum at the surface, dropping quickly as one moves into the bulk. As a result the sum of wave amplitudes from every three bilayers is nonzero: the amplitude from the top layers dominates that from below. Suppose that at 1000 K atoms on the sample surface pop-out randomly, leaving vacant sites behind. This reduces the amplitude from the top layer of atoms. The net scattering intensity from the top three bilayers of Ge atoms reduces due to more effective cancellation. At 1100 K, the cancellation is optimized. At higher temperature, the random vacancy at the surface layer may be so large that the amplitude from the bottom layers now dominates. Since intensity is proportional to the modulus squared of the total wave amplitude from every layer, the intensity starts to increase once the random vacancy exceeds some critical value. In this model there is no broadening of the surface peaks, which is consistent with our observation. The mass spectroscopy measurement also supports this picture. Of course, this model is by no means unique. Further studies are required.

2.4 Rare Gases in Graphite

We have studied the phases and the phase transitions for a xenon solid layer on graphite in the monolayer coverage regime. The incommensurate solid undergoes the sequence of transitions: aligned → rotated → reentrant aligned, before the solid transforms into the commensurate solid. The current theory of orientational epitaxy correctly predicts only the point at which the rotation to the reentrant aligned phases occurs. None of the current theories can explain the whole picture of orientational epitaxy. Neither the high temperature aligned solid nor the reduction of the rotation angle from that of the static prediction are explained.

The reentrant aligned phase at low temperatures is an incommensurate solid with a network of superlight domain walls. The observed first-order phase transition can be explained within the domain-wall theory. The incommensurability at constant coverage decreases approximately as $[(T - T_0)/T_0]^{1/3}$ until the first order C-IC transition point is hit. This one-third power law is close to the behavior seen for Kr on graphite following a similar thermodynamic pathway.

We estimated the potential corrugation of the surface adsorption from the intensity ratios between the main and satellite peaks in the domain-wall incommensurate phase. The corrugation of the potential estimated was near the one predicted by Steele. Along with the estimation from the onset of the rotated

phase, we set the limits for the dimensionless wall width, $36 < \ell_0 < 42$.

At low temperatures the xenon layer on vermicular graphite did not transform into the commensurate phase as on the single-crystal substrate. Instead, the xenon layer seems to have a pinned domain-wall network due to defects.

2.5 Publications

Evans-Lutterodt K., R.J. Birgeneau, E.D. Specht, J.W. Chung, J.D. Brock, M.S. Altman, P.J. Estrup, I.K. Robinson, and A.A. MacDowell. "X-Ray Study of W (001) With and Without Hydrogen." *J. Vac. Sci. Technol. A* 7:2209 (1989).

Evans-Lutterodt, K.W. *Synchrotron X-ray Diffraction Studies of Surface Phase Transitions.* Ph.D. diss. Dept. of Physics, MIT, 1989.

Held G. A., J.L. Jordan-Sweet, P.M. Horn, A. Mak, and R.J. Birgeneau. "X-ray Scattering of the Deconstruction and Thermal Roughening of the Au(110)1 x 3 Reconstructed Surface." *Solid State Comm.* 72:37 (1989).

Held G. A., J.L. Jordan-Sweet, P.M. Horn, A. Mak, and R.J. Birgeneau. "Disordering Transitions of Metal Surfaces." *J. de Physique* Colleque C7(50):245 (1989).

Hong, H., and R.J. Birgeneau. "X-ray Diffraction Study of the Structure of Xenon Multilayers on Single Crystal Graphite." *Z. Phys. B* 77:413 (1989).

Hong, H., C.J. Peters, Mak A., R.J. Birgeneau, P.M. Horn, and H. Suematsu. "Synchrotron X-ray Study of the Structures and Phase Transitions of Monolayer Xenon on Single-Crystal Graphite." *Phys. Rev. B* 40:4797 (1989).

Robinson I.K., A.A. MacDowell, M.S. Altman, P.J. Estrup, Evans-Lutterodt K., J.D. Brock, and R.J. Birgeneau. "Order-Disorder Transition of the W (001) Surface." *Phys. Rev. Lett.* 62:1294 (1989).

Chapter 3. Semiconductor Surface Studies

Academic and Research Staff

Professor John D. Joannopoulos, Dr. Efthimios Kaxiras, Dr. Oscar L. Alerhand

Graduate Students

Tomas A. Arias, Mark Needels, Andrew M. Rappe, Eugen G. Tarnow, Jing Wang

3.1 Introduction

Sponsor

Joint Services Electronics Program
Contract DAAL03-89-C-0001

Understanding the properties of surfaces of solids and the interactions of atoms and molecules with surfaces is extremely important from both a technological and academic point of view. The recent advent of ultrahigh vacuum technology has made microscopic studies of well-characterized surface systems possible. The way atoms move to reduce surface energy, the number of layers of atoms involved in this reduction, the electronic and vibrational states that result from this movement, and the final symmetry of the surface layer are all important in achieving a fundamental and microscopic understanding of the nature of clean surfaces, chemisorption processes, and the initial stages of interface formation.

The theoretical problems associated with surface systems are quite complex. We are currently, however, beginning to solve for the properties of these real surfaces systems (rather than for simple mathematical models). In particular, we continue to pursue our goal of calculating the total ground-state energy of a surface system from "first principles," to provide accurate theoretical predictions of surface geometries. In this program, we are concentrating our efforts on the areas of surface growth, surface reconstruction geometries, structural phase transitions, and chemisorption.

3.2 Thermal Amplitudes of Surface Atoms

The vibrational excitations of semiconductor surfaces provide a direct probe of the structural and bonding properties that result from their reconstruction. Moreover, studies of the vibrational properties of surfaces are necessary to understand the dynamical processes that occur on these surfaces (such as kinetics of adsorbates, diffusion and desorption, epitaxial growth, and possibly surface melting). The thermal fluctuations of the surface atoms are directly related to these phenomena. Furthermore, the analysis of a number of experimental probes requires a detailed knowledge of the vibrational amplitudes and correlations of the surface atoms. The Debye-Waller factors, which appear in the expressions for the intensity of radiation scattered from a surface, and the displacement-displacement correlations of the surface atoms enter into the interpretation of ion scattering and other experiments.

New developments in a number of experimental techniques for studying vibrational properties of surfaces have generated further interest, the need for realistic calculations, and better theoretical understanding. These include He-atom scattering, high-resolution electron-energy-loss spectroscopy, surface infrared spectroscopy, medium- and high-energy ion scattering, and surface extended x-ray-absorption fine-structure experiments. From a theoretical point of view, an underlying formalism for surfaces exists within the general framework of the theory of lattice dynamics, but we have made a few realistic calculations for specific surfaces.

In this work, we have made calculations of the atomic displacement-displacement correlation functions for atoms on the Si(111)

2×1 and Si(001) 2×1 surfaces. Both of these surfaces have been the subject of intense research for many years, and even though we have made considerable progress, several questions regarding their structure and basic excitations remain unresolved. Using a semi-empirical tight-binding theory for structural energies in Si, we investigate the thermal fluctuations of the atoms on these surfaces. Specifically, we determine the anisotropy of the vibrational amplitudes of the surface atoms between vibrations parallel and normal to the surface plane, their temperature dependence, and the interatomic vibrational correlations.

The Si(111) 2×1 surface is currenlty understood in terms of a π-bonding chain model. According to this model, the surface reconstructs by forming zigzag chains of surface atoms that run parallel to each other. The bonding along the chain is provided by the π interaction between the surface electrons. Figure 1 shows a side view of the Si(111) 2×1 surface. The chain model also helps us understand the unique vibrational properties observed on this surface. Its lattice dynamics are dominated by the chain geometry and the strong coupling between the electronic surface states and the structural degrees of freedom of the zigzag chains. In fact, the most salient features in the surface phonon spectrum are related to modes that have the same form and elementary vibrational excitations of the surface zigzag chains.

The appearance of a small-wavelength surface phonon with an unusually low energy is particularly relevant to the thermal fluctuations of the surface atoms. Indeed, one of the main reasons for this study is to investigate the thermal effects of this mode. This intrinsic vibration of the surface is dispersionless across the surface Brillouin zone, having an energy of $\hbar\omega = 10$ meV. Near the zone edge, it is located well below the acoustic continuum. Because of the low energy of this phonon and its lack of dispersion (leading to a large contribution to the phonon density of states at that energy), this mode is thermally populated with a large probability. Thus, one might expect that the vibrational amplitudes of the surface atoms on Si(111) 2×1 would be greatly enhanced.

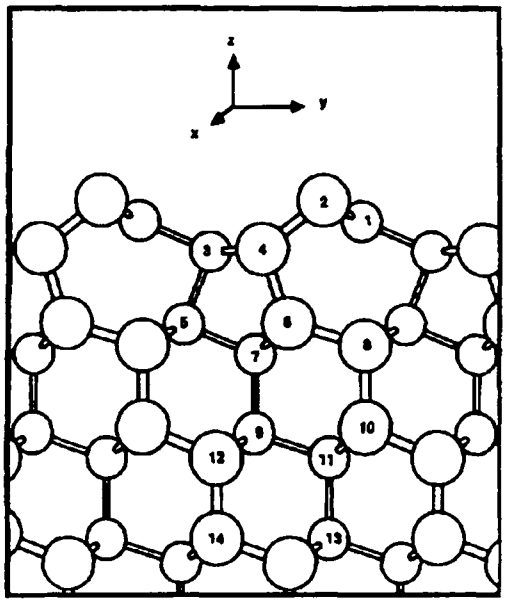

Figure 1. Side view of the π-bonded chain model of Si(111) 2×1. The two surface atoms, numbered 1 and 2, form zigzag chains that run parallel to the [112] direction (into the page); these chains are tilted with up (2) and down (1) atoms.

In contrast with the result for Si(111) 2×1, this low-energy small-wavelength surface phonon does not appear in the phonon spectrum of Si(001) 2×1. The basic building block in the reconstruction of Si(001) involves the formation of surface dimers between two neighboring surface atoms, halving the number of dangling bonds on the surface. Figure 2 shows a side view of the Si(001) 2×1 surface. The surface dimers do not remain symmetrical, tilting so that each dimer is formed by an up and down atom. With this model, we can understand the different periodicities observed on the surface [2×1, p(2×2) and c(4×2)] in terms of different ordered arrangements of the tilted surface dimers. We find that the normal modes of vibration of the higher-order reconstructions p(2×2) and c(4×2) are essentially the same as for the 2×1 reconstruction, since the surface phonons are essentially characterized by the vibrations of the nearly isolated surface dimers. Consequently, we concentrate only on the 2×1 reconstruction.

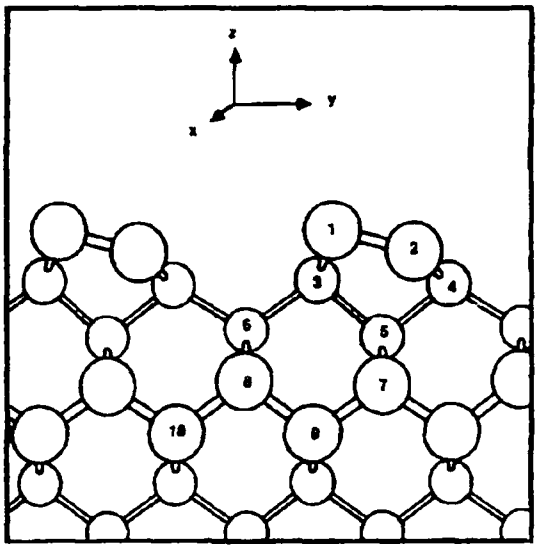

Figure 2. Side view of the tilted dimer model of Si(001)2 × 1.

In the harmonic approximation, the correlation function between the displacement $u_{i\nu}$ of atom i along the direction μ (from its equilibrium position), and the displacement of atom $u_{j\nu}$ of atom j along the direction v, can be expressed in terms of the phonons or normal modes of the system:

$$\langle u_{i\mu} u_{j\nu} \rangle = \frac{h}{2N(M_i M_j)^{1/2}}$$

$$\times \sum_{q,\lambda} \frac{e_{i\mu}(q,\lambda) e^{*}_{j\nu}(q,\lambda)}{\omega_\lambda(q)}$$

$$\times e^{iq(R_i - R_j)}\{1 + 2n[\omega_\lambda(q)]\}, \qquad (1)$$

where the sum is over normal modes λ and wave vectors q in the Brillouin zone, $\omega_\lambda(q)$ $e(q,\lambda)$ are the phonon frequencies and eigenvectors, respectively, R_i denotes the two-dimensional lattice vector of the surface unit cell where atom i is located, M_i is its mass, and N is the number of unit cells within the periodic boundary conditions used in the calculations. The temperature T enters through the Bose-Einstein distribution function $n[\omega]$.

The main difficulty in evaluating eq. (1) is that it requires the knowledge of the phonon energies and eigenvectors of the system over the entire Brillouin zone. Therefore, the calculation of vibrational correlation functions is usually limited to simple systems where the normal modes are determined by symmetry. Also, eq. (1) is usually approximated by low- and high-temperature expansions using models for the dispersion of phonon energies and the density of states, like the Debye model.

To make reliable predictions and to extract microscopic information from the thermal vibrational amplitudes of the system, eq. (1) must accurately represent the system's phonon energies and eigenvectors. For semiconductors surfaces, this representation is further complicated because their reconstruction leads to bonding configurations that can be quite different from the bulk; thus, dynamical properties cannot be simply described using force constants calculated for the bulk and transferred to the surface.

A realistic theory must be used to calculate phonon energies and eigenvectors for each particular reconstructed surface. In this work, we use a formalism based on a semi-empirical tight-binding theory for structural energies in semiconductors. To explain the model briefly, the total energy of the system is expressed in terms of the band-structure energy, an empirical potential energy of interionic interactions, and the Coulomb energy of on-site electronic repulsions. The band-structure energy is calculated using an sp^3 tight binding representation of the valence electrons, and the interionic interactions are approximated with a sum of pairwise potentials. The on-site Coulomb repulsion term for the electrons is added to incorporate the effects of charge transfer. With this model, the dynamical matrix of a system can be calculated using perturbation theory, in which the bare ion-ion forces are renormalized by the electron polarizability; exponentially decaying interactomic forces are generated by the exchange of virtual electron-hole pairs between lattice distortions at different sites on the lattice. Because this approach incorporates the effects of reconstruction into the lattice dynamics of the surface, it successfully pro-

vides a description of the vibrational properties of Si surfaces.

The results of our calculations are presented in figures 3 and 4. Here we notice that for both Si(111) 2 × 1 and Si(001) 2 × 1, the surface atoms have thermal vibrational amplitudes that are larger along the direction perpendicular to the surface plane than parallel to it. This is usually expected, since the surface atoms have reduced coordination normal to the surface. However, we find that the degree of anisotropy between normal and in-plane vibrations is very different for the two surfaces. Indeed, for Si(111) 2 × 1 we find that this anisotropy is quite large (1.8 in the mean-squared amplitudes of vibration), while on Si(001) 2 × 1 the fluctuations of the surface atoms are nearly isotropic. Furthermore, in the case of Si(111) 2 × 1, the anisotropy increases rapidly with increasing temperature, a feature we attribute to the presence of a low-energy dispersionless surface phonon. This large temperature enhancement is not observed for the surface atoms of Si(001) 2 × 1, which does not support a similar low-energy surface phonon. In comparing the atomic vibrational amplitudes on the two surfaces, the most salient feature is that, in the case of Si(111) 2 × 1, the surface atoms have very large amplitudes of vibrations normal to the surface. The difference in the vibrational amplitudes of surface atoms on Si(111) 2 × 1 and Si(001) 2 × 1 shows that the specific microscopic properties of the surface must be considered in the calculation of the atomic vibrational correlation functions.

Specifically, we predict the degree of anisotropy between normal and in-plane vibrations and the difference in vibrational amplitudes between inequivalent surface atoms. Experimental techniques exist that can directly measure these variables. Perhaps the most important contribution of the calculations we have presented here is in their use in the analysis of experiments. Our calculated atomic vibrational amplitude and correlation function results might greatly reduce the uncertainties in the interpretation of scattering experiments that probe the structure of the surface; Debye-Waller factors might also be easily calculated with the information we have provided.

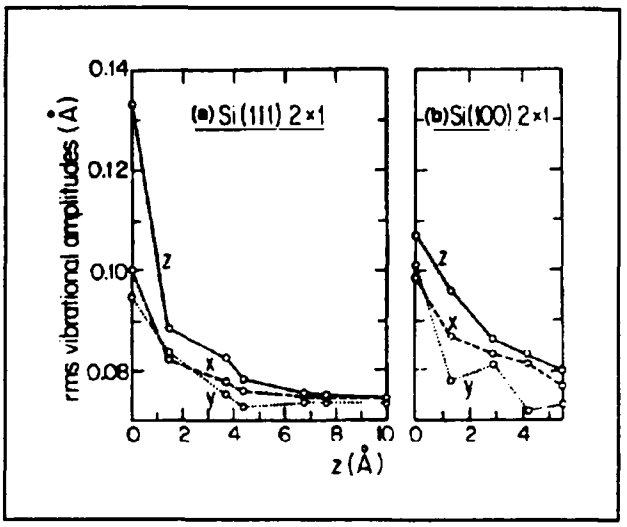

Figure 3. Atomic rms vibrational amplitudes at T= 270K as a function of penetration from the surface for (a) Si(111) 2 × 1 and (b) Si(100) 2 × 1. The Cartesian directions are defined in figures 1 and 2, respectively.

3.3 Heteroepitaxial Growth

Heterostructures of semiconductors, elemental or compound, have recently been the subject of intense study as technologically promising artificial materials. GaAs on Si is a system of particular interest, not only from a technological but also from a theoretical point of view. Usually GaAs growth is initiated on Si substrates oriented along the (100) direction. The quality of the GaAs overlayers is far from ideal with a very high density of defects and dislocations present, presumably due to lattice mismatch and polarity differences. However, it is not known to what degree other interface factors, such as surface reactions or substrate morphology, play an important role in growth inhibition or initiation. These issues are at the core of current growth models of GaAs on Si(100).

In this work, we investigate, from an ab initio theoretical point of view, the possibility of layered growth of GaAs on atomically flat regions (terraces) of the Si surface. We shall focus on the initial stages of growth by considering very low coverages (one to two monolayers) where a number of important issues can be isolated and addressed in detail. For example, what is the structure of the initial monolayers? Are the Ga and As

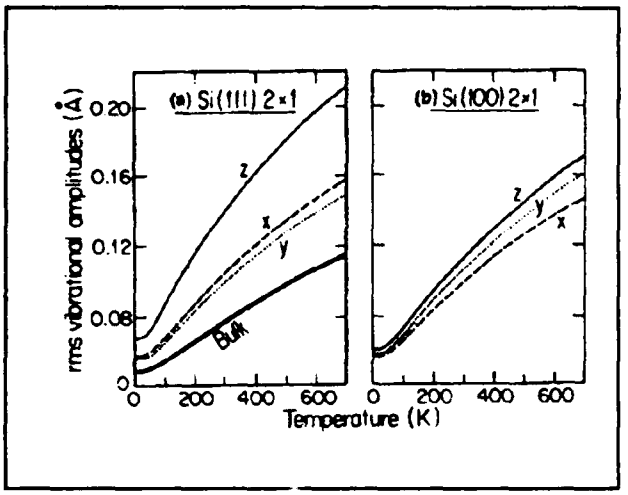

Figure 4. Atomic rms vibrational amplitudes of surface atoms on (a) Si(111) 2 × 1 (surface atom 2) and (b) Si(001) 2 × 1 (surface atom 1) as a function of temperature. The bold line is for a bulk atom.

atoms locally mixed or do they separate into domains of each species? Is the Si surface covered by Ga and As atoms to the largest possible extent at monolayers thickness or do these atoms form GaAs bilayer islands on part of the surface? What is the structure of the initial bilayer of GaAs? Does it resemble that of bulk GaAs with alternating places of Ga and As or does it have a novel structure?

To address the possibility of two-dimensional growth on Si terraces, we consider a slab of Si bounded by (100) surfaces on which we place Ga and As atoms. The issue of interest is the lowest-energy local structure and its effects on prospects for growth. There are two possibilities: the lowest-energy local structure may be the same as the structure of bulk GaAs, so that two-dimensional growth can proceed, or the structure may be different, in which case layered growth of zincblende GaAs will be inhibited. The easiest way to envision formation of the lowest-energy structure is to consider a Si surface covered by a monolayer of one species (corresponding to pre-deposition, for example, of Ga or As) and to introduce some amount of the opposite species. One must then consider the possible local atomic configurations and identify the lowest-energy structure. In this sense, the exact relative abundance (chemical potential) of Ga and As atoms is not important, but the presence of both species is crucial.

Each surface layer of the slab is taken to be reconstructed, for simplicity, in the standard (2 × 1) dimer pattern (this choice will be justified below). The Ga and As atoms are placed on the slab in five different ways as shown in figures 5(a)–5(e). The total energies resulting from ab initio calculations allowing these geometries to fully relax, are presented in table 1.

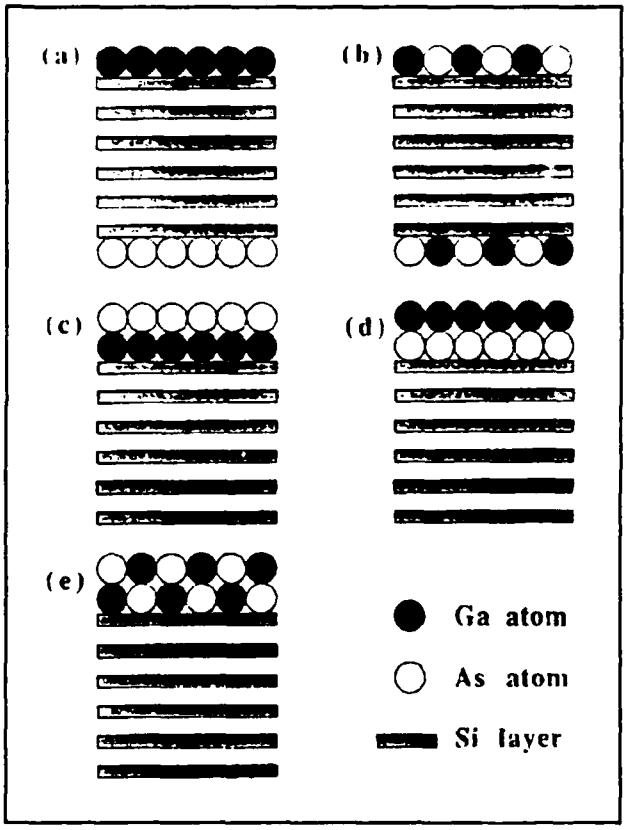

Figure 5. Schematic representation of overlayer arrangements. (a) Pure monolayer coverage, (Ga)[Si](As). (b) Mixed monolayer coverage, (GaAs)[Si](AsGa). (c) Bilayer coverage with pure layers and As-exposed surface, (As)(Ga)[Si]. (d) Same as (c) with Ga-exposed surface, (Ga)(As)[Si]. (e) Bilayer coverage with mixed layers, (GaAs)(AsGa) [Si].

Figure	Configuration	Relative Energy Difference
5(a)	(Ga)[Si](As)	0.8
5(b)	(GaAs)[Si](AsGa)	0.0
5(c)	(As)(Ga)[Si]	2.2
5(d)	(Ga)(As)[Si]	2.8
5(e)	(GaAs)(AsGa)[Si]	1.5

Table 1. Relative energy difference of the various overlayer configurations as depicted in figure 5 in eV/(2X1) SUC.

Based on the energies of the different configurations, a number of important conclusions can be drawn:

1. When the available amount of Ga and As atoms is less than a full monolayer, under equilibrium stoichiometric conditions, it wets the Si surface and formation of thicker GaAs islands is inhibited.

2. At monolayer coverage, the two species of atoms do not separate into pure Ga or pure As domains, but are locally mixed on the Si surface.

3. When GaAs is available in stoichiometric amounts sufficient for bilayer coverage, the equilibrium structure of the bilayers is not a succession of pure Ga and As layers as in bulk GaAs along the (100) direction. Rather, chemical and rehybridization reactions are energetically very favorable, leading to a passivating mixed overlayer configuration. Once this mixed layer is formed, it could persist in a disordered phase even under non-stoichiometric conditions because of its considerable stability. The mixed layer resembles locally a wurtzite structure under large uniaxial stress. A structural barrier (requiring creation of extensive defects at large energy cost) is encountered in reverting from the mixed layer structure to the zincblende structure of bulk GaAs.

This conclusion has important implications: Since the mixed layers have very different structure from the thermodynamically stable zincblende phase of bulk GaAs, the growth of mixed layers on terraces will be undermined by any surface topology which could lead to nucleation of zincblende GaAs. Thus, nucleation centers of zincblende GaAs at specific surface topologies will prevail in the growth process. It is possible to grow bulk GaAs experimentally on vicinal Si(100) surfaces, that is, surfaces with large density of steps. It is likely that surface steps are precisely the topology that nucleates zincblende GaAs, and growth occurs directly on the steps. Indeed, experimental evidence appears to support this view. Search for a possible microscopic mechanism for the initiation of this kind of growth, which involves formation of zincblende GaAs seeds at double-layer steps on the Si surface, is currently in progress.

Chapter 4. Ultralow Temperature Studies of Nanometer Size Semiconductor Devices

Academic and Research Staff

Professor Marc A. Kastner, Professor Dimitri A. Antoniadis, Dr. Stuart B. Field, Professor Henry I. Smith

Visiting Scientists and Research Affiliates

Mordehai Heiblum,[1] Shalom Wind[1]

Graduate Students

Udi Meirav, Samuel L. Park, John H.F. Scott-Thomas

Technical and Support Staff

Angela R. Odoardi

4.1 Project Description

Sponsor

Joint Services Electronics Program
Contract DAAL03-89-C-0001

In the late 1970s, the rapidly improving theoretical description of disordered metals combined with the rapidly evolving technology of submicron lithography to create a new subfield of condensed-matter physics. The electronic properties of artificial structures — which are large compared with atomic size scales but comparable to quantum mechanical coherence lengths — have been shown to be fundamentally different from both those of larger and smaller structures. For this reason, the term "mesoscopic" was coined to differentiate them.

Almost from the start, the hallmark of mesoscopic structures has been the random, noise-like, but reproducible fluctuations in their conductance. These fluctuations were first seen in the insulating regime of one-dimensional field-effect transistors when their Fermi energy was varied. The most dramatic discovery was that, in metallic samples, independent of their size and geometry, the fluctuations had magnitude of order e^2/h in the limit of zero temperature. These Universal Conductance Fluctuations were seen when the magnetic field, Fermi energy, or impurity configuration was varied, consistent with the theory of Altshuler, Lee and Stone.[2]

Recently, we reported the discovery of a new phenomenon in mesoscopic field effect structures. In the same regime where exponentially large random fluctuations had been seen in earlier devices,[2] we found fluctuations which, while still exponentially large, were accurately periodic in the density of the electron gas. We were the first to observe these oscillations in Si MOSFETs[3] fabricated at MIT and in novel GaAs inverted semiconductor-insulator-semiconductor field

---

[1] IBM Thomas J. Watson Research Laboratories.

[2] For a review see M. A. Kastner, R. F. Kwasnick, J. C. Licini, and D. J. Bishop, "Conductance Fluctuations near the Localized-to-Extended Transition in Narrow Si MOSFETs," *Phys. Rev. B* 36: 8015 (1987).

[3] J.F.H. Scott-Thomas, M.A. Kastner, D.A. Antoniadis, H.I. Smith, and S.B. Field, "Si Metal-Oxide Semiconductor Field Effect Transistor with 70-nm Slotted Gates for Study of Quasi-One-Dimensional Quantum Transport," *J. Vac. Sci. Technology B* 6: 1841 (1988); J.F.H. Scott-Thomas, S.B. Field, M.A. Kastner, H.I. Smith, and D.A.

effect transistors ISIS structures fabricated at IBM.[4] An example of the latter is shown in figure 1.

A rich phenomenology is associated with this oscillatory behavior. The conductance is thermally activated between 1 K and about 0.3 K, and the activation energy oscillates with the number of electrons per unit length. At a lower temperature there is a tunneling component which also oscillates. The conductance is highly non-ohmic, showing dramatic threshold behavior with threshold voltage that oscillates out of phase with the conductance. Most surprising of all, the oscillations are independent of magnetic field. This is probably why the phenomenon was not observed earlier by other groups that typically study MODFETs in which the carrier density can not be varied over a wide range. For the quantum Hall effect, the variation of carrier density is equivalent to the variation of magnetic field. This is not the case for our new phenomenon.

The phenomenology suggests that the oscillations result from the opening of an energy gap whenever an integral number of electrons resides in a subsection of the one-dimensional channel. Several models have been proposed to explain the observations. It is probable that the electron-electron interactions are crucial. If so, this will be the first time that many-body effects will have been shown to dominate the behavior of mesoscopic systems.

The silicon device fabrication and part of the GaAs fabrication was sponsored by the National Science Foundation under Grant ECS 88-13250. A portion of the ultralow temperature measurements was sponsored by the Joint Services Electronics Program under Contract DAAL03-89-C-0001.

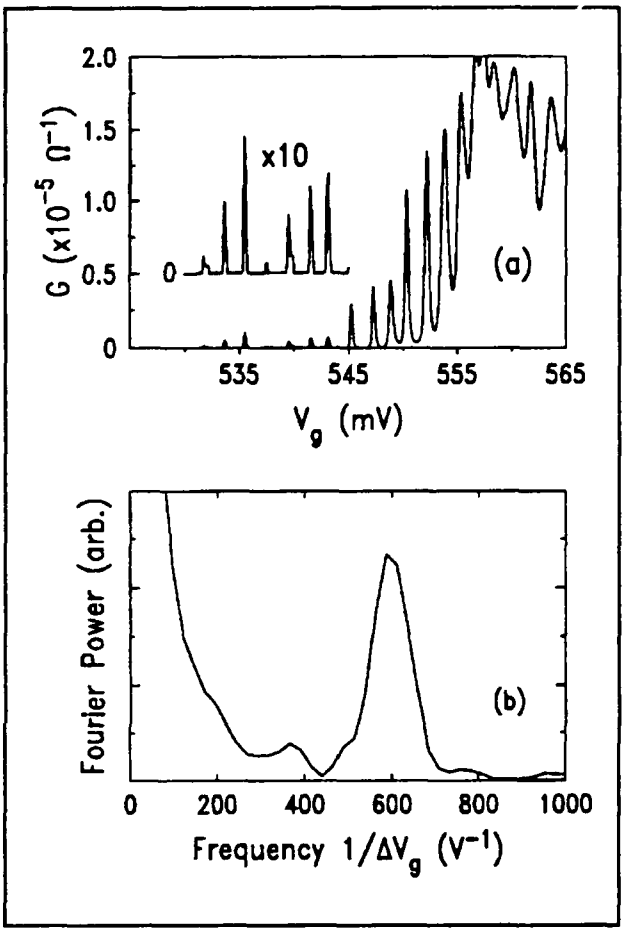

Figure 1. (a) Conductance vs. gate voltage of a narrow channel, 2 μm long, measured at T = 50 mK. The inset shows an expansion of the first few oscillations. (b) Fourier power spectrum of the above. The peak corresponds to a period of $\Delta V \approx 1.7$ mV.

Antoniadis, "Conductance Oscillations Periodic in the Density of a One-Dimensional Electron Gas," *Phys. Rev. Lett.* 62: 583 (1989).

[4] U. Meirav, M.A. Kastner, M. Heiblum, and S.J. Wind, "A One-Dimensional Electron Gas in GaAs: Periodic Conductance-Oscillations as a Function of Density," *Phys. Rev. (Rapid Comm.) B* 40: 5871 (1989); U. Meirav, M. Heiblum, and F. Stern, *Appl. Phys. Lett.* 52: 1268 (1988).

Chapter 5. The Quantum Hall Effect in Narrow MOSFETs

Academic and Research Staff

Professor Patrick A. Lee

Visiting Scientists and Research Affiliates

Dr. Alfred Gold[1]

Graduate Students

Jari Kinaret

Technical and Support Staff

Imadiel Ariel

5.1 Project Description

Sponsor

Joint Services Electronics Program
Contract DAAL03-89-C-0001

We are investigating the conductance of narrow MOSFETs that are subject to a strong magnetic field. This investigation was motivated by an experiment conducted by Professor Marc A. Kastner's group two years ago,[2] in which the group studied the transport properties of narrow MOSFETs (width ~ 500Å) subject to a large magnetic field of 5T to 10T. In these fields, only the lowest few Landau levels — in the quantum Hall regime — are occupied. At the same time, the cyclotron orbit is comparable to the sample width, making the finite size effect of the sample important. The experimentalists observed thresholds for large increases in conductance as a function of magnetic field, as well as ill-defined steps in the conductance of approximately $2e^2/h$. We tackled this problem using both computer simulation and analytic treatment of many-body effects.[3]

We use computer simulation to model disordered conductors subject to a large magnetic field. The model is defined on a tight binding lattice of finite width and length which is extended to infinity in both directions by connecting it to ideal lattices without randomness to simulate the source-drain leads. The novel feature of the model is that the leads are also subject to the same quantizing magnetic fields so that (1) the edge states in the leads consist of Landau level subject to a lateral boundary condition, and (2) the states at the Fermi level are edge states which are bound to the edge and propagate to the right along the upper edge and left along the lower edge. The conductance is then related to the transmission probability of these edge states using the Landauer formula. These transmission probabilities are computed numerically.

When the width of the wire is large compared with the cyclotron radius, the edge states are basically forward scattered in the disorder region so that the transmission probability is unity, leading to quantized Hall conductance of e^2/h. It is only when the width becomes comparable to the cyclotron

---

[1] Department of Physics, University of Munich, Germany.

[2] J. Scott-Thomas, S.B. Field, M.A. Kastner, H.I Smith, and D.A. Antoniades, *Phys. Rev. Lett.* 62:583 (1989).

[3] J. Kinerot and P.A. Lee, to be published.

radius that the edge state can scatter across the width of the sample and is then reflected. The reduction in the transmission probability leads to ordinary metallic conduction. As the field is increased, the simulation shows a threshold for the appearance of quantized steps in the conductance in agreement with the experiment. The simulation also shows that in the step between plateaus, the system behaves as a metal in the sense that it exhibits conductance fluctuations in the order of e^2/h. The period of the fluctuation as given by the condition that the flux through the sample area is a flux quantum just as in universal conductance fluctuation.

The next puzzle to be resolved is understanding why the quantum Hall step is in units of $2e^2/h$. We believe that the $2e^2/h$ step is due to the presence of two degenerate valleys in the silicon interface, which is not resolved. In ordinary two dimensional samples, the valley degeneracy is resolved due to the exchange effect. It is more energetically favorable to occupy one valley first, rather than occupying both valleys equally, because the exchange energy is nonlinear in the density. However, this mechanism will be weakened in narrow wires, because the Landau level is no longer completely flat and it costs kinetic energy to preferentially occupy one valley. We calculated the exchange energy for a model system confined by a parabolic potential demonstrating this competition between kinetic and exchange terms in quasi-one-dimensional MOSFETs. We conclude that the combination of numerical simulation and analytic work to account for the many-body effect gives a quite satisfactory account of the transport properties of a narrow MOSFET wire in a quantizing magnetic field.

Chapter 6. Epitaxy and Step Structures on Semiconductor Surfaces

Academic and Research Staff

Professor Simon G.J. Mochrie

Graduate Student

Douglas A. Abernathy

6.1 Project Description

Sponsor

Joint Services Electronics Program
Contract DAAL03-89-C-0001

Under the Joint Services Electronics Program, we have studied the Pt(001) surface as a model for the behavior of an incommensurate overlayer on a substrate.[1] This research will lead to a more complete understanding of what determines the orientation of a thin film on a substrate.

The (001) surface of platinum, like the (001) surfaces of gold and iridium, exhibits a radical reconstruction in which the topmost layer of atoms forms a hexagonal layer, in spite of the layers of square symmetry beneath. At T = 300 K, the hexagonal overlayer is rotated by 0.75 degrees away from a high symmetry direction of the cubic lattice (the substrate). Our recent synchrotron x-ray measurements have revealed, however, that the overlayer experiences a completely new class of rotational transition at high temperatures. For T > 1670 K, the hexagonal overlayer is aligned with the cubic substrate. The temperature $T_c = 1670$ K marks the onset of rotation, and as the temperature decreases further the rotation angle increases continuously, reaching 0.75° at T = 1300K. Figure 1 shows typical experimental profiles. The two peaks are arranged symmetrically about the high symmetry [1, 1, 0] direction and correspond to positive and negative rotation angles of the overlayer. The accompanying change in the overlayer lattice constant is on the order of one part in 1000.

Current theories of orientational epitaxy predict a definite relationship between the overlayer lattice constant and the rotation angle,[2] but our observations contradict this understanding. Nevertheless, the evolution of rotation angle with temperature follows a power-law behavior (see figure 2). In fact, the observed exponent is one-half, indicative of so-called mean-field behavior. An exponent of one-half is unusual for a two-dimensional phase transition because the effect of fluctuations are expected to be particularly severe in two-dimensions. However, an elegant interpretation is possible: If one supposes that the rotational transition occurs as a result of a rotational elastic constant becoming zero, then by considering the effect of such behavior on the low-energy modes (lattice vibrations) of the Pt overlayer, it emerges that there is no mode that becomes soft as the transition is approached. In other words, there simply are no fluctuations, and character of the transition must be mean-field.[3] With this observation, we can

---

[1] D.L. Abernathy, S.G.J. Mochrie, D.M. Zehner, G. Grübel, and D. Gibbs, "Rotational Transitions of the Pt(001) Surface," unpublished.; D. Gibbs, G. Grübel, D.M. Zehner, D.L. Abernathy, and S.G.J. Mochrie, "Phase Behavior of the Pt(001) Surface: X-Ray Measurements," unpublished.

[2] J.P. McTague and A.D. Novaco, *Phys. Rev. B* 19: 5299 (1979); J. Villain, *Phys. Rev. Lett.* 41:36 (1978); H. Shiba, *J. Phys. Soc. Jap.* 46:1852 (1979), 48:211 (1980).

[3] R.A. Cowley, *Phys. Rev. B* 13: 4877 (1976).

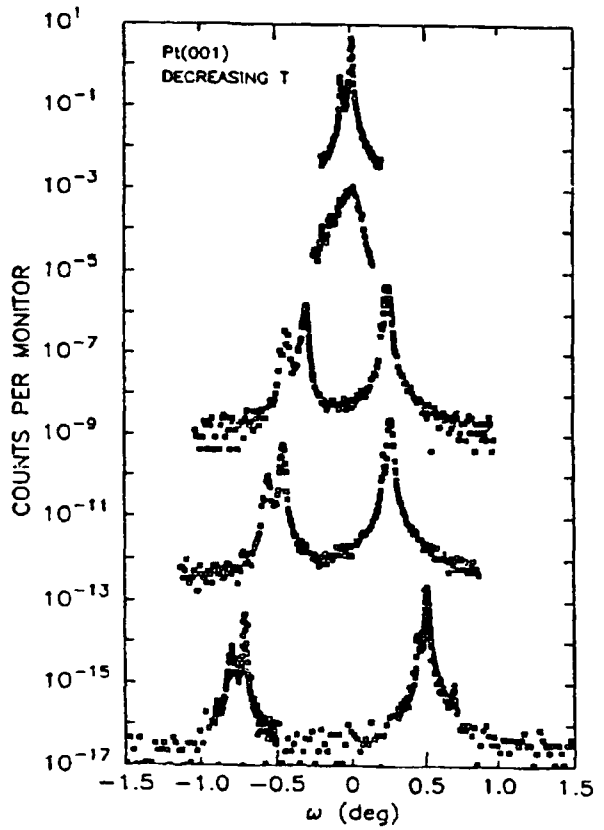

Figure 1. Transverse scans through a near hexagonal peak of the reconstructed Pt(001) surface for temperatures decreasing from the aligned phase (single peak) into the rotated phase (two peaks).

also understand the mean-field character of other high temperature rotational transitions.[4]

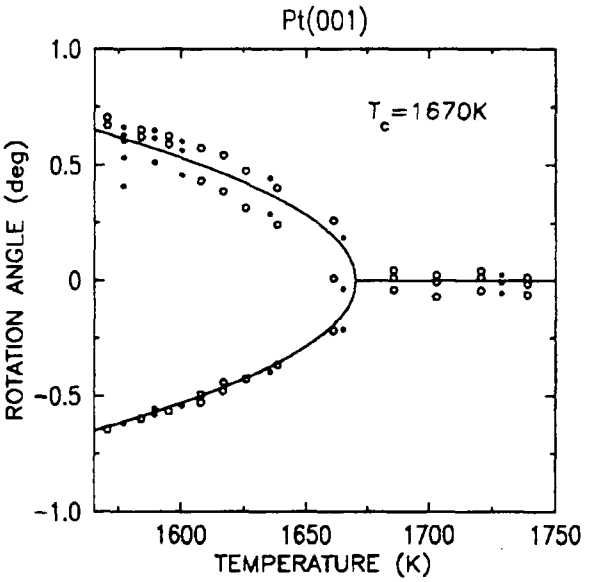

Figure 2. Evolution of the rotation angle vs. temperature for the Pt(001) surface.

[4] K.L. D'Amico, D.E Moncton, E.D. Specht, R.J. Birgeneau, S.E. Nagler and P.M. Horn, *Phys. Rev. Lett.* 53: 2250 (1984).

Chapter 2. Basic Atomic Physics

Academic and Research Staff

Professor Daniel Kleppner, Professor David E. Pritchard, Dr. Min Xiao

Visiting Scientists and Research Affiliates

Dr. Theodore W. Ducas[1]

Graduate Students

Kevin R. Boyce, Pin P. Chang, Eric A. Cornell, Michael W. Courtney, Chris R. Ekstrom, Thomas R. Gentile, Kristian Helmerson, Long Hsu, Barbara J. Hughey, Chun-Ho Iu, Michael A. Joffe, David W. Keith, Robert P. Lutwak, Bruce G. Oldaker, Scott Paine, Ke-Xun Sun, George R. Welch

Undergraduate Students

Deborah Kuchnir, James P. Schwonek, Quentin Turchette

Technical and Support Staff

Carol A. Costa

2.1 Experimental Study of Small Ensembles of Atoms in a Microwave Cavity

Sponsor

Joint Services Electronics Program
Contract DAAL03-89-C-0001

Project Staff

Barbara J. Hughey, Thomas R. Gentile, Dr. Theodore W. Ducas, Professor Daniel Kleppner

Cavity quantum electrodynamics — the study of interactions of individual atoms with quantum fields in cavities — has grown into an active area of quantum optics.[2] A seminal experiment in this area was the inhibition of spontaneous emission of an excited atom, first demonstrated in our laboratory some years ago.[3] During this past year, we have completed a study of the evolution of small ensembles of atoms in a microwave cavity. Our goal is to observe the dynamics of an atom-vacuum system in the quantum regime.

The states of our collective N-atom system are Dicke states.[4] The total atom-field Hamiltonian for the system is[5]

$$H_{tot} = H_A + H_F + H_{AF}$$

$$= \hbar\omega_o D^\circ + \hbar\omega(a^\dagger a + \tfrac{1}{2})$$

$$+ \tfrac{1}{2}\hbar\omega_a(aD^+ + a^\dagger D^-), \qquad (1)$$

---

[1] Department of Physics, Wellesley College, Wellesley, Massachusetts.

[2] S. Haroche and D. Kleppner, *Phys. Today B* 42(1): 24 (1989).

[3] R.G. Hulet, E.S. Hilfer, and D. Kleppner, *Phys. Rev. Lett.* 55: 2137 (1985).

[4] R.H. Dicke, *Phys. Rev. B* 93: 99 (1954).

[5] S. Haroche, in *New Trends in Atomic Physics*, eds. G. Grynberg and R. Stora (Amsterdam: North Holland, 1984), 190.

where H_A and H_F are the atomic and field Hamiltonians, respectively, and H_{AF} describes the atom-field interaction. a and a† are the conventional destruction and creation operators for the electromagnetic field. D^+ and D^- are collective atomic raising and lowering operators, respectively, that act on the Dicke states like standard angular momentum raising and lowering operators. D° acts on the Dicke states like the $z-$ component of the angular momentum operator.

The evolution of the system can be described by the density matrix equation

$$\frac{d\rho_{A+F}}{dt} = \frac{1}{i\hbar}[H_{tot}, \rho_{A+F}] + \Lambda_F \rho_{A+F}, \quad (2)$$

The last term in equation (2) accounts for dissipation. The probability that a member of the system is excited at time t is related to the expectation value of D° by

$$P_e(t,N) = \frac{1}{N} < D^\circ > + \frac{1}{2} \quad (3)$$

For more than fifty atoms, an alternative method based on the Bloch vector model becomes more practical than the above approach. The time derivatives of the quantum mechanical operators D°, D^+, and a† are found in the Heisenberg picture. The atomic operators are related to the components (η, ρ) of the Bloch vector, a classical angular momentum vector with length $J = N/2$
$D^\circ \rightarrow \eta \equiv \frac{1}{2}N \cos\theta$ and $D^+ \rightarrow \rho \equiv \frac{1}{2}N \sin\theta e^{i\phi}$, where θ and ϕ are the standard angles in spherical coordinates. The field operator a† is identified with ε, a classical electric field in the cavity. The evolution of the system is described by[6]

$$\frac{d\eta}{dt} = \frac{-i\omega_a}{2}(\varepsilon^*\rho - \varepsilon\rho^*), \quad (4a)$$

$$\frac{d\rho}{dt} = -i\omega_a \varepsilon \eta, \quad (4b)$$

$$\frac{d\varepsilon}{dt} = i\delta\varepsilon - \gamma\varepsilon + \frac{i\omega_a}{2}\rho + \tilde{F}^\dagger(t) \quad (4c)$$

where $\delta \equiv \omega - \omega_o$. Equation (4c) includes a damping term and a random force $F^\dagger(t)$ that account for the coupling of the radiation mode to the thermal reservoir of the cavity walls. It can be shown that the probability of excitation at time t is given by

$$P_e(t,N) = \frac{1}{N} < \eta(t,N,\theta(0)) >_{\theta(0)} + \frac{1}{2} \quad (5)$$

where the average over $\theta(0)$ is carried out over an appropriate distribution of initial angles arising from thermal fluctuations.

There is no general way to parametrize the behavior of the atom-cavity system, but for underdamped motion one feature is particularly easy to observe experimentally: this is the time τ_{min} at which $P_e(t,N)$ achieves its first minimum. We define the "collapse frequency" ν_{col} by

$$\nu_{col} \equiv (2\tau_{min})^{-1} \quad (6)$$

Although $P_e(t,N)$ is a complicated function of the system parameters, Haroche[5] has pointed out that the variation of ν_{col} with the number of atoms N can be accurately parameterized by

$$\nu_{col}(N) = \frac{a\sqrt{N}}{b + \ln N} \quad (7)$$

where a and b are adjustable parameters that depend on ω_a, γ, and β. The accuracy of this expression is illustrated by figure 1 which displays values of ν_{col} obtained from the exact solution [equation (3)] for $N \leq 50$ and from the Bloch method [equation (5)] for $N \geq 200$, along with the best fit of equation (7) to the calculations.

The experiments employ an atomic beam of calcium Rydberg atoms and a split superconducting cavity operated at 35 GHz. At the ambient temperature of 2 K, the mean blackbody photon number is 0.8. Selective

[6] B.J. Hughey, *Cavity Modified Atom-Photon Interaction*, Ph.D. diss., Dept. of Physics, MIT, 1989.

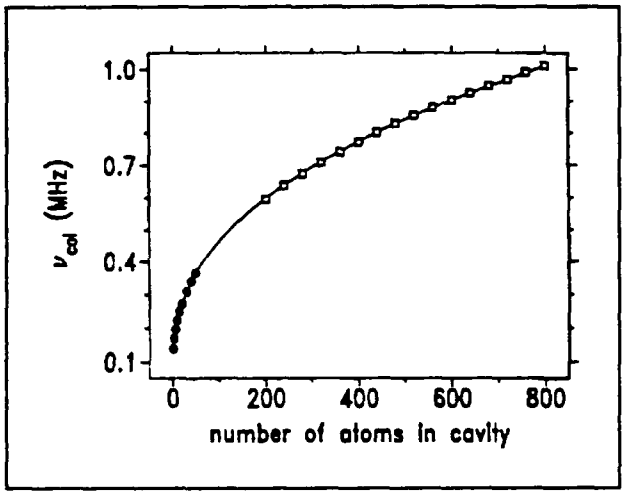

Figure 1. Dependence of the "collapse" frequency ν_{col} on number of atoms N for $Q = 1.2 \times 10^7$ and T = 2.17K. The filled circles are obtained from the exact method and the open squares from the Bloch method, as discussed in the text. The solid curve is a fit of the calculations to equation (7), which yields a = 0.3187MHz and b = 2.245.

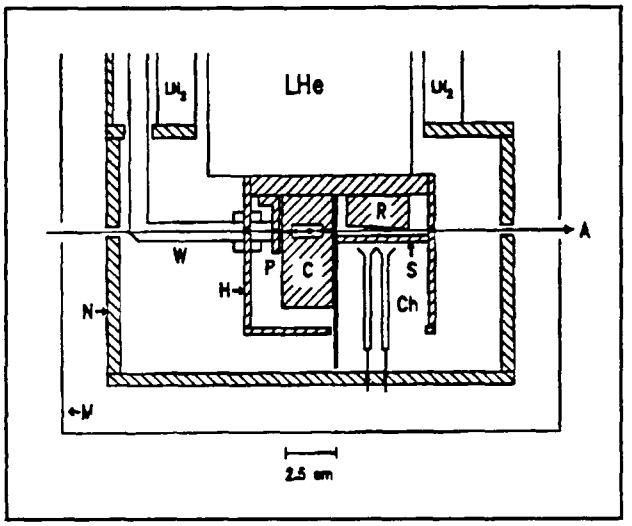

Figure 2. Diagram of the apparatus, side view. A: atomic beam, H: liquid helium temperature shield, N: liquid nitrogen temperature shield, M: single layer mu-metal shield, P: collimating plate of 2 channel field ionization detector, C: cavity, R: ramped plate, S: slotted plate, Ch: channel electron multipliers, W: waveguide, L: laser beams, B: waveguide holder, Co: coupler. The tuning mechanism is not shown for clarity.

field ionization allows us to monitor simultaneously the populations of the initial and final states. The time evolution of the atomic system is probed by "Stark switching." The collective oscillations of energy between ensembles of atoms and a cavity with $Q > 10^7$ are being studied for one to several hundred atoms.

The experiment is carried out with the apparatus shown in figure 2. A calcium atomic beam is prepared in the 46p state (abbreviation for the 4s46p $^1P_1$ state) inside the cavity using a three-step pulsed dye laser system. The final laser beam is polarized along the cavity electric field so that the 46p(m=0) state is excited relative to this quantization axis. The two states involved in the atom-cavity oscillations are thus the 46p(m=0) (upper state) and 46s (lower state). The frequency of the 46p → 46s transition in calcium is 35.332 GHz; the atom-cavity coupling frequency $\omega_a/2\pi$ calculated for this transition and our cavity dimensions is 105 kHz. Observing underdamped behavior for a single atom in the cavity requires $Q > 2 \times 10^5$. To avoid undesirable effects of blackbody radiation, the one-atom experiments require temperatures $\lesssim$2K, for which $\bar{n} \lesssim 0.8$.

The atoms are excited inside the cavity. The mean transit time to the cavity exit is 18 μsec, which corresponds to two cycles of the single-atom-cavity oscillation. After the atoms exit the cavity, they enter the detector region where selective field ionization is used to detect and differentiate the two states. We measure $\bar{P}_e(t, \bar{N})$ for each value of $\bar{N}$ by scanning the time t when a 200 mV pulse is applied between the cavity halves. ($\bar{N}$ is the mean number of atoms in the cavity.) In this way, we count the number of atoms detected in the 46p and 46s states as a function of the atom-cavity interaction time. Sample data are shown in figure 3.

An important feature of the experiment is the use of a split superconducting cavity. By applying an electric field between the two halves, the atomic resonance can be shifted far from resonance with the cavity, thereby terminating the atom-cavity interaction. This effectively freezes the atomic population at the moment at which the voltage pulse is applied. By using a carefully designed choke groove structure, we suppress leakage from the cavity and achieve a quality factor $Q > 10^7$ in niobium and lead-plated copper cavities.

A series of time evolution curves for various values of $\bar{N}$ was studied. Figures 4 and 5

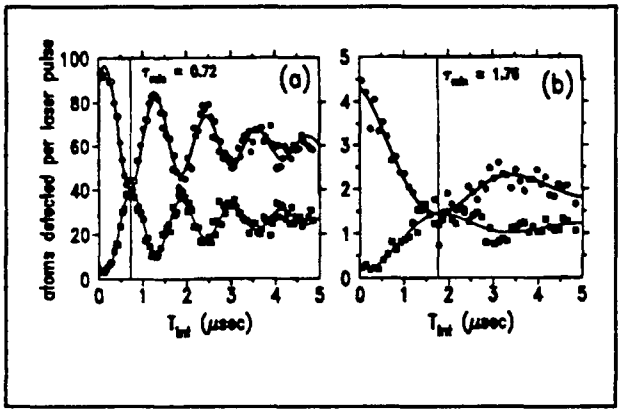

Figure 3. Observed atom-cavity oscillations for $Q = 1.18 \times 10^7$ and $T = 2.17K$ for two values of $\bar{N}_d$. The solid curves are fits of the data to damped sinusoids, from which ν_{col} is extracted. The open circles are the atoms detected in the 46p state, and the filled squares are the atoms detected in the 46s state. T_{int} is the atom-cavity interaction time.

display some of the data along with the calculated time evolution curves.

We also compared our results with theory for a single atom in the cavity. Single atom experiments are of special significance because they represent the limit of small systems. Furthermore, they have the experimental advantage of being free of much of the uncertainty in detection efficiency, assuming that the mean number of atoms detected per pulse is small compared to unity. For these studies, we generally operated with an average of 0.04 atoms detected per laser pulse. The observed and calculated evolution of a single atom in the cavity with $Q = 1.5 \times 10^6$ and $T = 1.95K$ are shown in figure 6. We believe that the damping which is evident in the data is due to stray electric and magnetic fields, and possibly thermal effects.

In support of these studies, we also carried out a high resolution study of the microwave spectrum of calcium Rydberg states. The results are described in a thesis,[7] and in the publications listed below.

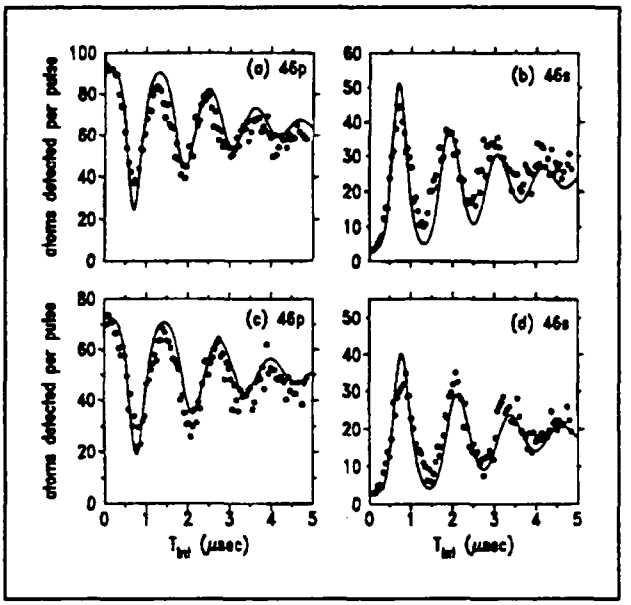

Figure 4. Comparison of calculated and observed evolution of the system for large ensembles of atoms in the cavity. The filled circles are the number of atoms detected in the 46p and 46s states as a function of atom-cavity interaction time T_{int}. The amplitudes of the theory curves are scaled to compare with data but there are no other adjustable parameters. (a) and (b): $\bar{N} = 380$. (c) and (d): $\bar{N} = 300$.

Publications

Gentile, T.R., B.J. Hughey, T.W. Ducas, and D. Kleppner. "Experimental Study of Two-Photon Rabi Oscillations." Paper presented at the Sixth Conference on Coherence & Quantum Optics, Rochester, New York, June 1989.

Gentile, T.R. *Microwave Spectroscopy and Atom-Photon Interactions in Rydberg States of Calcium.* Ph.D. diss. Dept. of Physics, MIT, 1989.

Gentile, T.R., B.J. Hughey, T.W. Ducas, and D. Kleppner. "Microwave Spectroscopy of Calcium Rydberg States." *Phys. Rev. A.* Accepted for publication.

Hughey, B.J., T.R. Gentile, T.W. Ducas, and D. Kleppner. "A Split High Q Superconducting Cavity." Submitted to *Rev. Sci. Instrum.*

[7] T.R. Gentile, *Microwave Spectroscopy and Atom-Photon Interactions in Rydberg States of Calcium,* Ph.D diss. Dept. of Physics, MIT, 1989.

polarizers. A scanned antenna-coupled pyroelectric detector system has been developed for mapping the millimeter wave beam profiles. A map of the radiation profile at the atomic beam is shown in figure 11.

We have begun designing the controlled field region in which the actual measurement will take place and hope to complete construction of the apparatus in the coming year. Efforts are also continuing to optimize the hydrogen beam source and the efficiency of the circular state production.

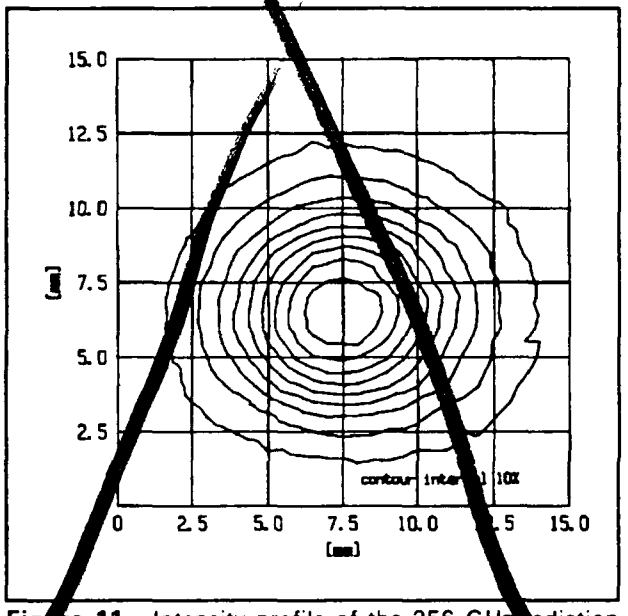

Figure 11. Intensity profile of the 256 GHz radiation used to drive the n = 29 → n = 30 circular transition.

2.4 Precision Mass Spectroscopy of Ions

Sponsors

Joint Services Electronics Program
Contract DAAL03-89-C-0001
National Science Foundation
Contract PHY 86-05893

Project Staff

Kevin R. Boyce, Eric A. Cornell, Deborah Kuchnir, Professor David E. Pritchard

In 1989, we made the first mass comparison of single trapped ions, raising the state of the art for fractional precision in mass measurement to 4×10^{-10}. This is a first step toward our ultimate goal of determining the mass of individual atomic and molecular ions with precisions of 10^{-11} or better. This precision will give us the capability of making experiments that address issues in both fundamental and applied physics:

- The $^3H^+ - ^3He^+$ mass difference is important in ongoing experiments to measure the electron neutrino rest mass.
- Excitation and binding energies of typical atomic and molecular ions can be determined by weighing the small decrease in energy: $\Delta m = E_{bind}/c^2$.
- Experiments that weigh γ-rays can be used in a new method to determine Avogadro's number, N_A, a key fundamental constant whose accurate determination would permit the replacement of the artifact mass standard by an atomic mass standard.
- Traditional applications of mass spectroscopy should benefit from the several orders of magnitude improvement in both accuracy and sensitivity which our approach offers over conventional techniques.

In our experimental approach, we measure ion cyclotron resonance on a single molecular or atomic ion in a Penning trap, a highly uniform magnetic field with axial confinement provided by weaker electric fields. We monitor ions, oscillating along magnetic field lines, by the currents induced in the trap electrodes. Working with only a single ion is essential because space charge from other ions leads to undesired frequency shifts. This work in trapping and precision resonance draws on techniques developed by Hans Dehmelt at the University of Washington and Norman Ramsey at Harvard University, for which they shared the 1989 Nobel Prize.

Our most notable accomplishment this year was determining the carbon monoxide-molecular nitrogen mass ratio to an accuracy

of 4×10^{-10}.[13] The ratio of the cyclotron frequencies of the two ions is the inverse of the ratio of the masses as long as the magnetic field remains constant. By trapping first a single N_2^+ ion and measuring its frequency, and then swapping to a single CO^+ ion, and then back again to N_2^+, we are able to correct for drifts in the magnetic field to about 0.5 parts per billion (see figure 12).

We have developed techniques for driving, cooling, and measuring the frequencies of all three normal modes of Penning trap motion. Thus, we can manipulate the ion position reproducibly to within 30 microns of the center of the trap, correcting for electrostatic shifts in the cyclotron frequency to great accuracy. We use a π-pulse method to coherently swap the phase and action of the cyclotron with the axial modes.[14] Therefore, although we detect only the axial motion directly, we can determine cyclotron frequency by measuring how much phase accumulates in the cyclotron motion in a known time interval (see figure 13).

Currently, precision is limited by magnetic field imperfections and temporal instabilities. Achieving our long range goal of 10^{-11} precision requires either dramatic improvements in field stability or simultaneous comparison of two different ions. With two ions of equal charge, the ion-ion perturbations are very similar for each ion and, hence, do not introduce significant uncertainty in the mass ratio. Our group has succeeded in trapping a single CO^+ ion and a single N_2^+ ion simultaneously.[15] In the coming year, we plan to develop techniques for making precision resonance measurements on two ions simultaneously.

Publications

Cornell, E.A., R.M. Weisskoff, K.R. Boyce, R.W. Flanagan, G.P. Lafyatis, and D.E. Pritchard. "Single-Ion Cyclotron Resonance Measurements of $M(CO^+)/M(N_2^+)$." *Phys. Rev. Lett.* 63:1674 (1989).

Cornell, E.A., R.M. Weisskoff, K.R. Boyce, and D.E. Pritchard. "Mode Coupling in a Penning Trap: π Pulses and a Classical Avoided Crossing." *Phys. Rev. A* 41:312 (1990).

Kuchnir, D.L. *Trapping and Detecting Two Different Single Ions at Once: A Step Towards Ultra-High-Precision Mass Comparison Measurements.* B.S. thesis. Dept. of Physics, MIT, 1989.

2.4.1 Atom Interferometry

Sponsors

Joint Services Electronics Program
Contract DAAL03-89-C-0001
U.S. Army Research Office
Contract DAAL03-89-K-0082
U.S. Navy - Office of Naval Research
Contract N00014-89-J-1207

Project Staff

Chris R. Ekstrom, David W. Keith, Bruce G. Oldaker, Quentin Turchette, Professor David E. Pritchard

Using fabricated transmission gratings as optical elements for the matter waves, we are constructing an atom interferometer to physically separate atom waves before recombining them. This interferometer will be useful in studies of atomic properties, tests of basic quantum physics, for metrology, as rotation sensors, and, perhaps, ultimately as devices to make ultra-small structures using atom holograms.

---

[13] E.A. Cornell, R.M. Weisskoff et al., *Phys. Rev. Lett.* 63:1674 (1989).

[14] E.A. Cornell, R.M. Weisskoff et al., *Phys. Rev. A* 41:312 (1990).

[15] D.L. Kuchnir, *Trapping and Detecting Two Different Single Ions at Once: A Step Towards Ultra-High-Precision Mass Comparison Measurements,* B.S. thesis, Dept. of Physics, MIT, 1989.

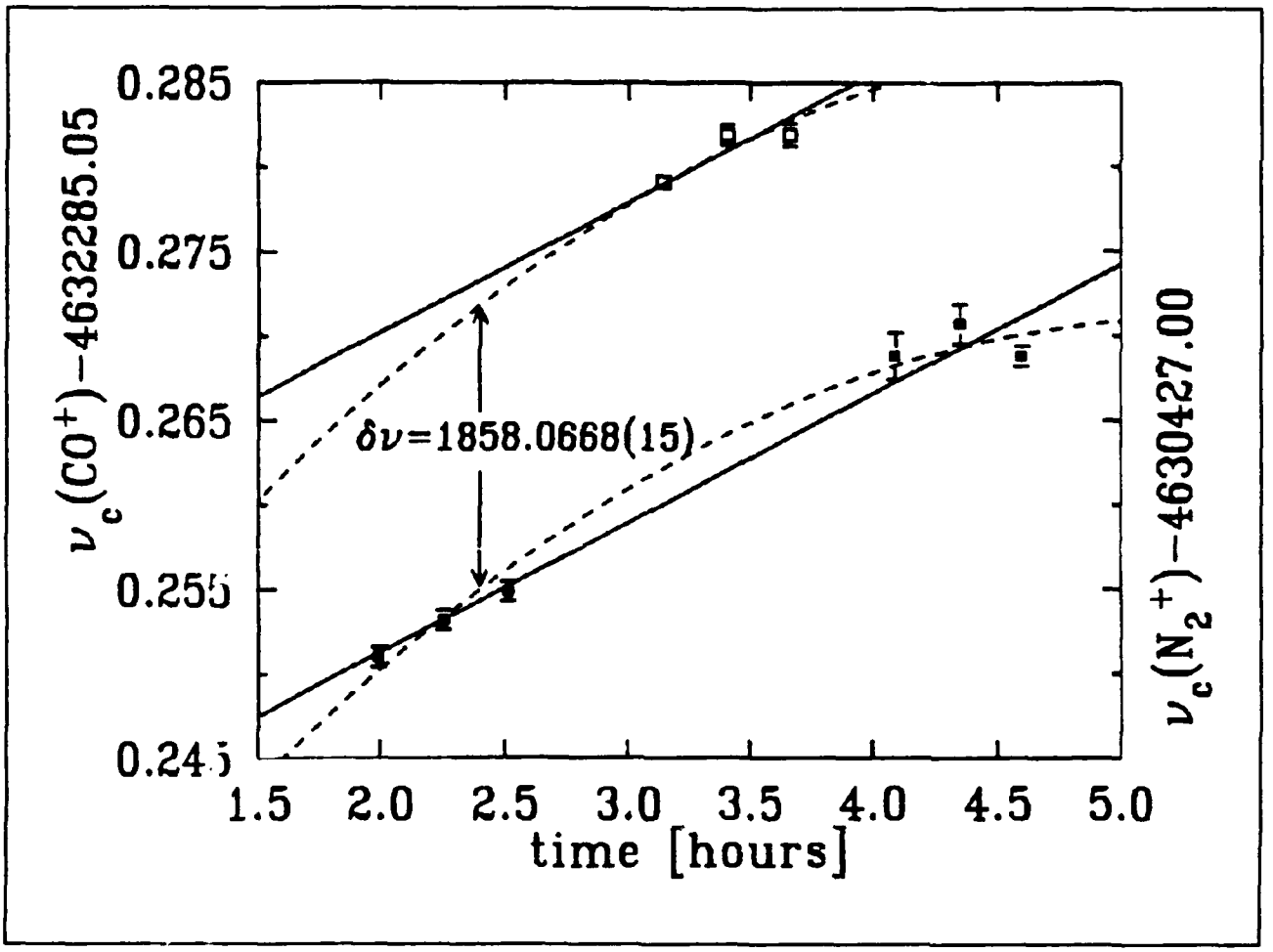

Figure 12. The data from a mass comparison run are shown. The solid squares (open squares) are the cyclotron frequency of $N_2^+(C^+)$. A total of three ions were loaded in the order $N_2^+ - CO^+ - N_2^+$. The solid lines are a fit to the two frequencies assuming a field drift that is linear in time. The dotted-line assumes a quadratic field drift. The indicated value for the difference frequency results from the latter assumption, and corresponds to $M(CO^+)/M(N_2^+)$ =0.9995988876(

During the last year, our atom interferometer evolved from a rough plan to an essentially complete device. At present, we have tested all its major components at least once. We will test the complete system during the coming year.

Our interferometer consists of three 0.2 μm-period diffraction gratings equally spaced $\sim$ 0.65 m apart in our atomic beam machine. The maximum separation of the beams will be $\sim 60\mu$m. The first two gratings separate and redirect the atomic beam forming a standing wave interference pattern in the atomic flux at the third grating, which acts like a mask to sample this pattern.

We can estimate our anticipated final signal strength from the properties of the individual gratings. Attenuation caused by the primary grating and the grating support structure gives an intensity in the 0^{th} order of $\sim$ one-eighth of the incident intensity and one-sixteenth in each of the $\pm$ 1 orders. The final intensity detected at the maximum of a fringe after transmission through all three gratings can be calculated by summing the amplitudes for the two sides of the interferometer and will be 0.005 of the incident intensity. The fringe constant will be 4 to 1, so the interference signal will be 0.004 of the incident intensity. We are anticipating that the final interference signal through the interferometer will be $\sim 4 \times 10^3$ counts per second. This should generously exceed the noise of the detector (≤ 100 sec^{-1}).

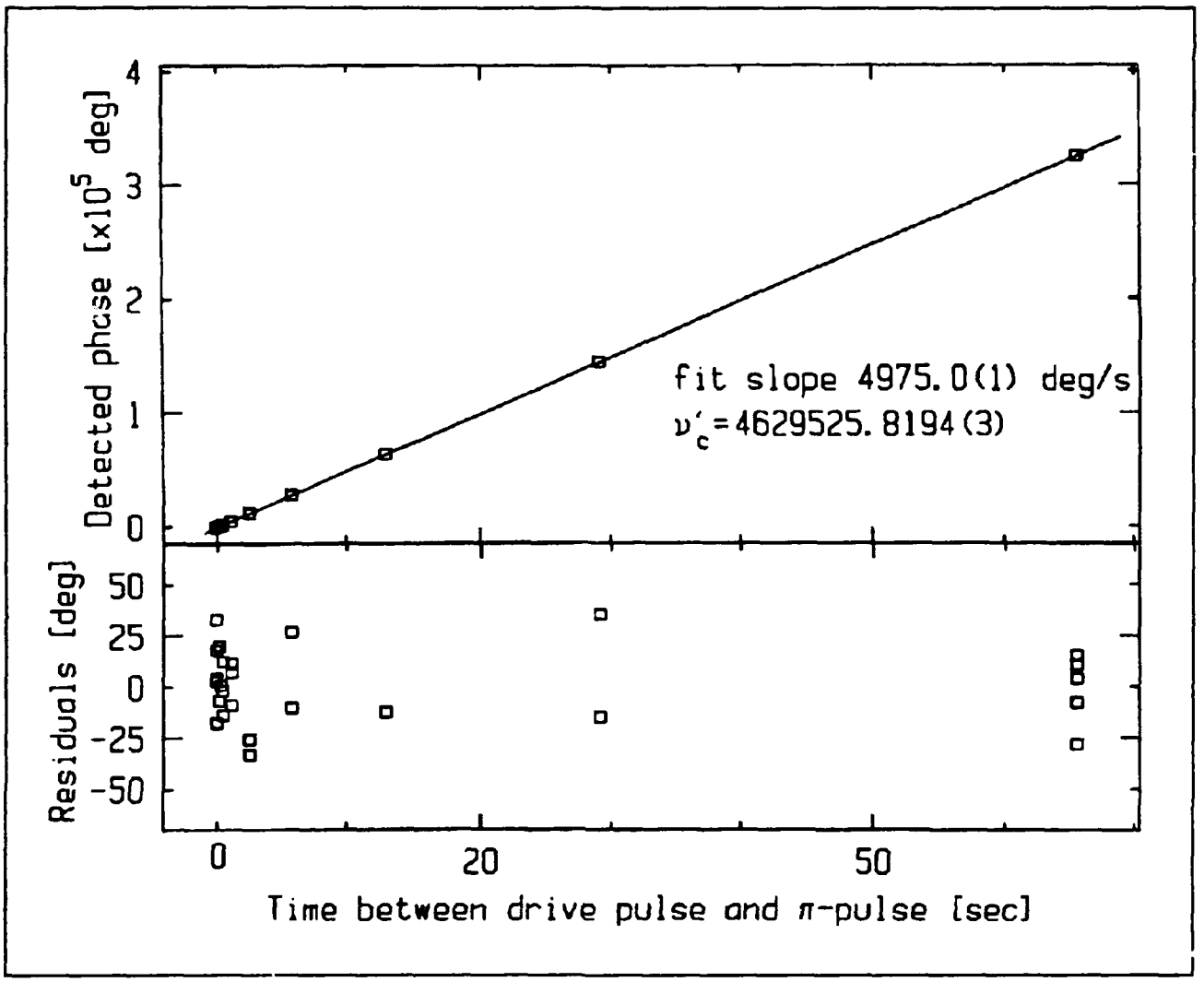

Figure 13. For each plotted point, we perform the following experiment: The initially cold ion is pulsed into a cyclotron orbit of known initial phase and then allowed to evolve "in the dark' for an indicated amount of time, t. Then a pulse is applied which exchanges cyclotron and axial motions, bringing the ion's cyclotron action and phase into the axial mode. As the ion's axial motion rings down, its phase is detected. The appropriate multiple of 360° is added, and a line is fitted to the points. The slope of the line is the frequency difference between the frequency generator and the trap cyclotron frequency.

The mechanical vibrations of our machine are a principal technical obstacle because they could blur the interference pattern. There are two types of required limits on vibrations. First, the three gratings must move relative to each other by less than ~ 1/4 period (50 nm) during the time the final grating samples the intensity at a given position. Thus, the rms amplitude of relative vibrations integrated over all frequencies greater than the reciprocal of the integration time must be less than ~ 50 nm. The second requirement is related to the motion of the gratings due to acceleration of, or rotation about, the center of mass of the grating system during the 1.3 ms time it takes for the atoms to traverse the interferometer. This means that below ~ 900 Hz the rms acceleration must be less than $10^{-2}ms^{-2}$, and the rms angular velocity must be less than 10^{-5} radians per second.

We have solved our vibration problem by using a combination of passive isolation and active feedback. The passive isolation system consists of small pneumatic feet which act like damped springs to support the machine and give it a 3-Hz resonant frequency. This isolates the machine from building noise at higher frequencies. We have used the active feedback system to stabilize the relative posi-

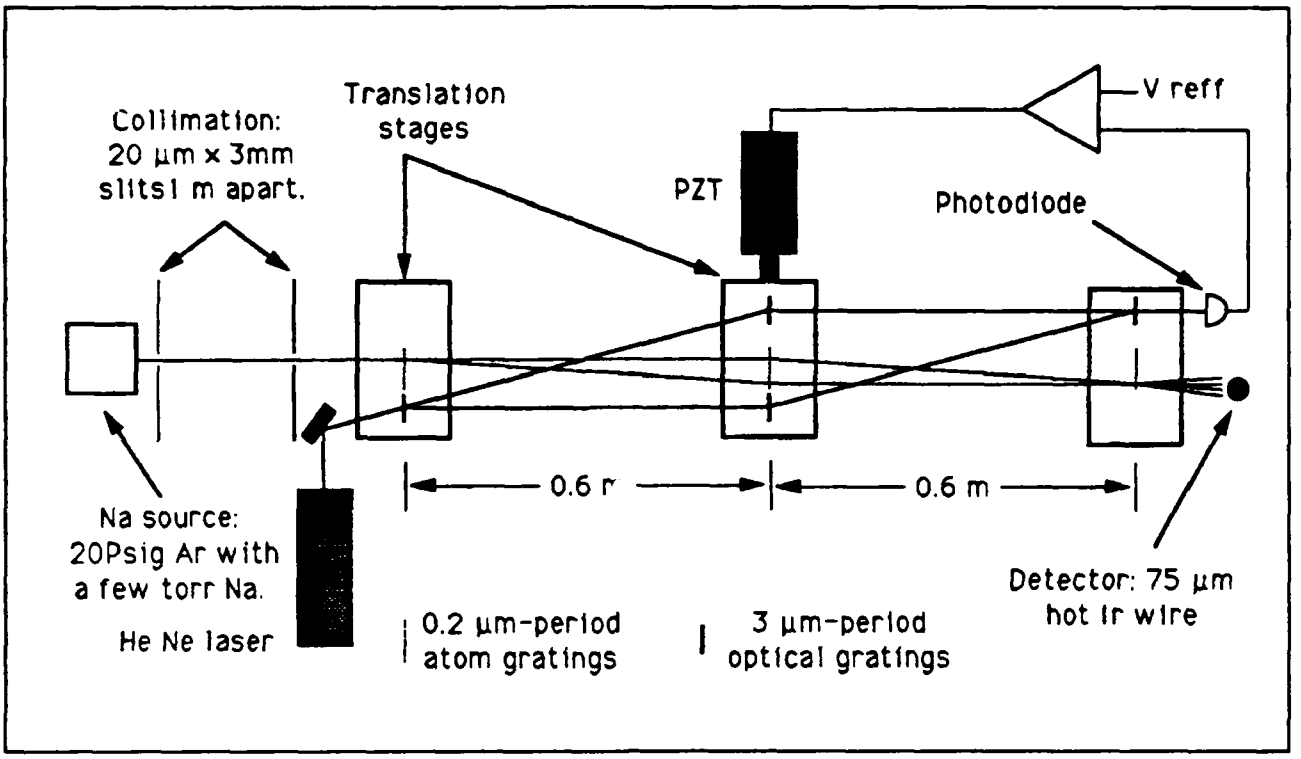

Figure 14. Our current atom interferometer with laser interferometer vibration isolation system is shown. (Not to scale.)

tions of the three gratings at frequencies below ~ 150 Hz. This system works best at low frequencies < 10 Hz) where the passive system is least effective. The reduction of relative motion provided by the active system will allow us to use much longer integration times when we are looking for the interference signal. The active feedback system uses a laser interferometer which has the same transmission grating geometry as the atom interferometer. We mounted the gratings for the optical interferometer on the same three translation stages as the matter wave gratings to record the exact relative orientation of the matter wave interferometer. We apply the signal from the optical interferometer to provide a measure of the relative alignment of the three grating platforms to a Piezoelectric translator (PZT) through a feedback network to stabilize the platforms (figure 14). With this system, we have adequately reduced the relative rms motion (at frequencies less than 0.3 Hz) of the gratings from ~ 1500 to 40 nm. We also reduced the rms acceleration in a frequency range to which the interferometer is sensitive from 1.1×10^{-2} to $2.3 \times 10^{-3} ms^{-2}$, which is safe by a factor ~ 5, ensuring sufficiently low angular velocities of the apparatus.

We have also made significant progress in overcoming another technical obstacle, the relative alignment of the atom gratings. For all points along the height (3 mm) of our ribbon shaped beam to have the same phase of interference signal, the gratings must be aligned to an angle of $\sim 10^{-5}$ rads. with respect to rotations about the beam axis. We accomplished this by using a technique based on the optical polarizing properties of the gratings.

In addition to the work on vibrations and alignment mentioned above, our main progress during 1989 was construction of the various mechanical components that position the gratings inside the vacuum envelope. Also, we have written computer software and built electronic hardware to control the position of the three grating platforms and the detector, and the height, angle and position of the second collimating slit. Instead of directly varying the voltage of the PZT that controls the position of the last grating, now we will use the computer to vary the null point of the active feedback

system when we are searching for interference fringes.

When we have successfully demonstrated this interferometer, our first experimental objective will be a demonstration of Berry's phase with bosons. Another experiment could be an improved measurement of the Aharonov-Casher effect.

Publications

Keith, D.W., and D.E. Pritchard. "Atom Optics." In *New Frontiers in QED and Quantumoptics*. New York: Plenum Press. Forthcoming.

Keith, D.W., M.L. Schattenburg, H.I. Smith, and D.E. Pritchard. "Diffraction Gratings from Atoms." *QELS Conference,* Baltimore, Maryland, April 1989.

Oldaker, B.G., P.J. Martin, P.L. Gould, M. Xiao, and D.E. Pritchard. "Experimental Study of Sub-Poissonian Statistics in the Transfer of Momentum from Light to Atoms." Submitted to *Phys. Rev. Lett.*

Pritchard, D.E., and B.G. Oldaker. "Light Forces and Atom Diffraction: An Illustrated Summary." Paper presented at the *Sixth Conference on Coherence,* Rochester, New York, 1989.

Pritchard, D.E. Experimental Studies of Atom Diffraction and the Mechanical Forces of Light on Atoms, *NICOLS Conference.* Bretton Woods, New Hampshire: Academic Press, 1989.

2.5 Neutral Atom Trap

Sponsors

U.S. Navy - Office of Naval Research
Contracts N00014-83-K-0695 and N00014-89-J-1207

Project Staff

Kristian Helmerson, Michael A. Joffe, Dr. Min Xiao, Ke-Xun Sun, Professor David E. Pritchard

We have trapped large numbers of neutral atoms, and cooled them to millikelvin temperatures. Our next objective is to cool them to microkelvin temperatures. Dense samples of atoms cooled to microkelvin temperatures promise to open up new and exciting areas of physics. The lack of interaction of the low velocity atoms due to their reduced thermal motion, together with the possibility of indefinitely long interaction times, make samples of trapped atoms ideal for high resolution spectroscopy and for use as atomic frequency standards. High density samples of ultra-cold atoms will also make possible new studies of interatomic collisions and collective effects, such as Bose condensation. We have made progress using our existing magnetic trap. In addition, we started a new project to develop a continuous source of slow atoms to load into future magnetic traps.

2.5.1 Magnetic Trap for Neutral Atoms

Now that techniques for trapping neutral atoms are well established,[16] the field of neutral atom trapping has moved from infancy to adolescence and the emphasis is now on doing experiments with the trapped atoms.

Currently, our main effort in neutral atom trapping is cooling trapped atoms to low temperatures. While this remains a difficult and elusive goal (to date, we have only achieved microkelvin temperatures with untrapped atoms), the rewards for supercooling trapped atoms are significant. The long confinement times, together with the reduced thermal motion of cold atoms, could result in a new era of ultra-high resolution spectroscopy and precise frequency standards. Potentially more exciting is the possibility of combining the high densities achievable in traps and the long deBroglie

[16] D.E. Pritchard, K. Helmerson, and A.G. Martin, "Atom Traps," in *Atomic Physics,*. 11, eds. S. Haroche, J.C. Gay, and G. Grynberg (Singapore: World Scientific, 1989), pp. 179-97.

Chapter 1. Electromagnetic Wave Theory and Applications

Academic and Research Staff

Professor Jin Au Kong, Dr. Sami M. Ali, Dr. Robert T. Shin, Dr. Ying-Ching E. Yang

Visiting Scientists and Research Affiliates

Dr. Pinchas D. Einziger,[1] Qizheng Gu,[2] Dr. Tarek M. Habashy,[3] Dr. Arthur K. Jordan,[4] Dr. Kevin O'Neill,[5] Dr. Soon Y. Poh,[6] Dr. Tsuneki Yamasaki,[7] Dr. Harold R. Raemer[8]

Graduate Students

Khurram K. Afridi, Jerome J. Akerson, David V. Arnold, Robert G. Atkins, Maurice Borgeaud, Ike Chang, Judy Chen, Nelson C. Chu, Hsiu C. Han, Yoshihisa Hara, Jean-Fu Kiang, Cheung-Wei Lam, Gloria W. Lau, Check-Fu Lee, Kevin Li, Victor Liau, Harold H. Lim, Son V. Nghiem, Kelly Savage, David M. Sheen, Mohammad A. Tassoudji, Michael J. Tsuk, Ann N. Tulintseff, Murat E. Veysoglu, Li-Fang Wang, Jiging Xia, Herng A. Yueh

Undergraduate Students

Daniel Chung, Laura Marmorstein

Technical and Support Staff

Margery Brothers, Kit-Wah Lai, Anh Lieu, Wei Ming-yu Lin

1.1 Electromagnetic Waves in Multilayer Media

Sponsors

Joint Services Electronics Program
Contract DAAL03-89-C-0001
National Science Foundation
Contract ECS 86-20029
Schlumberger-Doll Research
U.S. Army Research Office
Contract DAAL03 88-K-0057

Project Staff

Professor Jin Au Kong, Dr. Sami M. Ali, Dr. Tarek M. Habashy, Dr. Soon Y. Poh, Dr. Ying-Ching E. Yang, Robert G. Atkins, Ike Chang, Qizheng Gu, Check-Fu Lee, Kevin Li, David M. Sheen, Michael J. Tsuk, Ann N. Tulintseff, Jiging Xia

---

[1] Department of Electrical Engineering, Technion-Israel Institute, Haifa, Israel.

[2] Shanghai Research Institute of Mechanical and Electrical Engineering, Shanghai, China.

[3] Schlumberger-Doll Research, Ridgefield, Connecticut.

[4] Office of Naval Research, U.S. Navy, Arlington, Virginia.

[5] Civil and Geotechnical Engineering, Department of the Army, Hanover, New Hampshire.

[6] Digital Equipment Corporation, Andover, Massachusetts.

[7] Department of Electrical Engineering, College of Science and Technology, Nihon University, Tokyo, Japan.

[8] Electrical and Computer Engineering Department, Northeastern University, Boston.

We are developing a generalized formulation for the electromagnetic fields in multilayered uniaxially anisotropic media containing arbitrary distribution of current sources. A spectral domain dyadic Green's function for multilayered uniaxially anisotropic media containing three-dimensional sources is derived. Tractable forms are shown to be easily deduced from the physical picture of the waves radiated by the primary sources and the multiple reflections from the stratified medium. The formulation decomposes the dyadic Green's function into TE and TM waves. The dyadic Green's function in the source region is properly represented by extracting the delta function singularity. A simple procedure to obtain the fields in any arbitrary layer is described. Recursion relations for appropriately defined reflection and upward and downward propagating transmission coefficients are presented. Forms suitable for transmission line applications in multilayered media are derived.

Finite difference time domain (FDTD) techniques show great promise in their ability to solve three-dimensional problems with arbitrary geometry. Advantages of this method include the ability to model spatially or temporally varying media. These advantages are due to the complete discretization of both space and time. Considering the volume of information being calculated, these techniques are very efficient and well suited to calculation on future parallel processing computers. This method was first formulated by Yee in 1966, and his basic algorithm is still in use.

Recent work has demonstrated the applicability of the FDTD technique to microstrip problems. The centered finite difference approximations used are second order accurate in both space and time yielding good results for reasonable mesh sizes. Numerical techniques used to solve electromagnetic problems must limit the domain over which the fields are calculated. This mandates the use of an absorbing boundary condition to simulate the outward propagation of waves incident on the walls of the mesh. An absorbing boundary condition, developed by Mur and based on the work of Enquist and Majda, is used in this work.

Our work in this area includes development of the algorithms mentioned above into a general purpose computer code which can be used to solve for the transient response of electromagnetic problems having arbitrary geometries. In addition to the transient response, frequency domain parameters can be obtained by Fourier transform of the time domain results. Since the fields are calculated throughout space and time all other desired parameters can be calculated from the field quantities.

Specifically, we are analyzing rectangular microstrip structures with as many as two or more ports. Such structures can be used in MMIC filters or antennas. This problem is of interest for several reasons. First, there are existing frequency domain solutions to the resonance problem of a rectangular microstrip patch, which we compare with the FDTD solution. Secondly, the FDTD technique can be used to analyze coupling of microstrip lines to the rectangular structure. This coupling can be either a direct connection or a gap coupled connection. Advantages of the FDTD solution to this problem are that (1) the full wave solution allows for radiation or surface wave loss, (2) no empirical values such as "effective" dimensions are needed for the analysis, and (3) the geometry can be altered easily to allow for various connections or coupling to the patch. This method is a significant improvement over those that rely on a planar circuit approach in which the substrate thickness must be small compared to wavelength and inherently three-dimensional coupling problems are not easily handled. We will compare our results with various planar circuit approaches.

The leakage phenomenon is important in the area of millimeter-wave integrated circuits and integrated optics. We have performed theoretical analyses and experiments to investigate this phenomenon. The leakage is due to the TE-TM coupling occurring at the geometrical discontinuities, and the leaky power in the form of surface wave propagates in the background medium.

We are using various methods to analyze the dielectric strip waveguides including the approximate field matching, effective dielectric constant (EDC), and mode matching. Because the first two methods are approxi-

mate, they can not be used to predict the imaginary part of the propagation constant. When using the third method, we must place ground planes at some distance from the guiding structure and omit the effect of radiation loss.

To solve for the dispersion relation of single and coupled dielectric strip waveguides, we derive an integral equation formulation using dyadic Green's function. We also present a method for predicting the leakage. Three different dielectric strip waveguides are investigated: optical rib waveguide, strip dielectric guide, and insulated image guide. Both single and coupled strip waveguides are studied. The cross section of the dielectric strips are assumed to have rectangular shape. Applying the Galerkin's method, the field distribution on the cross section is represented by a set of unit pulse basis functions. By substituting these basis functions into the integral equations and choosing the same set of basis functions as the testing functions, we can obtain a determinant equation from which the propagation constant can be solved.

For single dielectric strip waveguide, we have observed that the leakage occurs when the effective refractive index is smaller than that of a surface wave mode in the background medium. We also observed that if the lowest TE-like (TM-like) mode is leaky, the lowest TM-like (TE-like) mode is non-leaky. When the lowest order mode leaks, the surface wave mode of opposite polarization is excited. When the higher order mode leaks, the surface wave modes of both polarizations can be excited.

For two symmetrical dielectric strip waveguides, we investigated both the even and odd modes. In the leaky mode, the total leakage is due to the leakage from each individual strip waveguide. At the separation where the even mode has a maximum leakage, it is implied that the surface wave modes excited by each waveguide add in phase. For the odd mode at about the same separation, these surface wave modes add out of phase; hence, a null in the leakage is observed.

We are analyzing the propagation properties of single and coupled inhomogeneous slab waveguides and propose an integral equation formulation using the dyadic Green's function which covers both the TE and TM modes. The dispersion relations are obtained by applying Galerkin's method to solve the integral equation. We also investigate the coupling between two symmetrical inhomogeneous slab waveguides. This method is applicable to arbitrary dielectric constant profiles.

Full modal analysis is used to study the dispersion characteristics of microstrip lines periodically loaded with crossing strips in a stratified uniaxially anisotropic medium. Dyadic Green's functions in the spectral domain for the multilayered medium in conjunction with the vector Fourier transform (VFT) are used to formulate a coupled set of vector integral equations for the current distribution on the signal line and the crossing strips. Galerkin's procedure is applied to derive the eigenvalue equation for the propagation constant. We investigate the effect of anisotropy for both open and shielded structures on the stopband properties.

We are analyzing the quasistatic fields generated by an electrode mounted on a perfectly conducting pad of finite extent buried in a planar stratified medium. An integral equation in the spectral domain is derived for the outflowing current density distribution on the pad-electrode surface. The method of moments is then applied to solve the integral equation. We are investigating the effects of the electric properties of the stratified medium and the standoff thickness on the total electrode current. Several conductivity profiles modelling different practical measurement environments are also considered. Numerical results reveal that the total electrode current is insensitive to the standoff thickness, and can be used to prospect for the conductivity of rock formation.

Based on a hybrid transmission lines-lumped element circuit model, we analyze the transient propagation characteristics of VLSI interconnects with discrete capacitive loads at various locations. Exact expressions of the Laplace transform of unit step responses are first obtained through the ABCD matrix formulation. We then apply the equivalent dominant pole approximation to the transfer function with the propagation delays fac-

tored out. The approximated transfer function can be inverted in closed form and quickly evaluated. These results provide efficient ways of finding approximately the effects on delays and rise time brought by VLSI off-chip interconnects.

Because of the dramatic increase in device densities on microelectronic chips, the propagation delay for off-chip interconnects has become the factor limiting the speed of VLSI packages. Typical scales of these interconnects will be comparable or larger than the characteristic wavelength of the high frequency components of the signal. Therefore, to calculate the delays caused by these interconnects properly, a hybrid circuit model containing transmission line sections as well as lumped elements must be used in place of the all-lumped elements. Nevertheless, most circuit simulation packages are based on the latter and have to resort to subsection approximation when dealing with transmission lines. This scheme will undoubtedly lead to lengthy computation — which is not desirable when a quick, heuristic estimate of bounds is needed for the initial phase of the design cycle.

We have developed two approaches for obtaining the approximate transient response without lengthy simulation. The first emphasizes the calculation of bounds to voltage responses from the differential equations either by direct integration or by using the optimal control theory. The second analyzes the properties of Laplace transform domain solution. Thus far, their applications are limited to all lumped-element and distributed RC networks, which can only handle on-chip interconnects. For off-chip delay estimation, we took the second approach by incorporating transmission line elements.

Extensive work has been published on radiation by a microstrip patch excited by a probe. Most of the published work did not rigorously model the correct current distribution on the probe. In the case of electrically thin substrates, the probe current is usually approximated as uniform along the probe. This leads to acceptable numerical results for the computation of the radiation pattern by the patch and the mutual impedance between the probe and the patch. However, this approximation is not sufficiently accurate to solve for the current distribution on the patch or for the computation of the self impedance across the terminals of the probe. Furthermore, this approximation is not appropriate in the case of electrically thick substrates.

We rigorously analyzed the radiation problem of a circular patch which is center fed by a coaxial-line driven probe over a ground plane and situated in an arbitrary layered medium. The current distribution on both the patch and the probe is rigorously formulated using a planar stratified medium approach. A set of three coupled integral equations is derived which governs the axial current distribution on the probe, the radial current distribution on the patch and the azimuthal magnetic current sheet across the aperture of the driving coaxial line. This set of equations is then solved using the method of moments. The resulting matrix equation is obtained in terms of Sommerfeld-type integrals that take into account the effect of the layered medium. These integrals are efficiently computed by a simple deformation in the complex wavenumber domain. The probe current distribution, input impedance and radiation pattern are presented and compared to the case of an uniform probe current distribution.

The analysis of microstrip antennas with electrically thick substrates has many applications pertaining to millimeter wave systems and to achieving wide bandwidth. Most of the published work on the input impedance and other parameters of a probe-fed microstrip antenna employ an approximation to the probe feed where it is replaced by a uniform current ribbon of equivalent dimensions. This approximation fails to give sufficiently accurate results for the input impedance of the probe especially for thick substrates. Recently, we have made some progress in this area — we obtained the current distribution on the metallic probe in a closed magnetic wall cavity. Then, we accounted for the radiation losses by lumping them artificially into an effective loss tangent.

We have formulated the problem of a center fed circular microstrip antenna in terms of a Weber transform, which allowed us to develop the Green's function of the layered medium with the probe and the microstrip

patch as part of the medium. Using the Weber transform automatically enforces the boundary conditions on the probe and the patch. This allows us to cast the problem as the solution of a set of two coupled integral equations governing the tangential component of the electric field across the aperture of the coaxial line feed and that aperture across the interface where the patch lies. Next, we solve this set of equations using the method of moments. We then compute the current distribution on both the probe and the patch from the component of the magnetic field tangential to their surfaces. Furthermore, from the computed electric field across the aperture of the coaxial line feed, we obtain the reflection coefficient for the TEM mode which allows us to compute the input impedance across the terminals of the probe. The probe current distribution, input impedance and radiation pattern are presented, and the obtained results compared with those using the stratified medium formulation.

The transient fields of a current source on a layered medium are calculated using the double deformation technique, in which complex integrals are deformed in the transverse wavenumber and frequency planes. Singularities from these complex planes correspond to physical modes of the structure, such as guided and leaky waves, and the relative importance of each to the overall response can be discovered. Unlike the Cagniard-de Hoop method, double deformation can be applied to dispersive and dissipative media. Also, the causality of the electromagnetic signal can be shown analytically.

We developed a modification to the double deformation technique, which splits the Fourier transform of the source current into two halves, one for times before the arrival at the observation point, and one after. This greatly increases the range of sources to which the double deformation technique can be applied. Another advantage of the modification is the individual causality and continuity of each mode.

We have computed results for both line and strip currents on the surface of a coated perfect conductor for cases where the dielectric coating is both lossless and dissipative. In most cases, only a small number of modes suffices to reproduce the important features of the response, including the arrivals of reflected and lateral rays. The importance of each type of arrival depends on certain features of the time function, especially the initial slope. The response due to a strip current resembles that of a line current although there is some smoothing of the sharper features.

The complex resonant frequencies of the open structure of a microstrip antenna consisting of two circular microstrip disks in a stacked configuration have been rigorously calculated as a function of the layered parameters and the ratio of the radii of the two disks. Using a dyadic Green's function formulation for horizontally stratified media and the vector Hankel transform, the mixed boundary value problem is reduced to a set of coupled vector integral equations. Employing Galerkin's method in the spectral domain, we calculated the complex resonant frequencies and demonstrated convergence of the results. We show that for each mode, the stacked circular microstrip structure has dual resonant frequencies which are associated with the two coupled constitutive resonators of the structure and a function of the mutual coupling between the two disk resonators. This mutual coupling is a function of the geometrical configuration of the stacked structure; the layered parameters, permittivities, permeabilities, and heights; and the ratio of the radii of the two disks. The dual frequency behavior of the stacked microstrip structure can be used to broaden the bandwidth or to provide for dual frequency use of the antenna.

Publications

Ali, S.M., T.M. Habashy, and J.A. Kong. "Dyadic Green's Functions for Multilayered Uniaxially Anisotropic Media." Submitted to *J. Electromag. Waves Appl.*

Ali, S.M., T.M. Habashy, and J.A. Kong. "Probe Excitation of a Center-Fed Circular Microstrip Antenna Employing a Stratified Medium Formulation." In *IEEE AP-S International Symposium and URSI Radio Science Meeting,* San Jose, California, June 26-30, 1989.

Habashy, T.M., S.M. Ali, and J.A. Kong. "Probe Excitation of a Center-Fed Circular Microstrip Antenna Employing the Weber Transform." In *IEEE AP-S International Symposium and URSI Radio Science Meeting,* San Jose, California, June 26-30, 1989.

Kiang, J.F., S.M. Ali, and J.A. Kong. "Integral Equation Formulation of Inhomogeneous Slab Waveguides." Submitted to *IEEE J. Quantum Electron.*

Kiang, J.F., S.M. Ali, and J.A. Kong. "Integral Equation Solution to the Guidance and Leakage Properties of Coupled Dielectric Strip Waveguides." In *IEEE Trans. Microwave Theory Tech.* Forthcoming.

Kiang, J.F., T.M. Habashy, and J.A. Kong. "Electrostatic Fields Due to an Electrode Mounted on a Conducting Pad of Finite Extent in a Planar Stratified Medium." *IEEE Trans. Antennas Propag.* 37 (9):1140-1149 (1989).

Kiang, J.F., S.M. Ali, and J.A. Kong. "Analysis of Dielectric Strip Waveguides Using Integral Equation Formulation." *Progress in Electromagnetics Research Symposium,* Boston, Massachusetts, July 25-26, 1989.

Lam, C.W., S.M. Ali, and J.A. Kong. "The Propagation Characteristics of Signal Lines with Crossing Strips in Multilayered Anisotropic Media." *J. Electromag. Waves Appl.* Forthcoming.

Poh, S.Y., M.J. Tsuk, and J.A. Kong. "Transient Response of Sources Over Layered Media Using the Double Deformation Method." *IEEE AP-S International Symposium and URSI Radio Science Meeting,* San Jose, California, June 26-30, 1989.

Sheen, D.M., S.M. Ali, M.D. Abouzahra, and J.A. Kong. "Application of the Three Dimensional Finite Difference Time Domain Method to the Analysis of Planar Microstrip Circuits." Submitted to *IEEE Trans. Microwave Theory Tech.*

Sheen, D.M., S.M. Ali, M.D. Abouzahra, and J.A. Kong. "Analysis of Multiport Rectangular Microstrip Structures Using a Three Dimensional Finite Difference Time Domain Technique." In *Progress in Electromagnetics Research Symposium,* Boston, Massachusetts, July 25-26, 1989.

Tulintseff, A.N., S.M. Ali, and J.A. Kong. "Resonant Frequencies of Stacked Circular Microstrip Antennas." In *IEEE AP-S International Symposium and URSI Radio Science Meeting,* San Jose, California, June 26-30, 1989.

Tulintseff, A.N., S.M. Ali, and J.A. Kong. "Resonant Frequencies of Stacked Circular Microstrip Antennas." Submitted to *IEEE Trans. Antennas Propagat.*

Yang, Y.E., and J.A. Kong. "Transient Analysis of Capacitively Loaded VLSI Off-Chip Interconnections," In *Progress in Electromagnetics Research Symposium,* Boston, Massachusetts, July 25-26, 1989.

1.2 Remote Sensing of Earth Terrain

Sponsor

National Aeronautics and Space Administration
Contract NAGW-1617

Project Staff

Professor Jin Au Kong, Dr. Pinches D. Einziger, Dr. Robert T. Shin, David V. Arnold, Robert G. Atkins, Nelson C. Chu, Harold H. Kim, Son V. Nghiem, Herng A. Yueh

We are developing models of various kinds of earth terrain using a two-layer configuration to investigate the polarimetric scattering properties of remotely sensed media. The scattering layer is an anisotropic random medium characterized by a three-dimensional correlation function with lateral and vertical correlation lengths and variances. Based on the wave theory under Born approximations, we applied this model to derive the fully polarimetric backscattering coefficients of the Mueller and covariance matrices. We considered a single scattering process, taking into account all the multiple reflections at the boundaries. For an anisotropic random

Chapter 6. Custom Integrated Circuits

Academic and Research Staff

Professor Jonathan Allen, Professor John L. Wyatt, Jr., Professor Srinivas Devadas, Professor Jacob White, Professor Dimitri A. Antoniadis, Professor Berthold K.P. Horn, Professor Hae-Seung Lee, Professor Bruce R. Musicus, Professor Tomaso Poggio, Professor Charles G. Sodini

Graduate Students

Robert C. Armstrong, Donald G. Baltus, Cyrus S. Bamji, Michael J. Bryan, Curtis S. Chen, Steven J. Decker, Ibrahim M. Elfadel, Mikko Hakkarainen, Craig Keast, Kevin Lam, Jennifer A. Lloyd, Andrew Lumsdaine, Steven P. McCormick, Ignacio McQuirk, Keith S. Nabors, Joel R. Phillips, Mark W. Reichelt, Mark N. Seidel, Luis M. Silviera, David L. Standley, Ricardo Telichevsky, Christopher B. Umminger, Filip Van Aelten, Woodward Yang

Technical and Support Staff

Dorothy A. Fleischer, Susan E. Nelson

6.1 Custom Integrated Circuits

Sponsors

Analog Devices, Inc.
International Business Machines Corporation
Joint Services Electronics Program
Contract DAAL03-89-C-0001
U.S. Air Force - Office of Scientific Research
Contract AFOSR 86-0164B

Project Staff

Professor Jonathan Allen, Robert C. Armstrong, Donald G. Baltus, Cyrus S. Bamji, Steven P. McCormick, Mark W. Reichelt, Filip Van Aelten

Through our VLSI CAD research, we seek the means to produce custom integrated circuits correctly, quickly, and economically. Traditionally, correctness has been checked at several representational levels such as layout (via design rule checking), circuit, and logic (both via simulation). The techniques for checking correctness are local to the particular representational level involved. While these techniques are important components of design testing, they do not attempt to provide alignment and consistency checks between the different levels of representation and an input behavioral specification. In addition, they do not characterize the set of possible designs at each representational level corresponding to the initial functional specification, while ranging over a variety of performance levels. For this reason, there is an increasing need to provide CAD tools that can serve as the framework for design exploration, providing the desired performance together with consistently aligned representations at all levels.

In this research group, we are studying a variety of research topics with an emphasis on performance directed synthesis of custom VLSI designs. Professor Allen has recently provided an overview of these issues,[1] in which he emphasizes the need for coordinating the design optimization process over the several levels of representation.

Since there is so much to be gained by aggressive circuit design, our research group has placed considerable emphasis on this level. In addition, the group has focused on optimized architectures for digital signal processing (1) because of the highly parallel nature of the algorithms involved, and (2) because of the need for a very high level of real time performance. We have also increased our emphasis on developing means for formally specifying designs that facilitate performance directed design exploration, as well as efficient verification of correctness of the coordinated set of design level represent-

[1] J. Allen, "Performance Directed Synthesis of VLSI Systems," *Proc. IEEE* 78(2): 366-355 (1990).

ations. All of these studies are taking on an increasingly theoretical approach, signifying the transition of digital system design from an art to a science.

The circuit level of design representation is the most abstract level at which performance can be characterized explicitly in terms of delay, and also where performance can be substantially manipulated through changes in circuit style and device sizing. It is an important level of design because optimization techniques which manipulate circuit representation can have great impact on resulting performance. More abstract representations can be transformed into a circuit representation, but the need to transform a circuit into layout in a general yet efficient way is needed for the rapid design of custom circuits. Baltus[2] has developed a very general yet efficient technique for compiling circuits into layout. The algorithm converts both NMOS and CMOS circuits in any style, and provides special means for the efficient layout of circuits with highly varying transistor width-to-length ratios. While initially focused on implementation technologies with only one level of metal, it is now being generalized to multiple levels of metal. Recent comparisons of this program with other techniques at a benchmark competition have demonstrated the effectiveness of these procedures.

Now that there is assurance of the generation of a high quality layout from any circuit specification, we are turning our attention to design performance exploration at the architectural level. For this research, our goal is to study the performance of quasi-regular architectures through manipulations of an initial behavioral specification. A new language has been developed for algorithms which can be compiled into either regular systolic architectures, or structures with a limited degree of irregularity. From the input language specification, a prototype descriptor is generated which compactly and efficiently represents both the structural hierarchy and the degree of replication of architectural elements. This descriptor can be readily expanded into a fully parallel data flow graph if necessary, but has the advantage that its complexity does not appreciably grow with circuit element replication.

After obtaining the prototype descriptor, we apply a series of three types of transformations in order to explore the architectural design space. First, various amounts of serialization can be instantiated, cutting down the amount of inherent parallelism in the input language specification, but also reducing the area of the resultant implementation. Next, we explore a variety of architectural transformations that map the index spaces associated with each array variable into a common global index space. Finally, we explore pipelining to localize communication between architectural elements. This approach is expected to lead to a flexible but powerful framework for architectural design exploration in the context of known capability for the conversion of the circuit form of the architectural elements into efficient layout. One important research issue is the degree of irregularity that is desirable in the resultant arrays due to non-local communication. It may be possible to make the distance of communication a designer-controlled parameter, thus providing a means to depart from regularity when the communication needs of the algorithm favor it, thereby expanding the class of designs that can be efficiently converted to layout.

Another example of the mapping of a high level specification to the circuit level representation has focused on the technology mapping process. Much research has focused on the conversion of a high-level functional specification to a highly optimized logic specification. This logic representation is usually then converted to the circuit form by means of a technology mapping in terms of a cell library. Heretofore the cell library was made up of typical restoring gates, such as

---

[2] D.G. Baltus and J. Allen, "SOLO: A Generator of Efficient Layouts from Optimized MOS Circuit Schematics," *Proceedings of the 25th Design Automation Conference*, June 1988.

NAND and NOR cells, but Kaplan[3] has recently expanded this process to include pass transistor gates as well as restoring forms. By broadening the class of circuit forms, and hence basic library gate cells, new flexibility is introduced into the technology mapping process. New logic-level representations have been introduced to facilitate the optimization of these circuits. By coupling to the existing SOLO layout generator, savings in the area of approximately 20 percent have been demonstrated for a number of designs that take advantage of the use of pass transistor gates as well as restoring gates. This research exemplifies the need to coordinate design at several levels. Logic synthesis must contemplate the class of library cells that will be used in implementations, while increased circuit flexibility leads to new layout savings by means of a more powerful technology mapping.

Driven by the requirements of performance optimization, we have devoted a considerable amount of research to delay characterization associated with circuit waveform transitions. McCormick[4] has developed an efficient scheme for computing these transitions accurately using a small number (four or less) of circuit transform moments. Interactions between interconnection lines, even as general as RLC lines, can be readily computed with these moments. In addition to passive interconnect, we have expanded these techniques to also include the efficient characterization of active circuits. Using these techniques, efficiency of delay calculation, together with accuracy, is obtained, thus avoiding the substantial numerical load of comprehensive circuit simulation. Moment calculations are thus part of an overall strategy of performance estimation that must be done quickly and accurately in order to facilitate rapid exploration of design alternatives. It is also important to note that delay due to interconnect is now dominating the delay caused by active circuits in large systems. The ability to accurately characterize circuit delay in complex branching interconnect structures, including the effect of interconnect material together with driving and terminating impedances, is essential to the accurate exploration of circuit performance.

With the advent of very small devices operating at very high speeds, we need to revise device models for circuit simulation. Rather than use average value parameters, we must now solve the device equations directly to provide the accuracy required. Unfortunately, direct use of these equations implies very long simulation run times, making it important to find ways of obtaining required accuracy with reduced computational expenditure. Reichelt[5] has applied waveform relaxation techniques to this problem in a way that readily allows for the use of parallel waveform relaxation simulators. Initial results have proved the effectiveness of this approach, which guarantees convergence of the simulation. Investigations of possible parallel architectures for this purpose are now under way.

Recently, our emphasis on verification techniques has grown as the complexity of designs, and the need for overall correctness, has increased. There are a variety of approaches to verification, including logical proofs that implementation structures correspond to behavior specifications, and symbolic simulation. Because the need for formal characterizations of design has grown, we are searching for representations that can compactly characterize the class of correct

---

[3] J.T. Kaplan, *Pass and Restoring Logic Technology Mapping for the Efficient Automated Generation of Combinational Leaf Cells,* S.M. thesis, Dept. of Electr. Eng. and Comput. Sci., MIT, 1989.

[4] S.P. McCormick and J. Allen, "Waveform Moment Methods for Improved Interconnection Analysis." *Proceedings of the 27th Design Automation Conference,* Orlando, Florida, June 1990.

[5] M. Reichelt, J. White, and J. Allen, "Waveform Relaxation for Transient Simulation of Two-Dimensional MOS Devices." *Proceedings of the International Conference on Computer Aided Design,* November 1989.

designs. Bamji[6] has applied context free formal grammars to the specifications for the class of MOS digital integrated circuits. Compact grammars can represent classes of infinite cardinality, so that, for example, the class of all CMOS static combinatorial circuits can be generated by only five grammatical rules. Many circuit styles can be characterized in this way, and the corresponding parsing procedures can deal with mixed styles in an efficient way. Bamji has represented the class of all layouts generated by a regular grammar by use of the Regular Structure Generator, and he has shown how to verify the correctness of the resulting layout by parsing techniques. Finally, both of these grammatical representations, one at the circuit level and the other at the layout level, have been combined into a coupled grammar that can be used to verify the proper correspondence between layout and circuit. Thus, not only can both layout and circuit structures be verified independently by similar grammatical techniques, but we can show that their alignment is correct so that they are both coordinated representations of the same underlying abstract circuit in a consistent fashion. Successful verification demonstrates that all circuit and layout structures have correspondents at related layout and circuit representations, respectively, so that no loose fragments at either level are isolated from those at other design levels. Since these grammatical techniques have been successful at the circuit and layout levels, we are now focusing on their application at higher levels of design.

Grammatical techniques are appropriate for characterizing correct structure of circuits, but they are not easily adapted to the verification of nonstructural circuit properties such as device sizing and allowable capacitance sizes that could lead to undesirable charge sharing. To deal with these attributes, Van Aelten[7] has developed an efficient technique for verification of circuit properties. This approach builds on the grammatical techniques of Bamji, parsing the circuit first to reveal its constituent structure. Semantic checks are then applied to the circuit to verify its specified performance. The circuit is effectively mapped into logic level representations by a process of recursive interpretation. Checks for electrical constraints are made at the level of the individual subcircuits, and the behavioral description of these elements is composed in order to provide a match with the user supplied specification. Extensions to this approach require more comprehensive circuit grammars that may have to be interleaved with the semantic interpretation process, thus breaking down the traditional separation of syntax and semantics.

To continually maintain a consistent set of design representations that are properly aligned, it is important to build a unified framework for all levels of representation. Armstrong[8] has developed a technique for specifying design at all levels of abstraction with a uniform formalism. The way in which each of these abstractions is a consistent projection of one underlying abstract design entity is explicitly described, thus facilitating the automatic alignment of these representations. In this way, when one design projection at a specific level of representation (e.g., circuit level) is manipulated, all other levels are changed automatically to provide the correct alignment. In general, this is a one-many process, since there is usually an infinite number of less abstract design projections corresponding to a more abstract projection of the same overall design. All that is required, however, is that all levels are consistent, so that performance optimization algorithms can select the best design projection at a given level, subject to some

---

[6] C.S. Bamji and J. Allen, "GRASP: A Grammar-based Schematic Parser." *Proceedings of the 26th Design Automation Conference,* June 1989.

[7] F. Van Aelten and J. Allen, "Efficient Verification of VLSI Circuits Based on Syntax and Denotational Semantics," *Proceedings, IMEC/IFIP Workshop on Applied Formal Methods for Correct VLSI Design,* Houthalen, Belgium, 1989.

[8] R.C. Armstrong, *A Formal Approach to Incremental Consistency Maintainence in Multirepresentation VLSI Databases,* Ph.D. diss. proposal, Dept. of Electr. Eng. and Comput. Sci., MIT, 1987.

overall optimization criterion. Upon completion, this new formal framework will provide a basis for interconnecting an entire suite of design tools and will easily contemplate the addition of new levels of representation without the need to provide an entirely new framework.

The above descriptions show how several aspects of performance-driven synthesis are being studied and adapted to new CAD tools. There is a clear trend toward adopting more formal notions of behavior, structure, and attributes, together with techniques for coordinating these several levels of description in one overall consistently maintained structure. In the future, we will emphasize completion of the theoretical framework and unification of optimization procedures across all levels of design.

6.2 The Vision Chip Project

Sponsors

DuPont Corporation
National Science Foundation
Grant MIP 88-14612

Project Staff

Professor John L. Wyatt, Jr., Professor Berthold K.P. Horn, Professor Hae-Seung Lee, Professor Tomaso Poggio, Professor Charles G. Sodini, Steven J. Decker, Ibrahim M. Elfadel, Mikko Hakkarainen, Craig Keast, Ignacio McQuirk, Mark N. Seidel, David L. Standley, Christopher B. Umminger, Woodward Yang

6.2.1 Overall Project Description

Problem Definition and Methods

Computational Demands of Vision and the Smart Sensor Paradigm: A major problem in machine vision is the extraordinary volume of input data that must be acquired, managed and processed. This large quantity of data in real-time grey-level images leads to communication bottlenecks between imager, memory and processors, while the computational demands remain high once data have reached the processors. The result is that conventional machines are incapable of any but the most rudimentary forms of real-time vision processing.

The *smart sensor paradigm* shows great promise as a new approach to this problem. Although potentially applicable to a variety of sensor types, e.g., tactile and acoustic arrays, in this project we are restricting its application to vision. The key idea is to incorporate signal processing as early as possible into a system's signal flow path to reduce demands for transmission bandwidth and subsequent computation.

In this paradigm, the major themes are:

- sensors and processing circuitry integrated on a single chip,
- parallel computation,
- processing circuits distributed throughout the array for spatially local operations in situ with minimal wiring overhead,
- use of analog circuits for early processing tasks to avoid the speed and area costs of analog-to-digital conversion on high-bandwidth data streams,
- selection of tasks and algorithms requiring low to moderate precision, and
- special emphasis on computations that map naturally to physical processes in silicon, e.g., to relaxation processes or to resistive grids.

Analog Integrated Circuits: Both continuous-time and sampled-data analog integrated circuits play a key role in our research. Analog circuits offer substantial advantages in speed, functionality per unit silicon area, and ease of interfacing to inherently analog input data, while digital circuits are easier to design and can obtain unlimited precision through use of progressively longer wordlengths.

The Gilbert 2-quadrant multiplier is a dramatic example of analog capability. Requiring only four transistors, its similar, although slightly more complex circuits, achieve 0.02 percent precision multiplication in under 200 nanoseconds with a dynamic

SUBJECT: Hold and Denial Records for FDAB FL-88 Orders(e.g. H-0475, D-0476)

PROBLEM: FDAB regularly generates FL-88 orders, resulting from user requests, work unit summaries, bibliographies, etc. On occasion, FDAC must hold one of our orders or return the document to the originator, resulting in a denial. Reasons for holds include lack of distribution statement, missing pages, improper classification markings, reproducibility, illegibility. If answers to the above reasons are not received, denials are the result. There is a lack of consistent communication between FDAB and FDAC regarding FDAB orders that are held or denied. For example, FDAB is not always informed if a hold or denial is taking place. Also, the AQ inputter in FDAC inputs her own record instead of using the AQ record established by FDAB.

PROPOSED SOLUTION: FDAB is requesting more control over holds and denials on FL-88 orders. The proposed solution is for FDAB to input the hold/denial information into the AQ database for FL-88 orders. With denials, FDAB will be able to close out the files and inform users, when appropriate. With holds, FDAB records will be more up-to-date. It is imperative that FDAB be informed of the outcomes on holds.

Sharon Serzan
16 Oct 89

Discussed with C. Gibson, Acting Chief of FDAC, and we will proceed with above procedures.

Sharon Serzan
23 Oct 89

DEPARTMENT OF THE AIR FORCE
USAF ENVIRONMENTAL TECHNICAL APPLICATIONS CENTER (MAC)
SCOTT AIR FORCE BASE, ILLINOIS 62225-5458

FROM: LDD (DSN 576-2625) 19 OCT 90

SUBJECT: Change in document status

TO: DTIC-FDAC

1. The distribution statement for four technical reports written by Air Weather Service personnel was changed to "Approved for Public Release; Distribution Unlimited." Photocopies of the title page, Review and Approval Statement, and Report Documentation Page for each are attached (Atch 1-4).

2. Please delete 7WW/TN-82/002, AD A 123352 from the DTIC database. It has been declared obsolete. The same photocopied pages are attached (Atch 5).

Susan A Tarbell

SUSAN A. TARBELL
Cataloging Librarian
Air Weather Service Technical Library

5 Atch
1. AD B 099412L
2. AD B 130894
3. AD B 066230L
4. AD B 082564L
5. AD A 123353

Table of Equivalents for Calculating Cubic Footage of Records

Letter size material and any material filed in letter size folders	1 full file drawer = 1.5 cubic feet or 1 linear foot = .75 cubic foot
Legal size material and any material filed in legal size folders.	1 full file drawer = 2 cubic feet or 1 linear foot = 1 cubic foot
Cards in vertical files:	
3 by 5 inch cards.	1 linear foot = .1 cubic foot
4 by 6 inch & tabulating size cards. .	1 linear foot = .17 cubic foot
5 by 8 inch cards.	1 linear foot = .25 cubic foot
Cards in visible index trays:	
3 by 5 inch cards.	1,000 full pockets = .07 cubic foot
4 by 6 inch & tabulating size cards. .	1,000 full pockets = .11 cubic foot
5 by 8 inch cards.	1,000 full pockets = .18 cubic foot
8 by 10 1/2 inch cards	1,000 full pockets = .36 cubic foot
EAM listings, 14 by 17 inches or larger.	1 linear foot = 1.5 cubic feet
EAM listings, small sizes.	1 linear foot = 1 cubic foot
Records Shipment and Storage Boxes (15 by 12 by 10 inches).	1 box = 1 cubic foot
Maps and Drawings (Mixed sizes). . . . . (Since a wide range of sizes are frequently interfiled, using these average conversion factors is sufficiently accurate. In the case of large collections or when documents are mostly a single size, a more accurate conversion factor may be determined and used.)	a 1-inch stack = .5 cubic foot or 1,000 documents = 3 cubic feet
ADPS magnetic tape	10 reels = 1 cubic foot
Film:	
16 millimeter, 100' reel	100 reels = 1 cubic foot
16 millimeter, 1000' reel	12 reels = 1 cubic foot
35 millimeter, 100' reel	50 reels = 1 cubic foot
35 millimeter, 1000' reel	6 reels = 1 cubic foot
Other records.	Estimate dimensions and compute cubic measurement

DEPARTMENT OF THE ARMY
THE JUDGE ADVOCATE GENERAL'S SCHOOL
CHARLOTTESVILLE, VIRGINIA 22903-1781

REPLY TO
ATTENTION OF

JAGS-DD (310) 4 September 1990

MEMORANDUM FOR Defense Logistics Agency, Defense Technical Information Center, ATTN: Mr. Norm Walton, Cameron Station, Building 5, Alexandria, VA 22304-6145

SUBJECT: Request for Inclusion in and Deletion From DTIC

1. Please add the following items to DTIC:

Legal Assistance Guide: Soldiers' and Sailors' Civil Relief Act, JA-260-90

Model Tax Assistance Program, JA 275-90

2. Please delete the following publications from DTIC:

AD B142445, Legal Assistance Guide: Soldiers' and Sailors' Civil Relief Act, JA-260-90, dated January 1990

AD B124120, Model Tax Assistance Program/JAGS-ADA-88-2

3. Point of contact for this action is Ms. Eva Skinner, AV 274-7110, extension 972-6396; commercial (804) 972-6396.

Enclosures

MATTHEW E. WINTER
CPT, JA
Publications Officer